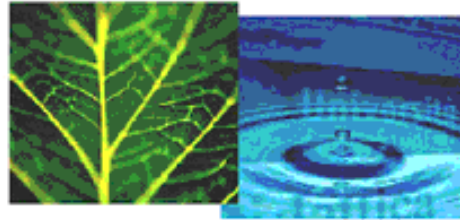


PhD Dissertation



International Doctorate School in Information and
Communication Technologies

DIT - University of Trento

ANALYSIS OF 3D SCANNING DATA FOR OPTIMAL
CUSTOM FOOTWEAR MANUFACTURE

Bitu Ture Savadkoohi

Advisor:

Dr. Raffaele de Amicis

2010

Acknolgment

I would like to express my deepest gratitude and thanks to my supervisor and the director of the Graphitech, Dr. Raffaele De Amicis for his enthusiasm, generosity, support and his patience with me. I feel truly honoured to have the opportunity of being Dr. De Amicis student; it was his experience and inspiration that kept the research going. I address my special thanks to Dr. Giuseppe Conti for helping and collaborating in different research areas during my Ph.D. studies.

My friendships along the way have been invaluable. For this I thank the entire Graphitech group. I owe special thanks to all of my office-mates and colleagues along the way: Gabrio Girardi, Stefano Piffer, Letizia Santato, Federico Prandi, Michele Andreolli, Daniele Magliocchetti, Marco Calderan and Bruno Simes. I would like to thank to my brother, Dr. Alireza Ture Savadkoohi and my sister, Dr. Parisa Ture Savadkoohi for helping me in all aspects of my life.

My parents and my aunt have been there for me throughout my life with advice, encouragement, love and support; thank you.

Bitā Ture Savadkoohi

July 2010, Trento

Abstract

Very few standards exist for fitting products to people. Footwear fit is a noteworthy example for consumer consideration when purchasing shoes. As a result, footwear manufacturing industry for achieving commercial success encountered the problem of developing right footwear which is fulfills consumer's requirement better than it's competeries.

Mass customization starts with understanding individual customer's requirement and it finishes with fulfillment process of satisfying the target customer with near mass production efficiency. Unlike any other consumer product, personalized footwear or the matching of footwear to feet is not easy if delivery of discomfort is predominantly caused by pressure induced by a shoe that has a design unsuitable for that particular shape of foot.

Footwear fitter have been using manual measurement for a long time, but the combination of 3D scanning systems with mathematical technique makes possible the development of systems, which can help in the selection of good footwear for a given customer. This thesis, provides new approach for addressing the computerize footwear fit customization in industry problem.

The design of new shoes starts with the design of the new shoe last. A shoe last is a wooden or metal model of human foot on which shoes are shaped.

Despite the steady increase in accuracy, most available scanning techniques cause some deficiencies in the point cloud and a set of holes in the triangle meshes. Moreover, data resulting from 3D scanning are given in an arbitrary position and orientation in a 3D space. To apply sophisticated

modeling operations on these data sets, substantial post-processing is usually required.

we described a robust algorithm for filling holes in triangle mesh. First, the advance front mesh technique is used to generate a new triangular mesh to cover the hole. Next, the triangles in initial patch mesh is modified by estimating desirable normals instead of relocating them directly. Finally, the Poisson equation is applied to optimize the new mesh. After obtaining complete 3D model, the result data must be generated and aligned before taking this models for shape analysis such as measuring similarity between foot and shoe last data base for evaluating footwear fit.

Principle Component Analysis (PCA), aligns a model by considering its center of mass as the coordinate system origin, and its principle axes as the coordinate axes. The purpose of the PCA applied to a 3D model is to make the resulting shape independent to translation and rotation as much as possible. In analysis, we applied "weighted" PCA instead of applying the PCA in a classical way (sets of 3D point-clouds) for alignment of 3D models. This approach is based on establishing weights associated to center of gravity of triangles. When all of the models are aligned, an efficient algorithm to cut the model to several sections toward the heel and toe for extracting counters is used. Then the area of each contour is calculated and compared with equal sections in shoe last data base for finding best footwear fit within the shoe last data base.

Keywords: [Advance front mesh, Poisson equation, Harmonic Function, "Weighted" Principle Component Analysis.]

Contents

1	Introduction	1
1.1	Mass customization concept	1
1.2	Problem statemnet and solution outline	3
1.2.1	Automated design and customized manufacturing	4
1.2.2	Reverse Engineering	6
1.2.3	Alignment of 3D models	8
1.2.4	3D comparization	9
1.3	Thesis Overview	9
2	Mass customization and Footwear research: An overview	11
2.1	Introduction	11
2.2	Why customization?	12
2.3	The product process matrix	13
2.3.1	Diagonal position	15
2.4	Level of mass customization	16
2.5	Success facture of mass customization systems	17
2.5.1	Customer demand for variety and customization must exist	18
2.5.2	Product should be customized	18
2.5.3	Technology must be available	18
2.5.4	value chain should be ready	19
2.5.5	Market conditions must be appropriated	19

2.5.6	Knowledge must be shared	19
2.6	Footwear Customization	20
2.7	Foot shape and shoe last	21
2.7.1	Foot shape	21
2.7.2	Shoe last	22
2.8	Footwear comfort and fit	23
2.9	Footwear research	25
3	Reconstruction of 3D model from 3D scanning data	29
3.1	Introduction	29
3.2	Acquisition Techniques	30
3.2.1	Practical problems of data acquisition	31
3.2.2	Contact-Based Acquisitions	34
3.2.3	Contactless Acquisitions	34
3.2.3.1	Passive scanners	35
3.2.3.2	Active scanners	38
3.3	Reconstruction of surface from 3D Data Points	43
3.3.1	Spatial subdivision	45
3.3.1.1	Surface-oriented cell selection	45
3.3.1.2	Volume-Oriented Cell Selection	53
3.3.2	Surface construction with distance functions	61
3.3.2.1	Calculation of Distance Functions	62
3.3.2.2	Bittar's et al. surface construction by medial axes	64
3.3.3	Surface construction by warping	66
3.3.3.1	Spatial free form warping	68
3.3.3.2	The approach of Algorri and Schmitt	69
3.3.3.3	Kohonen feature map approach of Baader and Hirzinger	70

3.3.4	Incremental surface-oriented construction	71
3.3.4.1	Boissonat's surface-oriented approach	72
3.3.4.2	Approach of Mencl and Muller	73
4	Filling hole in triangle mesh	77
4.1	Introduction	77
4.2	Preliminaries	77
4.3	Advance front mesh technique	79
4.4	Differential geometry background	79
4.4.1	Isometric mappings	81
4.4.2	Conformal mappings	82
4.4.3	Equiareal mappings	83
4.4.4	Planar mappings	84
4.4.5	Conformal and harmonic mappings	84
4.4.6	Equiareal mappings	89
4.4.7	Discrete harmonic mappings	91
4.4.8	Finite element method	92
4.5	Rotation about arbitrary axis in 3 dimensional	95
4.5.1	A translation matrix	96
4.5.2	Rotation matrices	96
4.5.3	Transformations for moving a vector to the z-axis	97
4.5.4	Rotations about the origin	98
4.6	Rotation about an arbitrary line in 3 dimensional	98
4.7	Filling hole in triangle mesh	99
4.7.1	Hole patching	100
4.7.2	Harmonic-based desirable normal computing	101
4.7.3	Poisson equation	104
5	Alignment of the scanned foot with shoe last data base	107
5.1	Introduction	107

5.2	Problem Description	108
5.3	Principal Component Analysis	109
5.4	Modifications of the PCA	114
5.5	Search for similarity estimation	117
6	Conclusion	121
	Bibliography	125

List of Tables

2.1	Generic Level of mass customization	16
3.1	<i>Shape – from – X</i> methods and their classification	36

List of Figures

2.1	Matching major stages of product and process life cycles . . .	14
2.2	Footwear customization	21
2.3	I) Phalanges. II) Metatarsas. III) Malleolus; tarsal 1) inner, 2) middle, 3) outer, 4) navicular, 5) cuboid 6) talus, 7) calcaneus	22
2.4	Foot Shoe last triangle	23
3.1	Out of a scanning process. a) Point. b) Profile. c) Range image. d) Volumetric output	30
3.2	The classification of the surveyed acquisition methods . . .	31
3.3	Example of contact based system	35
3.4	<i>StereoVision = Correspondences + Reconstruction</i> . . .	37
3.5	Coordinate relationship between the image plane and the surface plane	38
3.6	The basic geometry of active, optical triangulation (planar XZ view). The Y and y axes are perpendicular to the plane of the figure.	39
3.7	Triangulation: Moveing the camera and Illumination . . .	41
3.8	Time of flight scanner	43
3.9	A laser range-finder based on amplitude modulation . . .	44
3.10	The initial point set (left) and the desired reconstruction result (right)	44
3.11	The approach of Algorri and Schmitt	46

3.12	The approach of Hoppe et al.	48
3.13	An example for a reconstruction of a body. If α is too small, gaps in the surface can occur, or the surface may become fragmented.	51
3.14	Boissonnat's Volume-Oriented Approach	54
3.15	An example point set and the deletion process.	56
3.16	A Υ -indicator is a value associated to a sphere through three boundary points of a polyhedron which is positive or negative for an illustration of the 2D-case	57
3.17	Some intermediate stages during the construction of a surface	58
3.18	The selection of tetrahedra, uses a minimum spanning tree of the Voronoi graph	60
3.19	A consistent orientation of neighboring tangent planes is determined by computing the Riemannian graph	63
3.20	The desired surface is calculated by distributing center of sphere on the medial	65
3.21	A sharp field function preserves details while a soft function smoothes out the details	66
3.22	The connectness of the resulting solid can be influenced by the shape function	67
3.23	The approach of Algorri and Schmitt	69
3.24	Kohonen's feature map is a two-dimensional array of units (neurons),	70
3.25	The combination of this normal and reverse training completes the algorithm of Baader and Hirzinger and has to be used in the training of the network.	72

3.26	The point is taken which maximizes the angle between at its edges in the new triangle, that is, the point sees edge boundary edge under the maximum angle	73
3.27	The algorithm terminates if there is no free edge available any more.	73
3.28	Approach of Mencl and Muller	75
4.1	Preliminaries related to triangle mesh and hole.	78
4.2	The mapping f from $StoS^*$ and the parameterization x of S induce the parameterization $X^* = f \circ fS^*$	81
4.3	Orthographic (a), stereographic (b), Mercator (c), and Lambert (d) projection of the Earth.	82
4.4	One-to-one harmonic mappings.	86
4.5	A harmonic mapping which is not conformal	87
4.6	An equiareal mapping.	90
4.7	Piecewise linear mapping of a triangular mesh.	92
4.8	Atomic map between a mesh triangle and the corresponding parameter triangle.	94
4.9	Angles for the discrete harmonic map and the mean value coordinates.	94
4.10	Moving the axis of rotation to the z axes	95
4.11	Rules for generating initial patch over the hole.	101
4.12	1-ring vertex of v_i and angles opposite to edge $v_i v_j$	102
4.13	a) Initial patch mesh in triangle mesh, (b) A triangle red is initial patch mesh and its locally rotated is version green.	103
5.1	Models of shoe last are initially given in arbitrary units, position, and orientation (a, b, and c). The out come of the pose estimation procedure is the canonical positioning of each model (d, e, and f) which is parallel with x-y space.	108

5.2	The analyzed image (left) and the pixels of the image in the color space (right). Axes x , y , and z represent values of red, green, and blue components, respectively. The PCA coordinate axes are denoted by P_1 , P_2 and P_3	113
5.3	<i>a)</i> Input 3D smooth triangle. <i>b)</i> Translated center of gravity to the origin. The red, green and blue lines are eigenvectors. <i>c)</i> Rotated 3D model with its eigenvectors. <i>d)</i> Target model.	115
5.4	<i>a)</i> Translated center of gravity to the origin. <i>b)</i> Rotated 3D foot model. <i>d)</i> The alignment of 3D foot in <i>b</i> with shoe last in <i>c</i>	116
5.5	Preliminaries related to triangle mesh with intersection planes for cutting shape to several sections.	118
5.6	Steps for cutting shape to several sections.	119
5.7	The illustrated contour after cutting mesh.	120

Chapter 1

Introduction

As consumers are becoming increasingly selective of what they wear on their feet, manufacturers are experiencing problems developing and fitting the accurate footwear that fulfils the consumer's requirement better than it's competitors for achieving commercial success. Thus production of custom tailored product is widely required in manufacturing industry nowadays and the business paradigm is moving from producer-centered productivity to consumer-centered customization.

In this chapter, we first describe the general concept of Mass customization. Then the main motivation of work presented in the thesis will be introduced. Finally the structure of the thesis will be presented.

1.1 Mass customization concept

Mass customization is become an important for manufacturing strategy. MC enables manufacturers to customize the products or services to fulfill the exact needs of customers. Generally, mass customization (MC) can be defined either broadly or narrowly.

MC is defined broadly as the ability to provide products and services that are individually designed for each customer through high-process agility, flexibility and integration [17]. Some authors defined MC narrower as in-

formation technology, flexible processes and organizational structures using a system that delivers a wide range of products and services in order to meet particular needs of each of their customers at a cost near that mass-customized item [97].

In any case, MC can be seen as a systemic idea involving all aspects of product sale, development, production, and delivery, full-circle from the customer option up to receiving the finished product. The development of MC systems can be justified as follow [53]:

- Delivering higher variety production system at lower cost by new flexible manufacturing and information system (IT).
- Increasing demand for product variety and customization.
- Shortening of product life cycles and expanding industrial competition has led to the breakdown of many mass industries, increasing the need for production strategies focused on individual customers.

Using the concept of "product-process matrix" [57], MC systems are positioned below the main diagonal of this matrix, i.e. having medium to high-volume process types such as manufacturing cells or assembly line that are able to deliver the high product varieties usually associated to function or fixed-type operation.

Annually, manufactures are produced thousands of new products to bring products closer to ever changing customers tastes [14]. However, providing variety can be costly. There by manufacture cannot take advantage of the economic scale in production and distribution. Mass customization can take place at different levels subject to the technological limitations and the product. There for, it is important to determine how much customization should be undertaken. For instance, if the market place is very competitive, there may exist a greater need for a high level of customization. For instance, Spencer [99] is introduced that automation can be take

place in the footwear industry for producing high variety, low volume and low cost products.

1.2 Problem statement and solution outline

The importance of product compatibility for comfort and satisfaction is well known. Fit is considered to be very importance since mis-fitting shoes are generally the major cause of foot related illnesses and injuries.

According to Janisse [49] properly fitting footwear are important in avoiding foot discomfort and are essential in patient with arthritis, diabetes, and other foot disorders such as calluses, corns, hallux valguses, plantar ulcera. Thus, a pair of shoes designed and manufactured with a good fit is very important for foot comfort and health. Unlike any other consumer product, personalized footwear or the matching of footwear to feet is not easy if delivery of discomfort is predominantly caused by a shoe that has a design unsuitable for that particular shape of foot.

Footwear fitters have been using manual measurements for a long time. Anthropometers and plastic tapes are commonly used for obtaining measurements on people [46]. Foot dimensions are measured using the device such as the Ritz Stick device [85], the Brannock device [8], the Scholl device [40], calliper.

Foot measuring always takes a lot of time and shoe making industry in order to make an accurate custom shoe last must manually measure the specific consumer's foot, and sometimes, more than thirty measurement are required. The last is also manually manufactured by experienced last maker. The process of foot measuring and last manufacturing process and custom footwear is expensive to produce and time-consuming because of the complexity constraints imposed by footwear manufacturing process.

Nowadays, the combination of 3D scanning system with mathematical tech-

nique makes it possible, automating the process of producing custom tailored footwear based on consumer's foot shape.

In this thesis, we provide new methods for addressing the computerized footwear fit customization in industry problems. In basic idea of solution is to compare the lasts which were used to manufacture the shoes and the scanned feet of the clients.

Depending on both the complexity of the object to be reverse engineered and accuracy of adopted data acquisition system technology, some area of the object outer surface may never be accessible and it cause some deficiencies in the point cloud and a set of holes in the triangle meshes. This deficiency is not acceptable when the 3D model is taking into actual application. Moreover, data resulting from 3D scanning are given in an arbitrary position and orientation in a 3D space. To apply sophisticated modeling operations on these data sets, substantial post-processing is usually required. Thus, the problem of geometric similarity measurement consists essentially of two sub problems:

- The pose estimation, where complete 3D models is reconstructed (all of the holes are filled) and properly positioned and aligned
- Comparison or similarity measurement of 3d models.

1.2.1 Automated design and customized manufacturing

In the last few years, three-dimensional models have become more and more important in several research and application fields of advance information technology. Following the growing demand of 3D models, the development of 3D acquisition systems has also become of key practical and scientific interest.

Automatic 3D acquisition device allow to build highly accurate models of real 3D objects in a cost- and time-effective manner. This technology en-

ables full customization of manufactured parts for individuals by scanning and generating a geometric model of a human body and its respective parts and then designing customized one-of-a-kind products.

It seems important to clearly distinguish between the concepts of a 3D copier and a 3D scanner. A photocopier takes a piece of paper and produces another piece of paper just like the original. A 3D copier is a device which takes a solid object and makes another one of just the same shape (let us ignore material). In fact, copy machining has been a well established technology for a long time. A scanner however, in 2D, not only inputs a page of text into the computer, but can also recognize the characters and figures, thus providing a text file and graphical structures. Similarly, a 3D scanner will not only capture raw data from the object, but the data will be interpreted and some computer model will be created. Now, not only may a single copy be generated, but knowledge of the shape is obtained, and thus we can derive new shapes, make variations, analyze properties and determine characteristic quantities such as volume or surface area. Many different systems have been proposed for data acquisition; a common characterization subdivides them into contact and non-contact devices [92].

Contact-based acquisition is performed by touching the object surface on each relevant side. This group of technology are very precise but very slow and expensive, in addition to begin very difficult to automate. For example, a Coordinate Measuring Machine (CMM) requires that the path of a physical probe be directed in such a manner that it comes into contact with the part. If the geometry of the part is not known beforehand, this path must be specified by a human operator, thus increasing the time and cost needed to measure an object.

Contactless acquisition is performed through indirect techniques based on a given energy source. Digital cameras or special sensors are used to measure the return signal. This group of technology have become more ubiquitous be-

cause of their low cost and speed in acquisition data and it can further be categorized as: active sensors and passive sensors.

Active sensors are made by an energy source and a sensor. The source emits a certain illumination and the sensor acquires the returned pattern reflected by the object's surface. The possible type of active sensors include imaging radar, triangulation, interferometry, active stereo.

Passive sensor use multiple camera systems with natural light and no special source of illumination, or a combination of more than one camera system coupled with some controlled illumination pattern. The possible type of passive sensors are shape from-X, where X represents the method used to determine the shape, that is stereo, shading, silhouette, depth from focused/defocus.

1.2.2 Reverse Engineering

In many area of industry, it is desirable to create geometric models of existing for which no such model is available. There are several application areas of reverse engineering. It is often necessary to produce a copy of a part, when no original drawings or documentation are available. In other cases we may want to re-engineer an existing part, when analysis and modifications are required to construct a new improved product.

In areas where aesthetic design is particularly important such as in the automobile industry, real-scale wood, clay and body models are needed because stylists often rely more on evaluating real 3D objects than on viewing projections of objects on high resolution is to generate custom fits for human request.

The ultimate goal of reverse engineering systems is to realize an intelligent 3D scanner. However, there is a long way to go. Even capturing shape and translating it into a CAD model is a difficult and complex problem. In spite of several encouraging partial results in particular areas, a fully

automatic solution to build a complete and consistent CAD model is still a goal.

There is a wide range of applications for which surface construction from scattered point data is important. However many algorithms have been developed which interpolate or approximate the input sampled points. The methods can be divided into four groups:

- **Warping**

Warping works on the basic idea that we deform some starting surface to the surface that forms the object[55].

- **Incremental surface construction**

The methods of incremental surface reconstruction start at some starting simplex(triangle, edge) and other simplices are incrementally added [86].

- **Distance function methods**

The distance function describes the shortest distance from the point to the surface. For closed surfaces, the value of the function is negative or positive depending on whether the point is inside or outside the object. This function is computed for each point using the tangent plane. The plane can be estimated from k-nearest neighbours (points, the parameter k is set by the user) by the least square approximation [72].

- **Spatial subdivision**

The basic feature of the spatial subdivision methods is the boundary hull (convex hull, box around points, etc.) division to the independent areas forming e.g. the regular grid, octree or tetrahedra. The surface is then extracted using the relationship to the surface described by the input set (e.g. the surface triangles should be small, etc.)[18].

We used Tight Cocone software for generating triangle mesh from cloud point [101]. During the surface reconstruction process, a mesh is calculated from a cloud point. Despite the steady increase in accuracy, most available scanning techniques cause some deficiencies in the point cloud and set of holes in triangles meshes. Thus certain repair must be done before taking these models into actual application.

Various techniques have been proposed to fill holes in the mesh. Existing approach to fill holes in meshes can be distinguished two main categories: the geometric and non-geometric approaches. In the chapter four, details about our original filling hole approach are given. A satisfaction hole filling method should:

- Run in reasonable time.
- Be able to patch an arbitrary holes for any model.
- Cover the missing geometry well.

Hole filling process that we implemented is summarized in following steps [94, 95]. First, holes is identified in triangle mesh and they covered by with Advance Front Mesh technique. Holes can be identified automatically by looking close loop of boundary edges. Next, modify the triangles in the initial patch mesh by estimating desirable normals instead relocating them directly and rotate triangle by local rotation. Then, Make algorithm more accurate by re-positioning these coordinate by solving the Poisson equation according to desirable normal and boundary vertices of the hole. Finally, Update the coordinate to make the smoothed patch mesh.

1.2.3 Alignment of 3D models

The obtained data from 3D scanning given in arbitrary position and orientation in the space. After obtaining complete 3D model, the result data

must be generated and aligned before taking these models for shape analysis.

The most prominent tool for solving the problem is the Principal Component Analysis (PCA) [102], also known as the discrete Karhunen-Loeve transform, or the Hotelling transform. Principal component analysis aligns a model by considering its centre of mass as the coordinate system origin, and its principle axes as the coordinate axes. The purpose of the PCA applied to a 3D model is to make the resulting shape feature vector independent to translation and rotation as much as possible. In analysis, instead of applying the PCA in a classical way (sets of 3D point-clouds) in order to account for different sizes of triangle, we established weights associated to the centre of gravity of triangles [93].

1.2.4 3D comparization

Due to the recent improvement in laser scanning technology, 3D visualization and modelling, there is an increasing need for automatic search for 3D objects in archive. Our new approach is based on the efficient algorithm for cutting 3D triangle mesh to several sections toward heel and toe. Then the area of each contour is calculated and compared with area of equal section in shoe last data base for finding footwear fit [94].

1.3 Thesis Overview

The **first chapter** has an introductory chapter and consists of three sections. The general concept of mass customization is presented in section 1.1. Section 1.2, which consists of four subsections, focuses on the topic of the thesis, analysis 3D scanning data for customize footwear manufacture. Since triangular mesh is the most common way of representing 3D-object, a

general 3D-model acquisition is explained in subsection 1.2.1. 3D-hole filling algorithm should fulfill certain criteria, which are defined and discussed in subsection 1.2.2. Alignment of 3D models are addressed in subsection 1.2.3. Measure of similarity (or dissimilarity) between 3D client's foot and shoe last data based are described in subsection 1.2.4.

In the **second chapter** detailed discussion of mass customization is given. In particular level of mass customization, success factors of mass customization systems and together with footwear research and customization of footwear will be discussed.

In the **third chapter**, current 3D-model acquisition using both active and passive vision techniques. Each technique is explained in terms of its configuration, principle of operation, and inherent advantages . and limitations. In addition methods for surface reconstruction from scattered point data will be discussed.

A brief description of the filling holes on surfaces reconstructed from point clouds is given in **fourth chapter**.

In the **fifth chapter**, details about our original pose estimation approach are given. we will describe the problem of finding the canonical coordinates of a mesh. Since applying the PCA to the set of vertices of a mesh model can produce undesired normalization results. Thus modifications of the PCA will be given. Examples as well as an evaluation of the weighted approach will be described. In addition for Similarity estimation for computerize footwear fit we will be described efficient algorithm for cutting the triangle mesh model toward heel and toe.

Finally we conclude in **sixth chapter** by reviewing our work.

Chapter 2

Mass customization and Footwear research: An overview

2.1 Introduction

For the last years the concept of mass customization has gained a broad attention within various branches of industry because the marketing interest is increasingly focused on delivering superior customer. The research area of manufacturing strategy is evolving, calling for a stronger focus on the manufacturing aspect of companies, and claiming that by strategically managing the manufacturing function it can become a competitive weapon. As a result, Mass Customization Manufacturing (MCM) has emerged as a new trend which aims at to provide customized product and services to individual customers using technology from their customers through engineering-to-order, product-to-order, or assembly-to-order production systems at optimal production efficiency and cost levels.

2.2 Why customization?

In the natural cycle of industrial evolution order-winner will over time turn into order-qualifiers . In the 1970's quality and function were order winners, but during the 1980's and 1990's product have become increasingly uniform regarding attributes such as quality and performance, and thereby they are turned into order qualifiers. Faced with this challenge manufactures are forced into the search for new parameters of differentiation.

Some manufactures are using mass customization as a tool to escape the enervating price competition between uniform products. Customization is one mean by which manufactures strive to differentiate their products in a world of similarity. Since customers are individual and have different preferences, there is a fertile soil for development towards personalized and adoption.

Customization is intended to add increased customer perceived value to a product, since a customized product (compared to a standard product) increasingly fulfils the need of its customer. Historically companies have made a strategies decision on craft production, build-to-order, or mass production. Within these traditional paradigms, a customer may select between a customized product with a high price and standardized product at low cost.

With the emergence of mass customization the added value of customization should now be manufactured with no or only little extract cost. The differentiation is, however, only effective (i.e. the product is sold) if the customers considers customization to be of value.

When looking at the customized product value generated from variation to be considered firstly. Authors in [82] have set up some basic question regarding customer orientation helping to define the value of mass customization:

- Do the customers really have unique needs?
- Do the customers really care about more customization of their products/services?
- Do they really want more choices or will they be overwhelmed by large variety?

Thus the goal of the customization process must be the reduction of the customer sacrifice and cost through the customization process. The manufactures must help the customer to configure the right product, since the manufactures holds the most knowledge of the products and its utilization and thereby can eliminate uncertainty.

2.3 The product process matrix

The process life cycle has been attracting increasing attention from business managers and researchers [57]over the past several years. Just as a product and market pass through a series of major stages, so does the production process used in the manufacture of that product.

The process evolution typically begins with a "fluid" process-one that is highly flexible, but is not very cost efficient and proceeds toward increasing standardization, mechanization, and automation.

- The rows of this matrix represent the major stages through which a production process tends to pass in going from the fluid form in the top row to the systemic form in the bottom row.
- The columns represent the product life cycle phases, going from the great variety associated with startup on the left-hand side to standardized commodity products on the right-hand side.

- Two corners in the matrix are void of industries or individual companies.
- The upper right hand corner characterizes a commodity product produced by a job-shop process that is simply not economical. Thus there are no companies or industries located in that sector.
- Similarly, the lower left-hand corner represents a one-of-a-kind product that is made by continuous or very specific process. Such process are simply too inflexible for such unique product requirements.

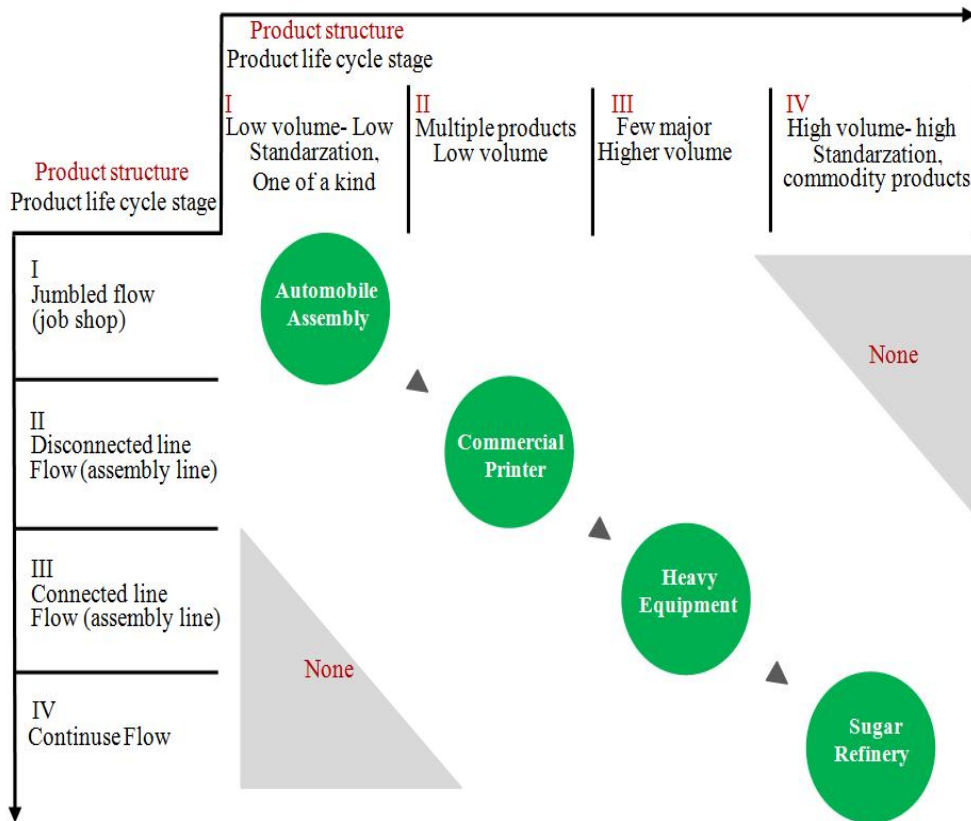


Figure 2.1: Matching major stages of product and process life cycles

2.3.1 Diagonal position

A business unit within a diversified company can be characterized as occupying a particular region in the matrix, determined by the stage of the product life cycle and its choice of production process for that product. Typical of a company positioned in the upper left-hand corner is a commercial printer. In such a job shop, jobs arrive in different forms and require different tasks, the equipment tends to be relatively general purpose and the workers typically have a wide range of production skills, and each job takes much longer.

Further down the diagonal in this matrix, the manufacturer of heavy equipment usually chooses a production structure characterized as a "disconnected line flow" process. Although the company may make a number of products (a customer may even be able to order a somewhat customized unit), economies of scale in manufacturing usually lead such companies to offer several basic models with a variety of options. This enables manufacturing to move from a job shop to a flow pattern in which batches of a given model proceed irregularly through a series of work stations, or possibly even a low volume assembly line.

Even further down the diagonal, for a product like automobiles or major home appliances, a company will generally choose to make only a few models and use a relatively mechanized and connected production process, such as a moving assembly line. Such a process matches the product life cycle requirements that the automobile companies must satisfy with the economies available from a standardized and automated process.

Finally, down in the far right-hand corner of the matrix, one would find refinery operations, such as oil or sugar processing, where the product is a commodity and the process is continuous. Although such operations are highly specialized, inflexible, and capital intensive, their disadvantages

are more than offset by the low variable costs arising from a high volume passing through a standardized process.

2.4 Level of mass customization

There are many methods to achieve mass customization [103]. Based on an analysis of existing framework to categorize the various levels of customization of product, Da Silverira et al.[97] proposed a set of eight generic levels of mass customization, ranging from pure customization (individually designed products) to pure standardization, see table 1.

Generic Levels	Approach by Cilmore&Pine [34]	Strategies by Lampel&Mintzberg [68]	Satge by Pine [78]	Types by Spira [100]
1. Standardization		Pure standardization		
2. Usage	Adaptive		Embedded customization	
3. Package and Distribution	Cosmetic	Segmented standardization		Customized packaging
4. Additional Services			Customized services; quick response	Providing additional services
5. Additional Custom work			point of delivery customize	performing additional custom work
6. Assembly		customized standardization	modular production	Unique config, out of standard components
7. Fabrication		tailored customization		
8. Design	collaborative; transparent	pure customization		

Table 2.1: Generic Level of mass customization

- Design

Design as the level 8 refers to collaborative product development, manufacturing and delivery of products according to individual customer preferences.

- Fabrication

The next level which is fabrication refers to manufacturing of customer-tailored products based on predefined designed.

- Assembly

Assembly as the level 6 deal with the arranging of modular components into different configurations according to customer orders.

- **Additional service and custom work**

On the level 5 and 4, mass customization is achieved by simply adding custom work or services to standard products (often at the point of delivery).

- **Package and Distribution**

In the level 3, MC is provided by alternative approaches for distributing or packaging of products (e.g. different labels and/or box sizes according to specific market segments).

- **Usage**

In level two, mass customization occurs only after delivery, through products that can be adapted to different functions and situations.

- **Standardization**

The level 1 refers to pure standardization of a strategy which can be useful in many industrial segments.

2.5 Success facture of mass customization systems

The ultimate success of mass customization depends on the perceived value of buying mass-customized products to mass-produced ones. Thus the success of mass customization is defined as the ability to provide superior customer value in contrast to mass manufacturer's offerings - through customization on a mass scale. Authors in [103] introduced the mass customization which is able to enhance customer loyalty by enabling the foundation of relationships through customer knowledge. However, this is only case when the frequency of purchasing is high.

Perceived customer value plays an important role in achieving sustainable competitive advantage [110]; it relates to customer perception of relative performance. The literature has often described perceived customer value as a trade-off between quality and price. The success of MC system depends on a series of external and internal factors.

2.5.1 Customer demand for variety and customization must exist

The need to deal with increasing customer demand for innovation and customized products is the fundamental justification for MC [69]. The success of MC depends on the balance between, on the potential sacrifice that customers make for MC products and the company's ability to produce and deliver individualized products.

2.5.2 Product should be customized

Independent units that can be assembled into different forms compose a modular products [27]. Successful MC products must be modularized, versatile and constantly renewed. Although modularity is not the fundamental characteristic of MC (true MC products are individually made), it enables simpler and lower-cost manufacturing of products with similar effectiveness compared to the true customization. Also, MC processes needs rapid product development and innovation capabilities due to typical short life cycles presented by MC products.

2.5.3 Technology must be available

The implementation of Advanced Manufacturing Technologies (AMTs) is a fundamental step to enable the development of MC systems [61]. One could argue that the early concept of MC appeared only after some compa-

nies were able to successfully integrate a series of information and process flexibility technologies. MC is one of the best opportunities offered by coordinated implementation of AMTs and Information Technology (IT) across the value chain.

2.5.4 value chain should be ready

MC is a value chain-based concept. Its success depends on the willingness and readiness of suppliers, distributors, and retailers to attend to the system's demands. The supply network must be at close proximity to the company to deliver raw materials efficiently [28]. Most important manufacturers, retailers and other value chain entities must be part of an efficiently linked information network [39].

2.5.5 Market conditions must be appropriated

According to Kotha [65], a company's ability to transform MC potential into actual competitive advantage greatly depends on the timing of this development. In other words, being the first to develop an MC system can provide substantial advantage over competitors, since the company may get well entrenched in this position and start being seen by people as innovative and customer-driven.

2.5.6 Knowledge must be shared

MC is a dynamic strategy and depends on the ability to translate new customer demands into new products and services. To achieve that, companies must pursue a culture that emphasizes knowledge creation and distribution across the value chain. That requires the development of dynamic networks along with manufacturing and engineering expertise [66], and in-house development of new product and process technologies [65].

2.6 Footwear Customization

Research indicates that customer focus can influence today's business. With growing product variety and opportunities in e-commerce, the old paradigm of mass production becomes sluggish especially when there is a change of the business paradigm from producer-centered productivity to consumer-centered customization. Mass customization begins with understanding individual customer requirements and ends with the fulfillment process of satisfying the target customer with near mass production efficiency.

By breaking down the product features into components and offering those components to the consumer as choices, customization of the whole or part-product is possible. Historically, there has been a trend to introduce product variety which covers varying consumer tastes and styles. For example, from 1970 to 1988, the number of running shoe models increased from 5 to over 285 (167 men and 118 women) [14]. In order to keep pace with ever changing customer tastes, thousands of new products are made annually and with each variation, manufacturers attempt to bring products closer to what the customer needs. Even though variety matters to consumers, each product variety may have a differing meaning to different consumers [34].

Hence, allowing a customer to choose one product from a "shelf" can be wasteful and can also constrain a customer's ultimate satisfaction even though a store shelf may have great marketing appeal [107]. The difficulty of selecting the right pair of shoes in a shoe store is a classic example. Mass customization means to generate these "right" products in order to fulfill customer's needs at different levels [99, 83, 37]. The footwear industry can adopt this methodology for the next generation of footwear manufacturing and product design, see figure 2.2.

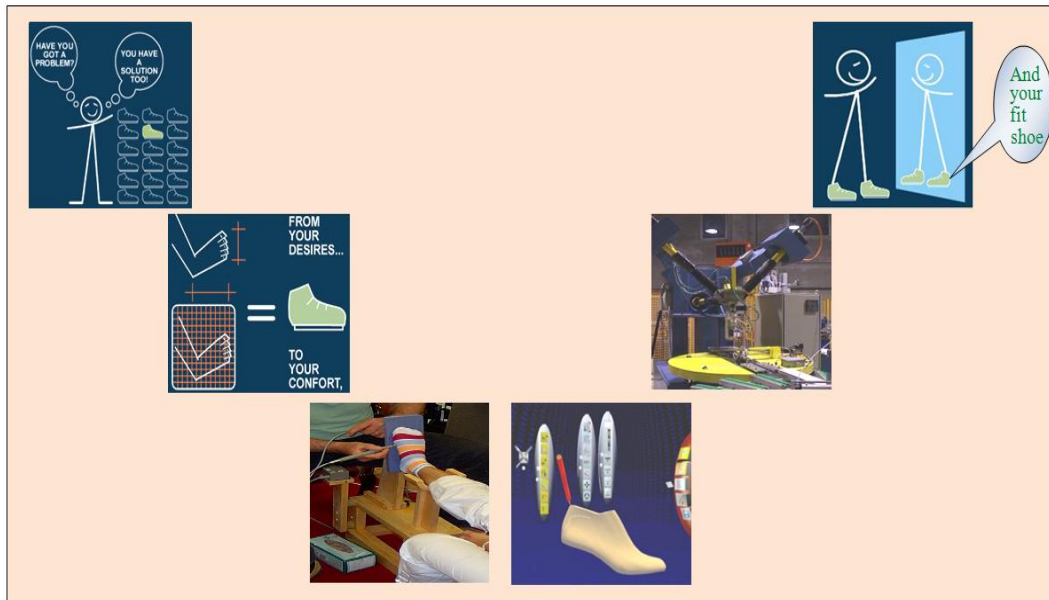


Figure 2.2: Footwear customization

2.7 Foot shape and shoe last

2.7.1 Foot shape

The human foot is an unsymmetrical object that has great flexibility and it supports the body and helps us to keep balance and to move forward or backward. There are 26 bones in each foot. The top view of foot bones is illustrated in Figure 2.3. In terms of functions, the foot bones can be categorized into three groups: the malleolus bones, the metatarsal bones and the phalanges. The malleolus bones are also called the tarsal bones, which are located at the back part of foot.

- **Ectomorph:** tall, slender, long-boned, slim-muscled.
- **Mesomorph:** stocky, muscular, heavy-boned.
- **Endomorph:** fleshy, plump, small-boned, fatty.

Nobodys physical shape is entirely any one of the above categories, but is usually a combination of all three, one type in the combination is dominant. Since, the foot type is in the same category as the body type, some of the subject demographic may play an important role when attempting to understand foot shape.

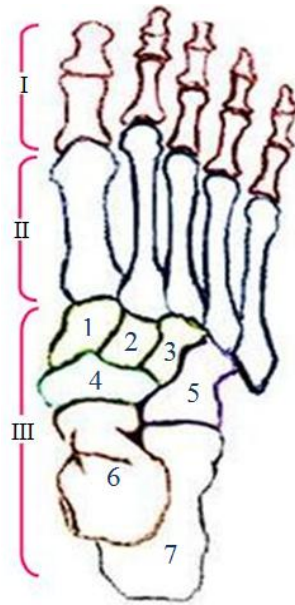


Figure 2.3: I) Phalanges. II) Metatarsals. III) Malleolus; tarsal 1) inner, 2) middle, 3) outer, 4) navicular, 5) cuboid 6) talus, 7) calcaneus

2.7.2 Shoe last

The shoe last is a wooden or metal model of human foot on which shoes are shaped. The design of new shoe last mainly determines the shoe shape, fashion, fit and comfort qualities [21, 22]. "A good last for shoe production has the same importance as a good foundation for a stability of a house" [23]. The last furnishes support and protection to the foot if properly constructed [24]. The key steps in the manufacture of a shoe last are:

- Data related to the foot, shoe fabrication materials, style, comfort and

type of construction should be collected.

- According to above data and the last maker's knowledge the last will be designed.
- A rough model according to design parameters will be made.
- The rough model turns into a finished last.
- To check the finished last if it is of the required dimensions.

Shoes are subordinate to the feet and are bound to protect them. As the mold for shoe making, the shoe last should be designed in accordance to the foot shape. A thorough understanding of the foot structure and its biomechanical characteristics is important for foot measurement, last design, and shoemaking. The foot shoe last triangle are introduced in figure 2.4.



Figure 2.4: Foot Shoe last triangle

2.8 Footwear comfort and fit

The importance of product compatibility for comfort and satisfaction is well known. Fit is considered to be very importance since mis-fitting shoes

are generally the major cause of foot related illnesses and injuries. Properly fitting footwear are important in avoiding foot discomfort, deforming and are essential in patient with arthritis, diabetes, and other foot disorders. For instance Hallux Valgus, Ankle Valgus and lesions (Chilblains, blisters, Corns, Calluses) are some of the foot deformation related to footwear [49]. Hallux Valgus is associated with abnormal pressure at the metatarsophalangeal joints (MPJ) of the great toe and is caused by footwear that is too narrow. The joint separation is enlarged and there may be inflammation of bursa at joint. Moreover the first metatarsal may be deflected away from the other metatarsals when the first toe overlap or underlie the second toe and bursa can be inflamed and then it is known as bunion.

The footwear squeezes the toes together. Ankle Valgus may not be painful in itself but it is caused by the inward rotation (toward the medial sides) of the back of foot such that the body weight falls on the inner side of the foot. In this case the arch apparently flattens. The condition is self-aggravating, since the more the foot twists the more the weight falls on the inner side of the foot.

Callouses, corns, blisters and chilblains belong to the deformities known as lesions. When there is intermittent pressure at some part of the foot Callouses will be occurred and this causes the outer skin to thicken and become hard. However, when the Callouses are under pressure pain and burning sensation will happen.

Friction associated with localized pressure causes Corns occur over toe joints. Blisters are caused by friction, when the outer skin becomes loose and fluid collects beneath it. If the friction continues, the blister breaks causing an inflamed area. This occurs normally at the back of heel due to heel slip. Chilblains are caused due to pressure normally at the back of heel in cold weather.

When the dimensional differences are comparatively large the shoe can be

either tight or loose depending upon the relative location of foot with that of the shoe. Loose shoes (even though function may be impaired) are not as uncomfortable as when the shoes are tight. When the shoe is tight, the pressure and force will produce compression which may result in discomfort, pain or injury. On the other hand, loose shoe causes discomfort, pain or even injury due to the friction between the shoe and foot. Thereby, ill-fitting shoes are generally associated with injuries and foot deformities [30,31,32] and by improving footwear fit stretching of the upper material will be reduced [33]. Thus properly constructed footwear may provide the right pressure and force at the different locations on the foot surface, and this may result in improved comfort, fit and foot health.

2.9 Footwear research

The issue of good shoe fit was posed as early as 1500 B.C. in "Ebers Papyrus". Researcher at the beginning gave attention on the relationships between biomechanical variable and the kinematics analysis of foot [108]. Most of the initial work was done on running, typical idea was that sport shoes should be built to reduce impact loading and to control (\approx reduce) foot and to guide take-off inversion. It was suggested that these functions would reduce movement-related injuries.

Researchers results and their tests were responsible for sport shoes that were developed into relatively bulky constructions with rigid heel counter, stiff heel stabilizers and wide lateral heel wedges, which may have been responsible for new problems and injuries.

In 1964 the anthropometric research in Taiwan organized several investigation regarding length and width of foot. From 1980 to 1982 [74], China organized several research about relationship between various features of

the foot, sole design and the size specification of the shoe last.

From 1982 to 1986 the main research topic included marketing research, function and quality study of sport swears and particularly, the static and dynamic tests and analysis of the foot. From 1986 to 1990, measurement techniques were improved but the measurement items seemed Not to be adequate.

A study on the incidence of fitting problems in footwear found that, for both men and women, tight fit was a problem in 22% of the items reported, width in 20%, narrow toes in 19%, arches in 14%, and sloppy fit in 9% [12]. Length was not a problem except for those people with very short or very long feet.

Unlike any other consumer product, personalized footwear or the matching of footwear to feet is not easy if delivery of comfortable shoes is to be the ultimate goal, even though footwear related discomfort is predominantly caused by localized pressure induced by a shoe that has a design unsuitable for that particular shape of foot.

The design of shoe last, which represents approximate shape of human foot is the "heart" of shoemaking because it mainly determines the foot shape, fit and comfort qualities. Because of the complexity and the constraints imposed by the footwear manufacturing process, most importantly, the last manufacturing process, the custom footwear is expensive to produce.

In traditional manufacturing, the device such as the Ritz Stick device [85], the Brannock device [8], the Scholl device [40], caliper and tape are always used for measurement of foot dimensions.

The process of foot measuring and making an accurate customer shoe last was always complicated and time consuming because the shoe maker must manually measure the specific consumer's foot and the last manufactured by last maker experience.

Nowadays, with development of 3D acquisition devices, automatic process,

producing custom-tailored footwear is reasonable, if the custom last can be automatically produced based on consumer's foot shape. There are already some approaches in literature [35, 73, 63]. The typical suggestion coming from literature is selecting a shoe last from a shoe last data base or deforming it into one that fits the scanned foot data. Authors in [87], quantify footwear fit and predict the fit-related comfort with colourcode mismatch between human foot and shoe last. Li and Jneja [35], suggested to store front and back part of shoe last separately, to generate smooth surface between two given disjointed surfaces of the front and rear parts of the shoe last to obtain the new shoe last. This method is helpful for companies which already maintain library of last rear parts, so they need only front parts of last shapes to be designed as fashion suggests. However, this method for custom tailored footwear designing is not very accurate because the consumers feet may change from time to time.

Chapter 3

Reconstruction of 3D model from 3D scanning data

3.1 Introduction

The problem of creating a CAD model for an existing physical object from a given set of points of the surface is important in many fields of science and industry. There are many methods available for solution of this problem. These methods are based on a great variety of principles, and have various properties, that in many cases allows choosing the most suitable algorithm for a given task.

In order to reconstruct complete 3D shape of object/scene, whole range data of the surface should be acquire in advance. Many types of range finders used for surface reconstruction are based on stereoscopic vision [13], laser scanning [51], time-of-flight laser [3], pattern projection [91]. Due to occlusions and limitation to field of view of the sensors the entire object can not capture at once. There for, in order to acquire whole range data of the surface, multiple range images which are represented different parts of the same object are fused. In order to register multiple images, Euclidean motion between views must be determined. After solving registration problem, the data must fuse into single shape, e.g., a dense triangle

mesh for further processing [92].

3.2 Acquisition Techniques

Fast, inexpensive and accurate 3D acquisition systems has evolved considerably in the last few years. Depending on the technique used the output of a scanning process can be simply a set of points, unstructured data, profile, range image or volumetric output (structured data), figure 3.1, is shown different output of scanning process. Many different systems have

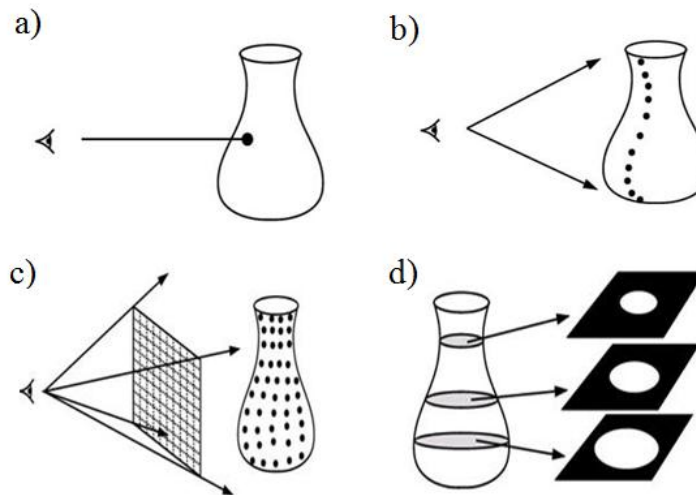


Figure 3.1: Out of a scanning process. a) Point. b) Profile. c) Range image. d) Volumetric output

been proposed; a common characterization subdivides them into contact and non-contact devices. An important subclass of the latter is one based on the adoption of optical technology, and it can be further subdivided into active and passive approaches, see figure 3.2.

3.2.1 Practical problems of data acquisition

There are many practical problems with acquiring useable data, the major ones being:

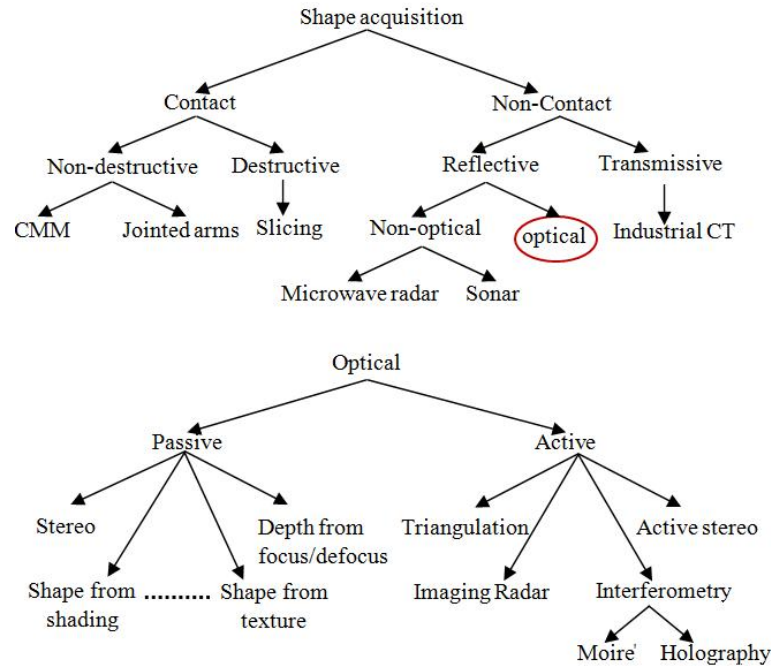


Figure 3.2: The classification of the surveyed acquisition methods

- Calibration.
- Accuracy.
- Accessibility.
- Occlusion.
- Fixturing.
- Multiple views.
- Noise and incomplete data.
- Statistical distribution of parts.
- Surface finish.

Calibration is an essential part of setting up and operating a position measuring device. Systematic sensing errors can occur through lens distortions, non-linear electronics in cameras, and similar sources. Most of the papers

cited present some discussion of accuracy ranges for the various types of scanners, but all methods of data acquisition require accurate calibration. Optical scanners' accuracies typically depend largely on the resolution of the video system used. Distance from the measured surface and accuracy of the moving parts of the scanning system all contribute to the overall measurement error.

Accessibility is the issue of scanning data that is not easily acquired due to the configuration or topology of the part. This usually requires multiple scans but can also make some data impossible to acquire with certain methods. Through holes are typical examples of inaccessible surfaces.

Occlusion is the blocking of the scanning medium due to shadowing or obstruction. This is primarily a problem with optical scanners. However, acoustic and magnetic scanners may also have this problem. Multiple scanning devices are one approach to obviate this problem. As well as self-occlusion, occlusion may also arise due to fixturing/typically parts must be clamped before scanning.

The geometry of the fixtures becomes a part of the scan data. Elimination of fixture data is difficult and often requires multiple views. Multiple views introduce errors in acquired data because of registration problems. Noise elimination in data samples is a difficult issue. Noise can be introduced in a multitude of ways, from extraneous vibrations, specular reflections, etc. There are many different filtering approaches that can be used. An important question is whether to eliminate the noise before, after, or during the model building stage. There are times when the noise should not be eliminated at all. Noise filtering, though, is often an unavoidable step in reverse engineering, but note, that this also destroys the "sharpness" of the data i.e. typically sharp edges disappear and are replaced by smooth blends, which in some cases may be desirable, but in other cases may lead to serious problems in identifying features [7]

A similar problem is restoration of missing data. This is partly necessary due to the above mentioned inaccessibility and occlusion problems. Moreover, because of the nature of optical and even tactile scanning, the data close to sharp edges is also fairly unreliable. Finally there are situations where only parts of a certain surface can be measured, there are missing parts or parts obscured by other elements, but we need to reconstruct the whole surface from just the visible parts.

Statistical distribution of parts deals with the fact that any given part which is scanned only represents one sample in a distributed population. When reverse engineering methods attempt to reproduce a given shape, the tolerance distribution of the scanned part must be considered. This gives rise to multiple part scans and the averaging of the resulting data. However, it may be somewhat impractical to attempt to sample many parts from a population, and indeed, often only one is available.

The final issue we bring up is surface finish of the part being measured. Smoothness and material coatings can dramatically affect the data acquisition process. Tactile or optical methods will produce more noise with a rough surface than a smooth one. Reflective coatings also can affect optical methods. When scanning human faces noise is often introduced when the light reflects of the eye or spectacles. Hair is an example of a rough surface which presents very difficult problems in scanning.

Imagine an ideal scanner: the object is 'floating' in 3D space, so it is accessible from all directions. The data is captured in one coordinate system with high accuracy, with no need for noise filtering and registration. Possibly, the measurement is adaptive, i.e. more points are collected at highly curved surface portions, etc.

3.2.2 Contact-Based Acquisitions

Acquisition based on contact is performed by touching the object on each relevant side. Recently, the use of contact-based technique has been limited due to the concerns arising when dealing with fragile or precious objects such as artifacts. These technologies have a number of disadvantages such as deforming the object during operations, errors in the estimations of the shape, not providing information on the object appearance. Moreover, this group of techniques are very slow. Contact-based techniques can be further classified into two main groups: destructive techniques, including slicing, and non-destructive techniques, like Jointed arms and Coordinate-measuring machine(CMM), see figure 3.3.



Figure 3.3: Example of contact based system

3.2.3 Contactless Acquisitions

Contactless acquisition, is performed through indirect techniques based on the a given energy source. Digital camera or special sensors are used to measure the return signal. This group of techniques have some advantages. In fact the shape can obtained in the present of delicate objects, hot environment, large scene, deformable objects, etc. Optical - and laser-based technologies are the most used in this class. This class of technique

can be further classified in two main groups, reflective and transmissive techniques.

Transmissive technologies are based computer tomography. This method is based on X-rays, is widely used in medical imaging. Other Transmissive scanners are based on time of flight lasers, is used in long distance measurement such as hundreds of meters or many kilometers. Non-optical techniques, such as sonars or microwave radars, are mainly used in robotics. Additionally, optical techniques can be sub-divided into two types, passive sensors and active sensors.

3.2.3.1 Passive scanners

In passive vision technique, no energy is emitted but instead rely on detecting the radiation reflected by objects. This scanner are simple to use because they do not need any special hardware. On the contrary, the quality and accuracy of the produced model can be quite low.

Such passive technique include shape from-X, where X represents the method used to determine the shape, such as: stereo, shading, texture, depth from focus/defocus, among others. 3D information recovery from only a single 2D image is difficulty of its group and it forms an ill-posed problem. The table 3.1, below, gives an overview of shape from X methods.

Stereo vision techniques

Stereo vision (or "stereopsis") is the process of recovering the *three – dimensional* location of points in the scene from their projection in the images. More precisely, if we have two images I_l and I_r (left and right from the left and right eyes), given a pixel p_l in the left image and the corresponding pixel p_r in the right image, then the coordinates (X,Y,Z) of

Shape from	How many images	Method type
Stereo	2 or more	Passive
Motion	A sequence	Active/Passive
Focus/Defocus	2 or more	Active
Zoom	2 or more	Active
Contours	Single	Passive
Texture	Single	Passive
Shading	Single	Passive

Table 3.1: *Shape – from – X* methods and their classification

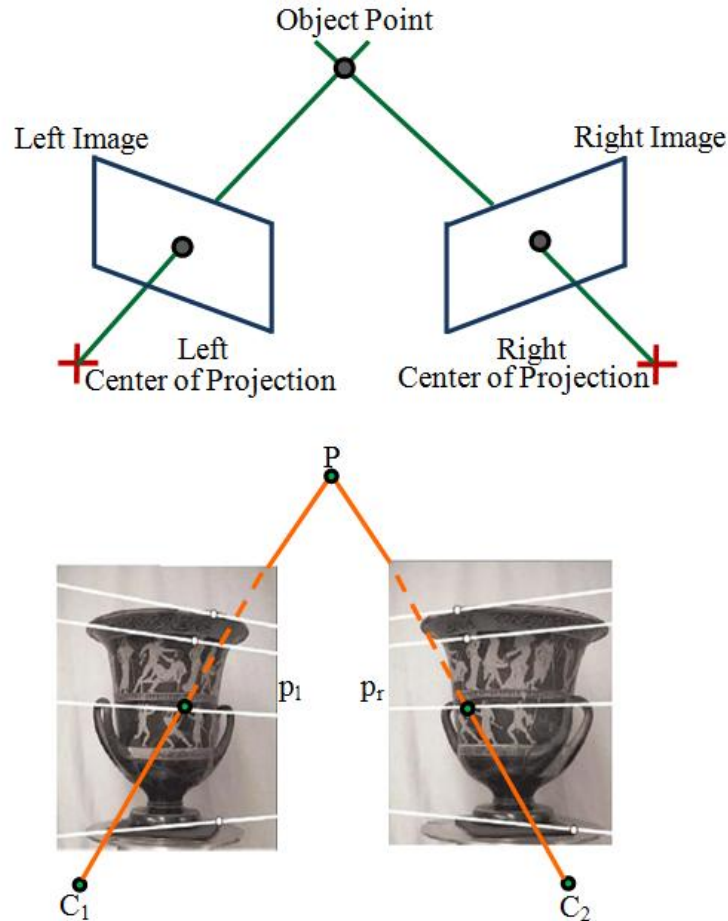
the corresponding point in space is computed.

Geometrically, given p_l , we know that the point P lies on the line L_l joining p_l and the left optical center C_l (this line is the viewing ray), although we don't know the distance along this line. Similarly, we know that P lies along a line L_r joining p_r and P. Assuming we know exactly the parameters of the cameras (intrinsic and extrinsic), we can explicitly compute the parameter of L_l and L_r . Therefore, we can compute the intersection of the two lines, which is the point P, see figure 3.4. This procedure is called triangulation. Thus stereovision involves two problems:

- Correspondences: Given a point p_1 in one image, find the corresponding point in the other image.
- Reconstruction: Given a correspondence (p_l, p_r) , compute the 3 – D coordinates of the corresponding point in space, P.

Shape from texture

Shape from texture is a computer vision technique where a 3D object is reconstructed from a 2D image. The first person who proposed that a shape can be perceived from a texture was Gibson in 1950 [54]. Gibson used the term texture gradient in order to denote that areas of a surface

Figure 3.4: *StereoVision = Correspondences + Reconstruction*

that have similar texture, with other neighbor areas, are perceived differently from the observer due to differences in orientation of the surfaces and the distance from the observer. In order to measure the orientation of the texels in a texture, we need to find the slant and tilt angles. Slant denotes the amount and tilt denotes the direction of the slope of the planar surface projected on the image plane. In figure 3.5 the angle ρ between z_s and z_i is the slant angle while the angle τ between X_i and the projection of the surface normal Z_S onto the image plane is the tilt angle.

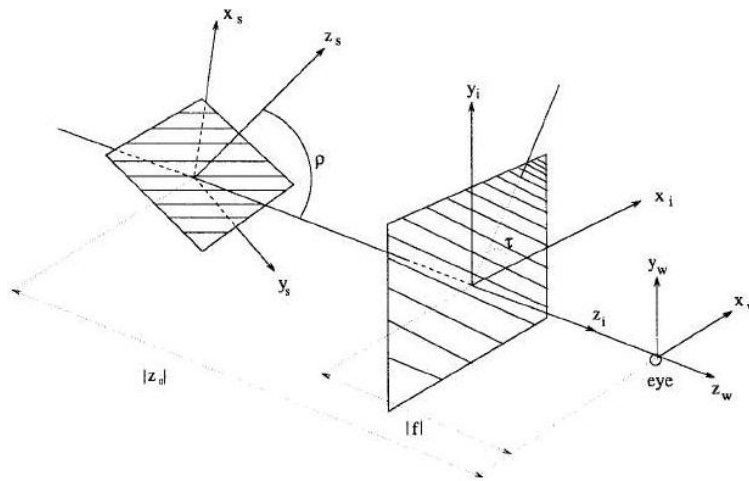


Figure 3.5: Coordinate relationship between the image plane and the surface plane

3.2.3.2 Active scanners

Scanner based on triangulation

Where the object geometry is reconstructed by the use of three information: the pattern emission direction and the relative positions of both source and sensor. Either laser sources or light sources can be used as pattern emission sources. These systems reach a good level of accuracy, measuring many points in a small area and returning a 3D points cloud (x, y, z coordinates). Triangulation scanner usually have shading problem, due to the separation of light source and detector, parts of non-convex objects may not be reach by light from the projector or may not be seen by the detector . Thus triangulation scanner usually have shading problems. The basic geometry for an active triangulation system is shown in Figure 3.6. A light projector is placed at a distance b (called baseline) from the centre of projection of a pin-hole camera. The centre of projection is the origin of the reference frame XYZ , in which all the sensor's measurements are expressed. The Z axis and the camera's optical axis coincide. The y and Y , and x and X axes are respectively parallel but point in opposite directions.

Let f be the focal length. The projector emits a plane of light perpendicular

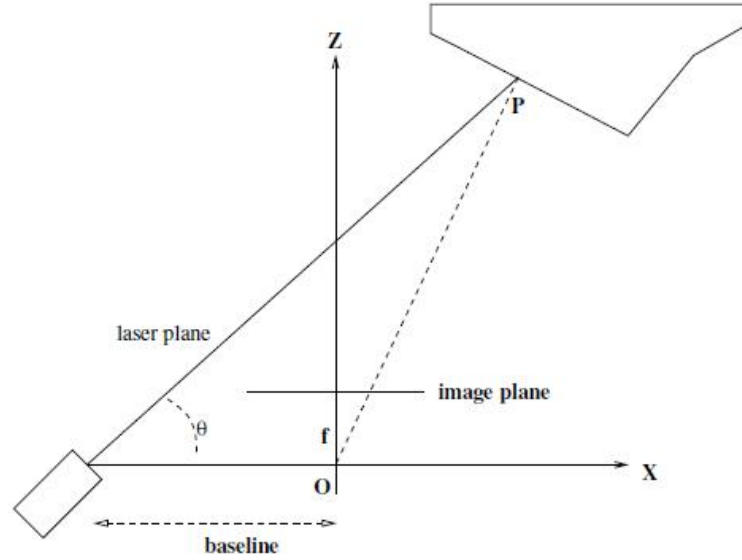


Figure 3.6: The basic geometry of active, optical triangulation (planar XZ view). The Y and y axes are perpendicular to the plane of the figure.

to the plane XZ and forming a controlled angle, θ with the XY plane. The Y axis is parallel to the plane of light and perpendicular to the page, so that only the profile of the plane of light is shown. The intersection of the plane of light with the scene surfaces is a planar curve called the stripe, which is observed by the camera. In this setup, the coordinates of a stripe point $P = [X, Y, Z]^T$ are given by:

$$\begin{bmatrix} x \\ y \\ z \end{bmatrix} = \frac{b}{f \cot \theta - x} \begin{bmatrix} x \\ y \\ z \end{bmatrix} \quad (3.1)$$

Applying this equation to all the visible stripe points, we obtain the 3-D profile of the surface points under the stripe (a cross-section of the surface). We can acquire multiple, adjacent profiles by advancing the object under the stripe, or sweeping the stripe across the object, and repeat the computation for each relative position of stripe and object. The sequence of all profiles is a full range image of the scene.

A slightly different triangulation device, called single point laser scanner do exist. The principle is to project a narrow laser beam (instead of a laser line) on the surface of the object being scanned. The produces a spot on the surface that will be imaged at different position in the CCD array, depending on the range. The 3D position can be recovered using the same triangulation principle as above. Figure 3.7 present different kind of triagualtion scanners.

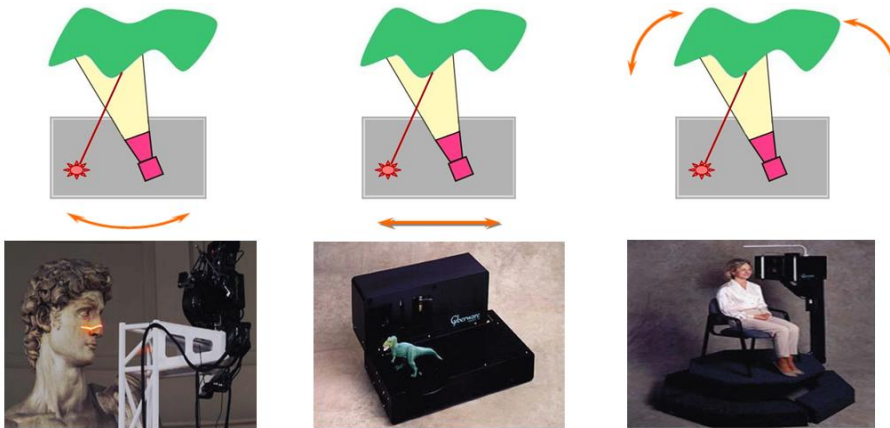


Figure 3.7: Taringualtion: Moveing the camera and Illumination

Imaging radar

Recently a new class of scanning methods, called imaging radar, is becoming popular. This class can be divided in two main sub-classes:

- Time of flight.
- Amplitude modulation.

The basic principle of these sensors is to emit a short electromagnetic or acoustic wave, or pulse, and detect the return (echo) reflected from surrounding surfaces. Distance is obtained as a function of the time taken by the wave to hit a surface and come back, called time of flight, which

is measured directly. By sweeping such a sensor across the target scene, a full range image can be acquired. Different principles are used in imaging laser radars; for instance, such sensors can emit a amplitude-modulated laser beam and measure the phase difference between the transmitted and received signals.

3D scanners based on imaging radar are preferred when scanning large structures [6], as range accuracy is usually relatively constant for the whole volume of measurement. In particular many companies are offering products and services for topographic surveys. The measurements carried with this class of instruments will be affected by drifts and jitter in the electronics, as since these systems require detection of the time light propagates through the air. In the following we give a brief introduction to the two classes of methods, more details can be found in [59].

Time of flight scanner

Time of flight (TOF) technique, computer the distance to the surface by timing the round-trip of the light puls. A laser is used to emit a light puls and the amount of time that passes before the reflected light is seen by the detector is timed. Since the speed of light is known, the round-trip time determines the travel distance of light, which is twice the distance between the scanner and the surface. The advantages of this group of sensors compare to triangulation is included offering greater operation range (up to tens of meters), which is valuable in outdoor navigation tasks. However these scanner speed is considerably slower than triangulation, see figure 3.8.

Amplitude Modulation

Amplitude modulation techniques are based on a continuous laser impulse

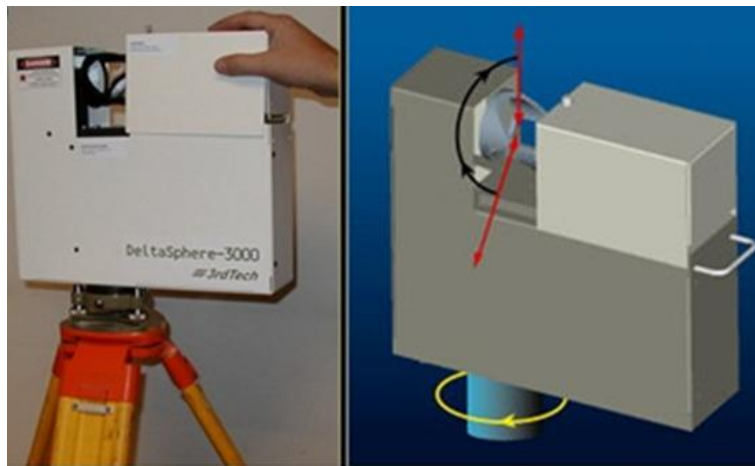


Figure 3.8: Time of flight scanner

that is modulated sinusoidally over the time. After the beam bounces on the object and returns back to the sensor, the signal presents a sinusoidal variation over the time, but out of phase with respect the emitted signal. The roundtrip distance to the object surface is measured by computing the phase difference between the emitted and the reflected power signals. It can be said [15] that amplitude modulation system may offer a better range resolution (0.3 mm), but however it generates an ambiguity interval problem (phase multiple of Π), see Figure 3.9

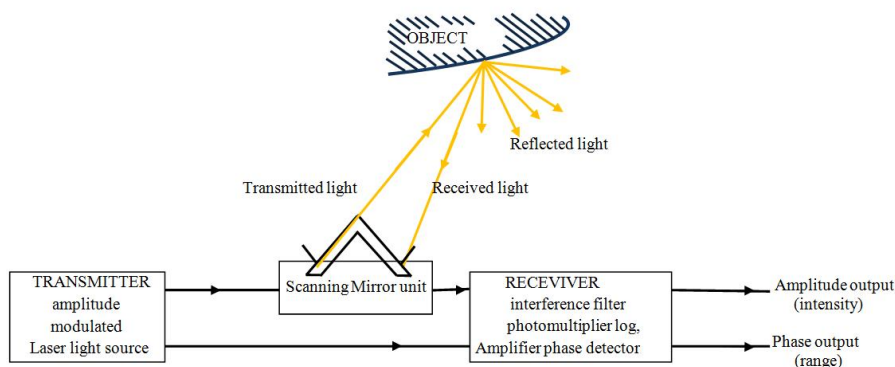


Figure 3.9: A laser range-finder based on amplitude modulation

3.3 Reconstruction of surface from 3D Data Points

There is a wide range of applications for which surface construction from scattered point data is important. In particular, depending on the field of application and the related properties of the data, many algorithms were developed in past. The problem treated in this contribution is Surfaces from scattered point data.

Input. A set P of points in space which are sampled from the surface.

Output. A surface S so that the points of P lie on or close to S .

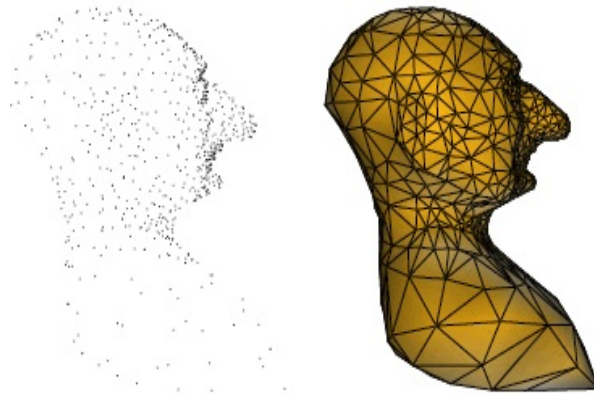


Figure 3.10: The initial point set (left) and the desired reconstruction result (right)

3.3.1 Spatial subdivision

Common to the approaches that can be characterized by "Spatial Subdivision" is that some bounding box of the set P of sampling points is subdivided into disjoint cells. There is a variety of spatial decomposition techniques which were developed for different applications [109]. Typical examples are regular grids, adaptive schemes like octrees, or irregular schemes like tetrahedral meshes. Many of them can also be applied to

surface construction. The goal of construction algorithms based on spatial subdivision is to find cells related to the shape described by P . The selection of the cells can be done in roughly two ways: surface-oriented and volume-oriented.

3.3.1.1 Surface-oriented cell selection

The surface-oriented approach consists of the following basic steps. Surface-oriented cell selection:

- 1- Decompose the space in cells.
- 2- Find those cells that are traversed by the surface.
- 3- Calculate a surface from the selected cells.

The approach of Algorri and Schmitt

An example for surface-oriented cell selection is the algorithm of Algorri and Schmitt [71] figure (3.11). For the first step, the rectangular bounding box of the given data set is subdivided by a regular voxel grid. In the second step, the algorithm extracts those voxels which are occupied by at least one point of the sampling set P . In the third step, the outer quadrilaterals of the selected voxels are taken as a first approximation of the surface. This resembles the cuberille approach of volume visualization [33].

In order to get a more pleasant representation, the surface is transferred into a triangular mesh by diagonally splitting each quadrilateral into two triangles. The cuberille artifacts are smoothed using a depth-pass filter that assigns a new position to each vertex of a triangle. This position is

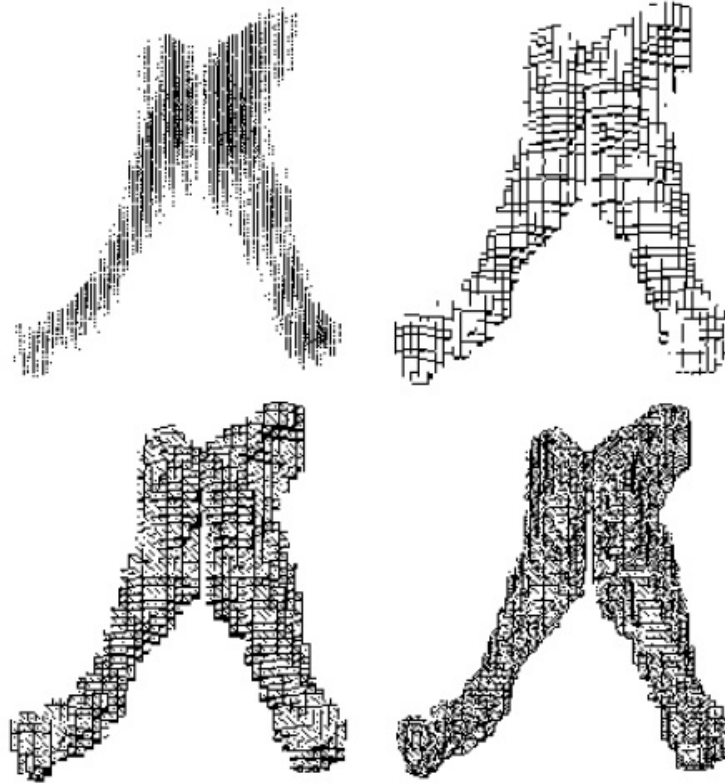


Figure 3.11: The approach of Algorri and Schmitt

computed as the weighted average of its old position and the position of its neighbors. The approximation of the resulting surface is improved by warping it towards the data points.

The approach of Hoppe et al.

Another possibility of surface-oriented cell selection is based on the distance function approach of Hoppe [43, 44, 45](figure3.12). The distance function of the surface of a closed object tells for each point in space its minimum signed distance to the surface. Points on the surface of course have distance 0, whereas points outside the surface have positive, and points inside the surface have negative distance.

The first step of the algorithm again is implemented by a regular voxel grid.

The voxel cells selected in the second step are those which have vertices of opposite sign. Evidently, the surface has to traverse these cells. In the third step, the surface is obtained by the marching cubes algorithm of volume visualization [109]. The marching cubes algorithm defines templates of separating surface patches for each possible configuration of the signs of the distance values at the vertices of a voxel cell. The voxels are replaced with these triangulated patches. The resulting triangular mesh separates the positive and negative distance values on the grid.

A similar algorithm was suggested by Roth and Wibowoo [38]. It differs from the approach of Hoppe et al. Furthermore, the special cases of profile lines and multiple view range data are considered besides scattered point data.

A difficulty with these approaches is the choice of the resolution of the voxel grid. One effect is that gaps may occur in the surface because of troubles of the heuristics of distance function calculation.

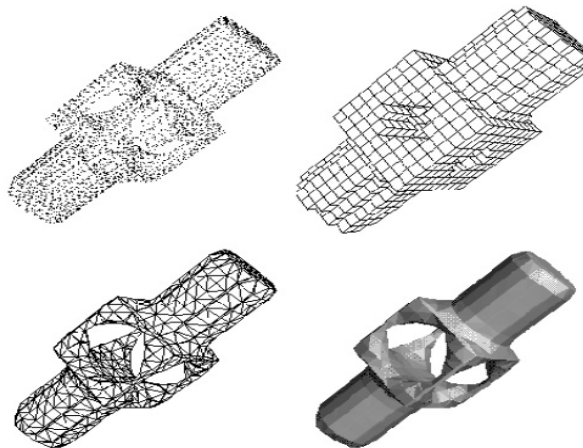


Figure 3.12: The approach of Hoppe et al.

The approach of Bajaj, Bernardini et al.

The approach of Bajaj, Bernardini et al. [10] differs from the previous ones in that spatial decomposition is now irregular and adaptive.

The algorithm also requires a signed distance function. For this purpose, a first approximate surface is calculated in a preprocessing phase. The distance to this surface is used as distance function.

Having the distance function in hand, the space is incrementally decomposed into tetrahedra starting with an initial tetrahedron surrounding the whole data set. By inspecting the signs of the distance function at the vertices, the tetrahedra traversed by the surface are found out. For each of them, an approximation of the traversing surface is calculated. For this purpose, a Bernstein-B'ezier trivariate implicit approximant is used. The approximation error to the given data points is calculated. A bad approximation induces a further refinement of the tetrahedrization. The refinement is performed by incrementally inserting the centers of tetrahedra with high approximation error into the tetrahedrization. The process is iterated until a sufficient approximation is achieved.

In order to keep the shape of the tetrahedra balanced, an incremental tetrahedrization algorithm is used so that the resulting tetrahedrizations always have Delaunay property. A tetrahedrization is said to have the Delaunay property if none of its vertices lies inside the circumscribed sphere of any of its tetrahedron [31].

The resulting surface is composed of trivariate implicit Bernstein-Bezier patches. A C^1 smoothing of the constructed surfaces is obtained by applying a Clough-Tocher subdivision scheme.

In Bernardini et al. [26] an extension and modification of this algorithm is formulated [11, 25]. The algorithm consists of an additional mesh simplification step to reduce the complexity of the mesh represented by the α -solid [9]. The reduced mesh is used in the last step of the algorithm for polynomial-patch data fitting using Bernstein-Bezier patches for each

triangle (by interpolating the vertices and normals and by approximating data points in its neighborhood). Additionally, the representation of sharp features can be achieved in the resulting surface.

Edelsbrunner's and Mcke's Alpha-shapes

Edelsbrunner and Mcke [42, 41] also use an irregular spatial decomposition. In contrast to the previous ones, the given sample points are part of the subdivision. The decomposition chosen for that purpose is the Delaunay tetrahedrization of the given set P of sampling points. A tetrahedrization of a set P of spatial points is a decomposition of the convex hull of P into tetrahedra so that all vertices of the tetrahedra are points in P . A tetrahedrization is a Delaunay tetrahedrization if none of the points of P lies inside the circumsphere of a tetrahedron. It is well known that each finite point set has a Delaunay tetrahedrization which can be calculated efficiently [34]. This is the first step of the algorithm.

The second step is to erase tetrahedra, triangles, and edges of the Delaunay tetrahedrization using so-called α -balls as eraser sphere with radius α . Each tetrahedron, triangle, or edge of the tetrahedrization whose corresponding minimum surrounding sphere does not fit into the eraser sphere is eliminated. The resulting so-called α -shape is a collection of points, edges, faces, and tetrahedra.

In the third step, triangles are extracted out of the α -shape which belong to the desired surface, using the following rule. Consider the two possible spheres of radius α through all three points of a triangle of the α -shape. If at least one of these does not contain any other point of the point set, the triangle belongs to the surface.

A problem of this approach is the choice of a suitable α . Since α is a global

parameter the user is not swamped with many open parameters, but the drawback is that a variable point density is not possible without loss of detail in the reconstruction. An example for reconstruction of a body is shown in figure 3.13

Guo et al.[5] also use make of α –*shapes* for surface reconstruction but they propose a so-called visibility algorithm for extracting those triangles out of the α –*shapes* which represent the simplicial surface.

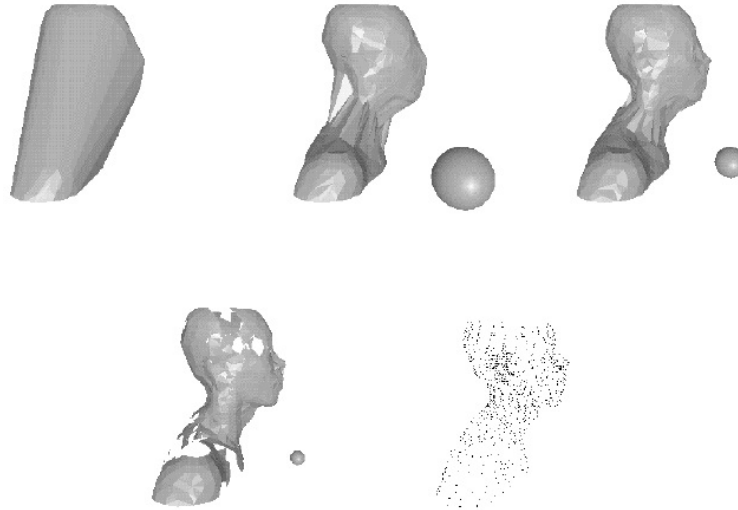


Figure 3.13: An example for a reconstruction of a body. If α is too small, gaps in the surface can occur, or the surface may become fragmented.

Attali's Normalized Meshes

In the approach of Attali [16], the Delaunay tetrahedrization is also used as a basic spatial decomposition. Attali introduces so-called normalized meshes which are contained in the Delaunay graph. It is formed by the edges, faces and tetrahedra whose dual Voronoi element intersects the surface of the object.

In two dimensions, the normalized mesh of a curve c consists of all edges between pairs of points of the given set P of sampling points on c which

induce an edge of the Voronoi diagram of P that intersects c . The nice property of normalized meshes is that for a wide class of curves of bounded curvature, the so-called r -regular shapes, a bound on the sampling density can be given within which the normalized mesh retains all the topological properties of the original curve.

For reconstruction of c , the edges belonging to the reconstructed mesh are obtained by considering the angle between the intersections of the two possible circles around a Delaunay edge. The angle between the circles is defined to be the smaller of the two angles between the two tangent planes at one intersection point of the two circles. This characterization is useful because Delaunay discs tend to become tangent to the boundary of the object. The reconstructed mesh consists of all edges whose associated Delaunay discs have an angle smaller than $\frac{\pi}{2}$. If the sampling density is sufficiently high, the reconstructed mesh is equal to the normalized mesh. While in two dimensions the normalized mesh is a correct reconstruction of shapes having the property of r -regularity, the immediate extension to three dimensions is not possible. The reason for that is that some Delaunay spheres can intersect the surface without being approximately tangent to it. Therefore, the normalized mesh in three dimensions does not contain all faces of the surface.

To overcome this problem, two different heuristics for filling the gaps in the surface structure were introduced.

The first heuristic is to triangulate the border of a gap in the triangular mesh by considering only triangles contained in the Delaunay tetrahedrization.

The second heuristic is volume based. It merges Delaunay tetrahedra to build up the possibly different solids represented in the point set. The set of mergeable solids is initialized with the Delaunay tetrahedra and the complement of the convex hull. The merging step is performed by pro-

cessing the Delaunay triangles according to decreasing diameters. If the current triangle separates two different solids in the set of mergable solids, they are merged if the following holds:

- No triangle from the normalized mesh disappears;
- Merging will not isolate sample points inside the union of these objects, i.e. the sample points have to remain on the boundary of at least one object.

The surface finally yielded by the algorithm is formed by the boundary of the resulting solids.

Weller's approach of Stable Voronoi Edges

Let P be a finite set of points in the plane. P' is an ε -perturbation of P if $d(p_i, p_i') < \varepsilon$ holds for all $p_i \in P, p_i' \in P', i = 1, \dots, n$. An edge p_i', p_j' of the Delaunay triangulation is called stable if the perturbed endpoints p_i', p_j' are also connected by an edge of the Delaunay triangulation of the perturbed point set P' .

It turns out that for intuitively reasonably sampled curves in the plane, the stable edges usually are the edges connecting two consecutive sampling points on the curve, whereas the edges connecting non-neighboring sampling points are unstable. The stability of an edge can be checked in time $O(\text{Voronoi neighbors})$ [24].

The extension of this approach to 3D-surfaces shows that large areas of a surface can usually be reconstructed correctly, but still not sufficiently approximated regions do exist. This resembles the experience reported by Attali [16]. Further research is necessary in order to make stability useful for surface construction.

3.3.1.2 Volume-Oriented Cell Selection

Volume-oriented cell selection also consists of three steps which at a first glance are quite similar to those of surface-oriented selection:

Volume-oriented cell selection:

- 1- Decompose the space in cells.
- 2- Remove those cells that do not belong to the volume bounded by the sampled surface.
- 3- Calculate a surface from the selected cells.

The difference is that a volume representation, in contrast to a surface representation, is obtained.

Most implementations of volume-oriented cell selection are based on the Delaunay tetrahedrization of the given set P of sampling points. The algorithms presented in the following differ in how volume-based selection is performed. Some algorithms eliminate tetrahedrons expected outside the desired solid, until a description of the solid is achieved [48, 29, 89]. Another methodology is the use of the Voronoi diagram to describe the constructed solid by a "skeleton" [105, 16].

Boissonnat's Volume-Oriented Approach

Boissonnat's volume-oriented approach starts with the Delaunay triangulation of the given set P of sampling points. From this triangulation of the convex hull, tetrahedra having particular properties are successively removed. First of all, only tetrahedra with two faces, five edges and four points or one face, three edges and three points on the boundary of the current polyhedron are eliminated. Because of this elimination rule only objects without holes can be reconstructed, see figure 3.14.

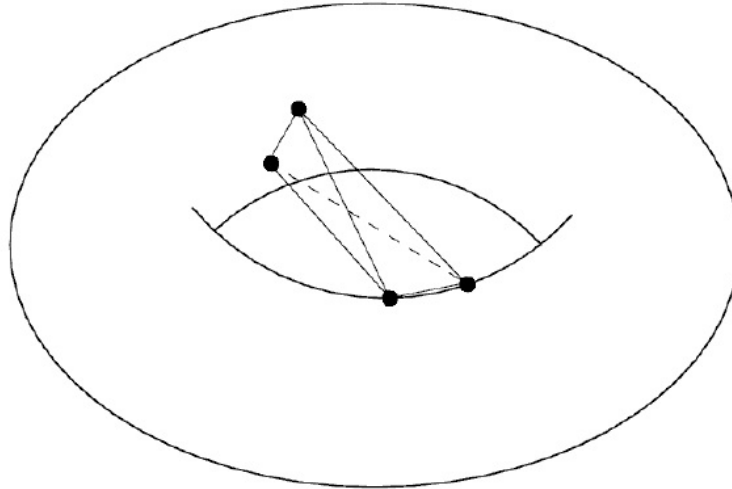


Figure 3.14: Boissonnat's Volume-Oriented Approach

Tetrahedra of this type are iteratively removed according to decreasing decision values. The decision value is the maximum distance of a face of the tetrahedron to its circumsphere. This decision value is useful because flat tetrahedra of the Delaunay tetrahedrization usually tend to be outside the object and cover areas of higher detail. The algorithm stops if all points lie on the surface, or if the deletion of the tetrahedron with highest decision value does not improve the sum taken over the decision values of all tetrahedra incident to the boundary of the polyhedron.

The approach of Isselhard, Brunnett, and Schreiber

The approach of [29] is an improvement of the volume-oriented algorithm of Boissonnat [48]. While Boissonnat cannot handle objects with holes, the deletion procedure of this approach is modified so that construction of holes becomes possible.

As before, the algorithm starts with the Delaunay triangulation of the point set. An incremental tetrahedron deletion procedure is then performed on tetrahedra at the boundary of the polyhedron, as in Boissonnat's algo-

rithm. The difference is that more types of tetrahedra can be removed in order to being able to reconstruct even object with holes. The additionally allowed types of tetrahedra are those with one face and four vertices or three faces or all four faces or on the current surface provided that no point would become isolated through their elimination.

The elimination process is controlled by observing an elimination function. The elimination function is defined as the maximum decision value (in the sense of Boissonnat) of the remaining removable tetrahedra. In this function, several significant jumps can be noticed. One of these jumps is expected to indicate that the desired shape is reached. In practice, the jump before the stabilization of the function on a higher level is the one which is taken. This stopping point helps handling different point densities in the point set which would lead to undesired holes through the extended type set of removable tetrahedra in comparison to Boissonnat's algorithm. If all data points are already on the surface, the algorithm stops. If not, more tetrahedra are eliminated to recover sharp edges (reflex edges) of the object. For that purpose the elimination rules are restricted to those of Boissonnat, assuming that all holes present in the data set have been recovered at this stage. Additionally, the decision value of the tetrahedra is scaled by the radius of the circumscribed sphere as a measure for the size of the tetrahedron. In this way, the cost of small tetrahedra is increased which are more likely to be in regions of reflex edges than big ones. The elimination continues until all data points are on the surface and the elimination function does not decrease anymore, see figure 3.15.

The Υ -indicator approach of Veltkamp

To describe the method of Veltkamp [89, 90] some terminology is required. A Υ -indicator is a value associated to a sphere through three boundary

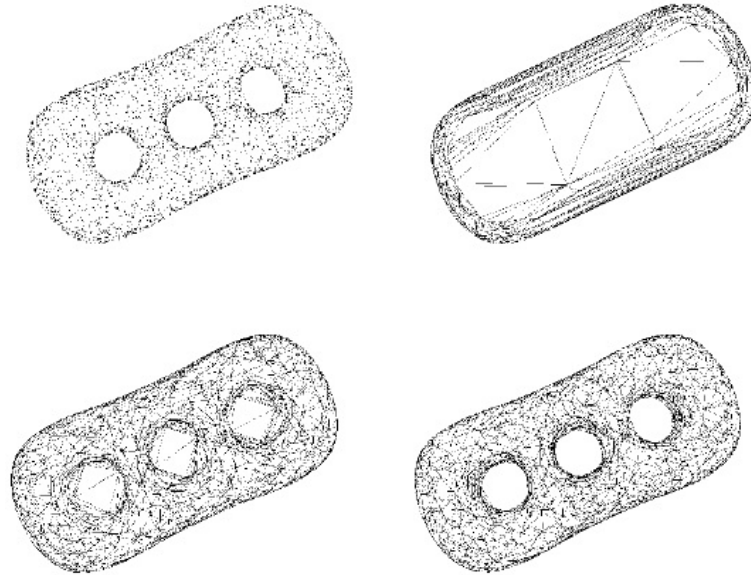
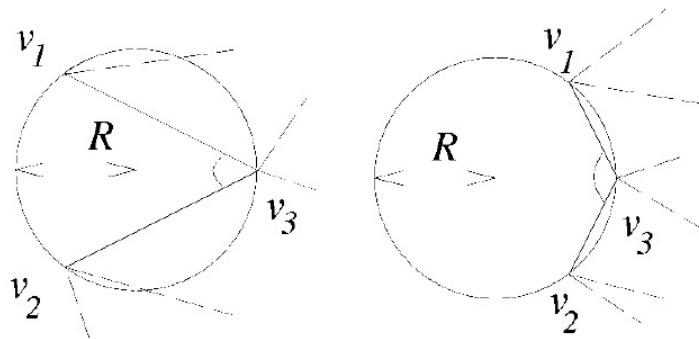


Figure 3.15: An example point set and the deletion process.

points of a polyhedron which is positive or negative, see figure 3.16 for an illustration of the 2D-case. Its absolute value is computed as $1 - \frac{r}{R}$, where r is the circle for the boundary triangle and R the radius of the boundary tetrahedron. It is taken to be negative if the center of the sphere is on the inner side and positive if the center is on the outer side of the polyhedron. Note, that the Υ -indicator is independent of the size of the boundary triangle (tetrahedron, respectively). Therefore, it adapts to areas of changing point density. A removable face is a face with positive Υ -indicator value.

Figure 3.16: A Υ -indicator is a value associated to a sphere through three boundary points of a polyhedron which is positive or negative for an illustration of the 2D-case

The first step of the algorithm is to calculate the Delaunay tetrahedrization.

In the second step, a heap is filled with removable tetrahedra which are sorted according to their Υ -indicator value. The removable tetrahedra are of the same boundary types as in Boissonnat's volume-oriented approach [48]. The tetrahedron with the largest Υ -indicator value is removed and the boundary is updated. This process continues until all points lie on the boundary, or there are no further removable tetrahedra. The main advantage of this algorithm is the adaption of the Υ -indicator value to variable point density. Like Boissonnat's approach, the algorithm is restricted to objects without holes. Some intermediate stages during the construction of a surface shown in figure 3.17

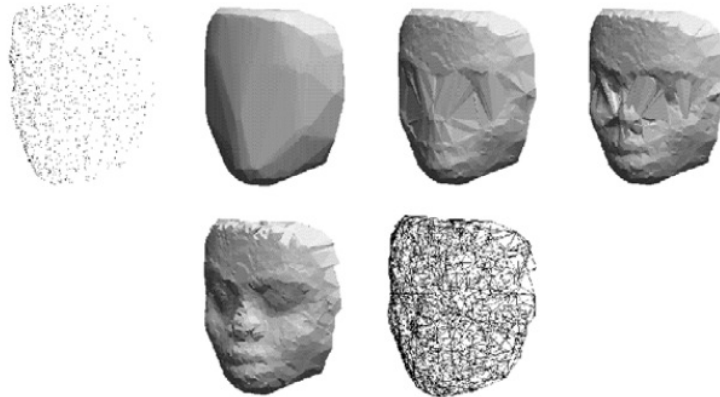


Figure 3.17: Some intermediate stages during the construction of a surface

The Approach of Schreiber and Brunnett

The approach of Schreiber and Brunnett [104, 105] uses properties of the Voronoi diagram of the given point set for tetrahedra removal. The Voronoi diagram of a point set P is a partition of the space in regions of nearest neighborhood. For each point p in P , it contains the region of all points in space that are closer to p than to any other point of P . It is interesting to

note that the Voronoi diagram is dual to the Delaunay tetrahedrization of P . For example, each vertex of the Voronoi diagram corresponds to the center of a tetrahedron of the tetrahedrization. Edges of the Voronoi diagram correspond to neighboring faces of the tetrahedra dual to its vertices. The same observation holds for Voronoi diagrams in the plane that are used in the following for the explanation of the 2D-version of the algorithm.

In the first step, the Delaunay triangulation and the dual Voronoi diagram of P is determined. The second step, the selection of tetrahedra, uses a minimum spanning tree of the Voronoi graph, see figure 3.18 The Voronoi graph is the graph induced by the vertices and edges of the Voronoi diagram. A minimum spanning tree (MST) of a graph is a subtree of the graph which connects all vertices and has minimum summed edge length. Edge length in our case is the Euclidean distance of the two endpoints of the edge.

In the second step, a pruning strategy is applied to it which possibly decomposes it into several disjoint subtrees. Each subtree represents a region defined by the union of the triangles dual to its vertices. Two pruning rules have been developed for that purpose:

- 1- All those edges will be pruned for which no end point is contained in the circumcircle of the dual Delaunay triangle of the other end point.
- 2- An edge will be pruned if its length is shorter than the mean value of the radii of both circumcircles of the dual Delaunay triangles of its voronoi end points.

The number of edges to be pruned can be controlled by using the edge length as a parameter.

The resulting regions are then distinguished into inside and outside. In order to find the inside regions, we add the complement of the convex hull as further region to the set of subtree regions. The algorithm starts

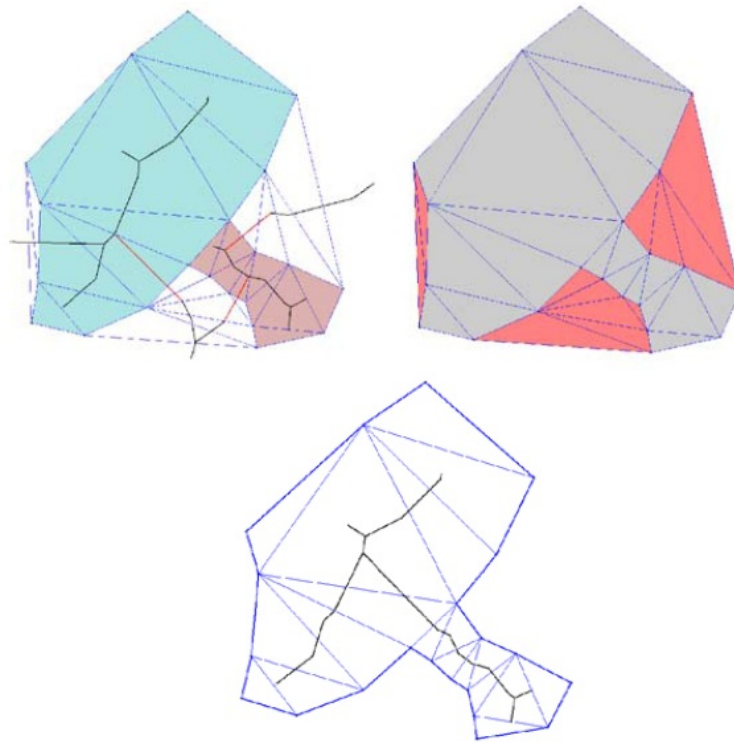


Figure 3.18: The selection of tetrahedra, uses a minimum spanning tree of the Voronoi graph

with a point on the convex hull which is incident to exactly two regions. The region different from the complement of the convex hull is classified "inside". Then the label "inside" is propagated to neighboring regions by again considering points that are incident to exactly two regions.

After all regions have been classified correctly, the boundary of the constructed shape is obtained as the boundary of the union of the region labeled "inside". An adaption of this method to three dimensions is possible.

The α -solids of Bajaj, Bernardini et al.

Bajaj, Bernardini et al. [10, 11, 25, 26] calculate so-called α -solids. While α -shapes are computed by using eraser spheres at every point in space, the eraser spheres are now applied from outside the convex hull, like in

Boissonnat's approach [48]. To overcome the approximation problems inherent to α -shapes a re-sculpturing scheme has been developed. Resculpturing roughly follows the volumetric approach of Boissonnat in that further tetrahedra are removed. This goal is to generate finer structures of the object provided the α -shapes approach has correctly recognized the larger structures of the object.

3.3.2 Surface construction with distance functions

The distance function of a surface gives the shortest distance of any point in space to the surface. For closed surface the distances can be negative or positive, dependent on whether a point lies inside or outside of the volume bounded by the surface. There the question remained open how a distance function can be calculated from the given set P of sample points. Solutions are presented in the next subsection.

Another possibility of calculating a distance function is to construct a surface to the given set P of data points and take the distance to this surface. The idea behind that is that this distance function may be used to get a better surface, for instance a smooth surface as in [10].

Besides marching cubes construction of surfaces, distance plays a major role in construction of surfaces using the medial axis of a volume. The medial axis consists of all points inside the volume for which the maximal sphere inside the volume and centered at this point does not contain the maximal sphere of any other point. Having the medial axis and the radius of the maximum sphere at each of its points, the given object can be represented by the union taken over all spheres centered at the skeleton points with the respective radius.

3.3.2.1 Calculation of Distance Functions

The approach of Hoppe et al.

Hoppe et al. [43, 45] suggest the following approach. At the beginning, for each point p_i an estimated tangent plane is computed. The tangent plane is obtained by fitting the best approximating plane in the least square sense [84] into a certain number k of points in the neighborhood of p_i . In order to get the sign of the distance in the case of close surfaces, a consistent orientation of neighboring tangent planes is determined by computing the Riemannian graph, see figure 3.19. The vertices of the Riemannian graph are the centers of the tangent planes which are defined as the centroids of the k points used to calculate the tangent plane. Two tangent plane centers o_i, o_j are connected by an edge (i, j) if one center is in the k -neighborhood of the other center. By this construction, the edges of the Riemannian graph can be expected to lie close to the sampled surface.

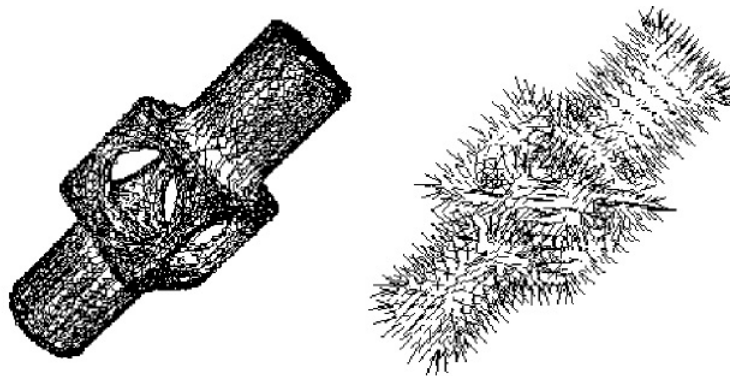


Figure 3.19: A consistent orientation of neighboring tangent planes is determined by computing the Riemannian graph

Each edge is weighted by 1 minus the absolute value of the scalar product between normals of the two tangent plane centers defining the edge. The orientation of the tangent planes is determined by propagating the orientation at a starting point, by traversing the minimum spanning tree

of the resulting weighted Riemannian graph.

Using the tangent plane description of the surface and their correct orientations, the signed distance is computed by first determining the tangent plane center nearest to the query point. The distance between the query point and its projection on the nearest tangent plane. The sign is obtained from the orientation of the tangent plane.

The approach of Roth and Wibowoo to distance functions

The goal of the algorithm of Roth and Wibowoo [38] is to calculate distance values at the vertices of a given voxel grid surrounding the data points. The data points are assigned to the voxel cells into which they fall. An "outer" normal vector is calculated for each data point by finding the closest two neighboring points in the voxel grid, and then using these points along with the original point to compute the normal.

The normal orientation which is required for signed distance calculation is determined as follows. Consider the voxel grid and the six axis directions $(\pm x, \pm y, \pm z)$. If we look from infinity down each axis into the voxel grid, then those voxels that are visible must have their normals point towards the viewing direction. The normal direction is fixed for these visible points. Then the normal direction is propagated to those neighboring voxels whose normals are not fixed by this procedure. This heuristic only works if the nonempty voxel defines a closed boundary without holes.

The value of the signed distance function at a vertex of the voxel grid is computed by taking the weighted average of the signed distances of every point in the eight neighboring voxels. The signed distance to a point with normal is the Euclidean distance to this point, with positive sign if the angle between the normal and the vector towards the voxel vertex exceeds 90° .

3.3.2.2 Bittar's et al. surface construction by medial axes

The approach of Bittar et al. [22] consists of two steps, the calculation of the medial axis and the calculation of an implicit surface from the medial axis.

The medial axis is calculated from a voxelization of a bounding box of the given set of points. The voxels containing points of the given point set P are assumed to be boundary voxels of the solid to be constructed. Starting at the boundary of the bounding box, voxels are successively eliminated until all boundary voxels are on the surface of the remaining voxel volume. A distance function is propagated from the boundary voxels to the inner voxels of the volume, starting with distance 0 on the boundary voxels. The voxels with locally maximal distance value are included to the medial axis. The desired surface is calculated by distributing centers of spheres on the

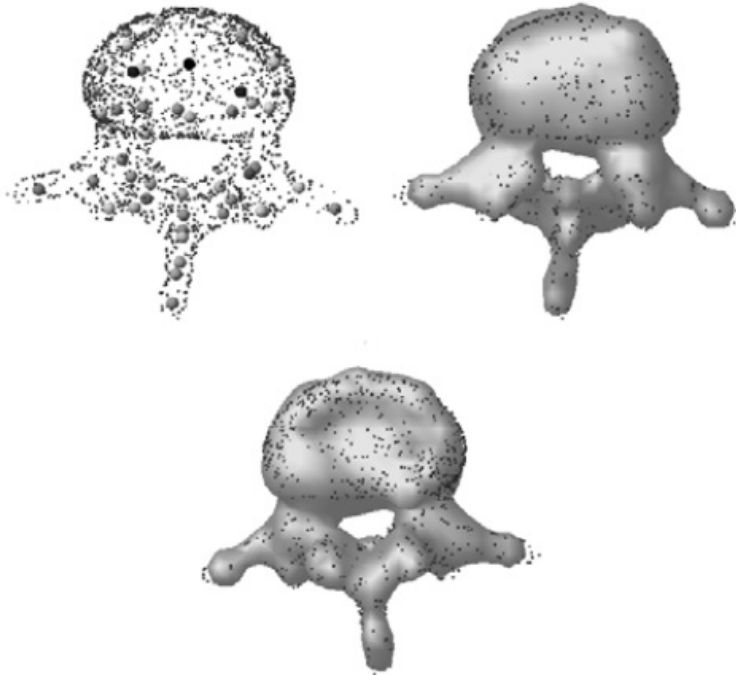


Figure 3.20: The desired surface is calculated by distributing center of sphere on the medial

medial, see figure 3.20. The radius of a sphere is equal to the distance

assigned to its center on the medial axis. For each sphere, a field function is defined which allows to calculate a scalar field value for arbitrary point in space. A field function of the whole set of spheres is obtained as sum of the field functions of all spheres. The implicit surface is defined as an iso-surface of the field function, that is, it consists of all points in space for which the field function has a given constant value.

In order to save computation time, a search strategy is introduced which restricts the calculation of the sum to points with suitable positions. The shape of the resulting surface is strongly influenced by the type of field function. For example, a sharp field function preserves details while a soft function smoothes out the details, figure 3.21. Also the connectness of the resulting solid can be influenced by the shape function, figure F3.22. function smoothes out the details, cf. figure 3.25. Also the connectness of the resulting solid can be influenced by the shape function, see figure 3.22. Because of the voxelization, a crucial point is tuning the resolution of the medial axis. If the resolution of the axis is low, finer details are not represented very accurately. The display of the surface detail is improved if the resolution is increased but can also tend to disconnect parts of the surface if the resolution is higher than the sample density at certain regions.

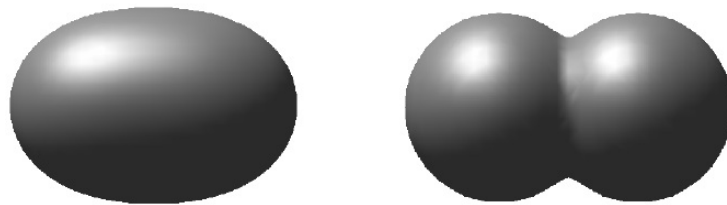


Figure 3.21: A sharp field function preserves details while a soft function smoothes out the details

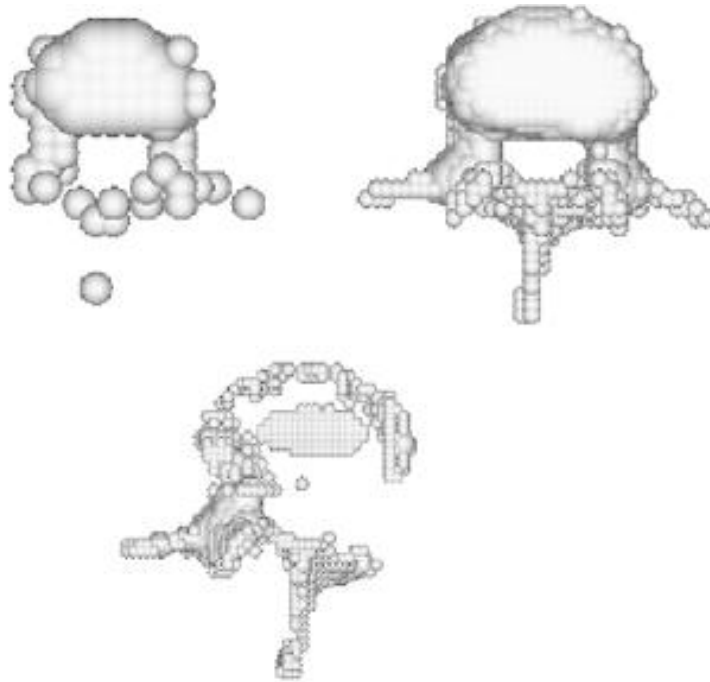


Figure 3.22: The connectness of the resulting solid can be influenced by the shape function

3.3.3 Surface construction by warping

Warping-based surface construction means to deform an initial surface so that it gives a good approximation of the given point set P . For example, let the initial shape be a triangular surface to some or all of its vertices corresponding points in P are determined to which the vertices have to be moved in the warping process. When moving the vertices of the mesh to their new locations, the rest of the mesh is also deformed and yields a surface approximation of the points in P .

Surface construction by warping is particularly suited if a rough approximation of the desired shape is already known. This simplifies detection of corresponding points.

Several methods of describing deformable surfaces were developed in the past. Muraki suggested a "blobby model" to approximate 2.5 D range images [98]. Terzopoulos, Witkin and Kass [21, 20] made use of deformable superquadrics which have to fit the input data points.

Miller et al. [56] extract a topologically closed geometric model from a volume data set. The algorithm starts with a simple model that is already topologically closed and deforms the model on a set of constraints, so that the model grows or shrinks to fit the object within the volume while maintaining it closed and a locally simple non-self-intersecting polyhedron that is either embedded in the object or surrounds the object in the volume data representation. A function is associated with every vertex of the polyhedron that associates costs with local deformation adherent to properties of simple polyhedra, and the relationship between noise and feature. By minimizing these constraints, one achieves an effect similar to inflating a balloon within a container or collapsing a piece of shrink wrap around the object.

A completely different approach to warping is modeling with oriented particles suggested by Szeliski and Tonnesen [88]. Each particle owns several parameters which are updated during the modeling simulation. By modeling the interaction between the particles themselves the surface is being modeled using forces and repulsion. As an extension Szeliski and Tonnesen describe how their algorithm can be extended for automatic 3D reconstruction. At each sample location one particle with appropriate parameters is generated. The gaps between the sample points (particles, respectively) are filled by growing particles away from isolated points and edges. After having a rough approximation of the current surface the other particles are rejected to smooth the surface.

In the following three subsections three approaches are outlined which stand for basically different methodologies, a purely geometric approach, a physical approach, and a computational intelligence approach.

3.3.3.1 Spatial free form warping

The idea of spatial free-form warping is to deform the whole space in which an object to be warped is embedded in, with the effect that the object is warped at the same time. Space deformation is defined by a finite set of displacement vectors consisting of pairs of initial and target point, from which a spatial displacement vector field is interpolated using a scattered data interpolation method. There is a huge number of scattered data interpolation methods known in literature, e.g. [52]. Among them that one can be chosen that yields the most reasonable shape for the particular field of application.

The resulting displacement vector field tells for each point in space its target point. In particular, if the displacement vector field is applied to all vertices of the initial mesh, or of a possibly refined one, the mesh is warped towards the given data points [19].

The advantage of spatial free form warping is that usually only a small number of control displacement vectors located at points with particular features like corners or edges is necessary.

3.3.3.2 The approach of Algorri and Schmitt

The idea of Algorri and Schmitt [71] is to translate given approximate triangular mesh into a physical model, cf. figure 3.23. The vertices of the mesh are interpreted as mass points. The edges are replaced with springs. Each nodal mass of the resulting mesh of springs is attached to its closest point in given set P of sampling points by a further spring. The masses and springs are chosen so that the triangular mesh is deformed towards the data points. The model can be expressed as a linear differential equation of degree 2. This equation is solved iteratively. Efficiency is gained by embedding the data points and the approximate triangular mesh into a

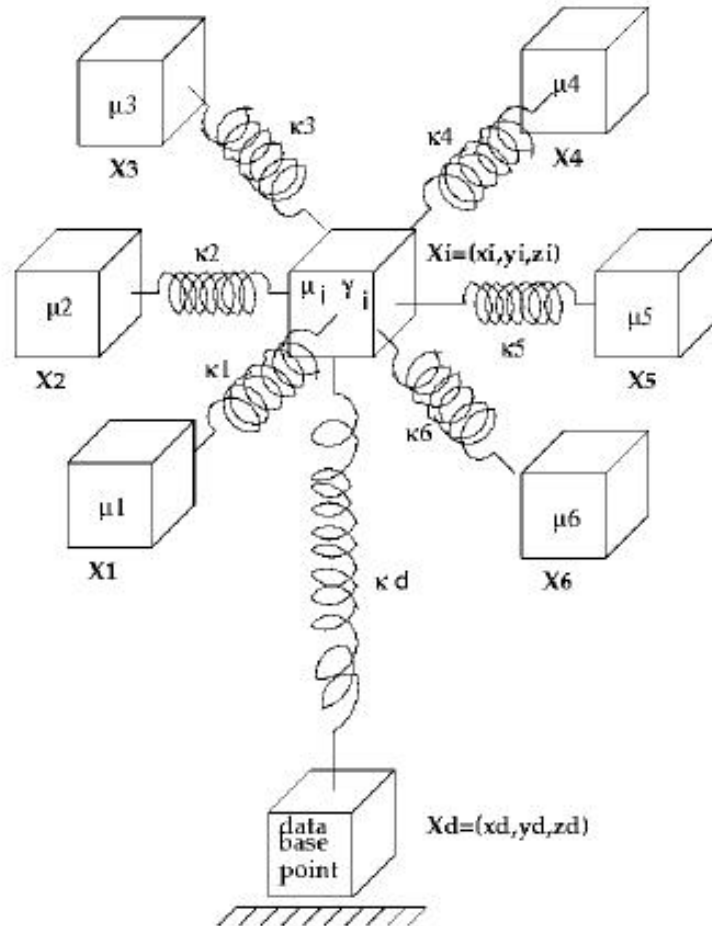


Figure 3.23: The approach of Algorri and Schmitt

regular grid of voxels.

3.3.3.3 Kohonen feature map approach of Baader and Hirzinger

The Kohonen feature map approach of Baader and Hirzinger [1, 2] can be seen as another implementation of the idea of surface construction by warping. Kohonen's feature map is a two-dimensional array of units (neurons), see figure 3.24.

Each unit u_j has a corresponding weight vector \vec{w}_j . In the beginning these vectors are set to normalized random values (of length equal

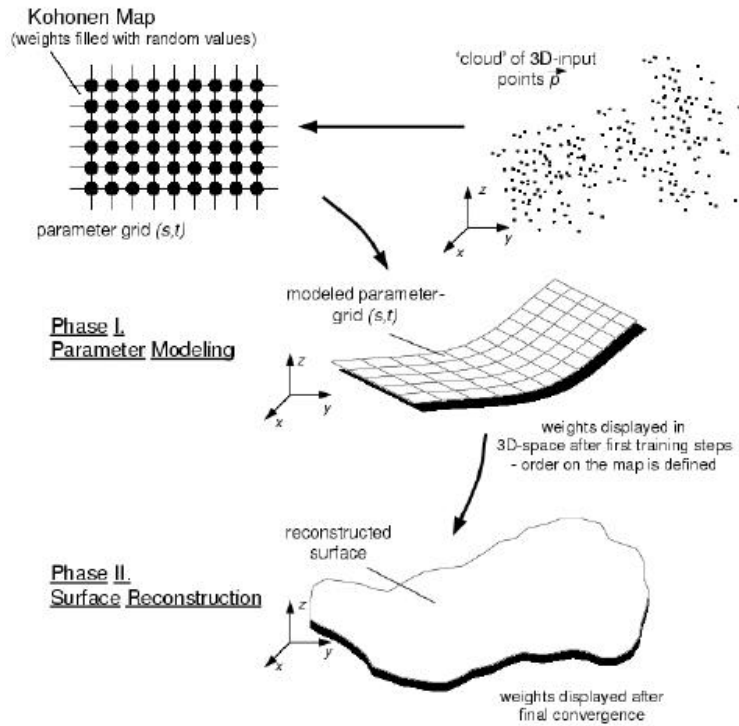


Figure 3.24: Kohonen’s feature map is a two-dimensional array of units (neurons),

to 1). During the reconstruction or training process the neurons are fed with the input data which affects their weight vectors (which resemble their position in three-space). Each input vector \vec{i} is presented to the units j which produce output o_j of the form $o_j = \vec{w}_j \cdot \vec{i}$. The unit generating the highest response o_j is the center of the excitation area. The weights of this unit and a defined neighborhood are updated by the formula $\vec{w}_j(t + 1) = \vec{w}_j(t) + \varepsilon_i(\vec{i} - \vec{w}_j(t))$.

Note that after this update the weight vectors have to be normalized again. The value $\varepsilon_j = \eta h_j$ contains two values, the learning rate η and the neighborhood relationship h_j . Units far away from the center of excitation are only slightly changed.

The algorithm has one additional difficulty. If the input point data do not properly correspond with the neuron network it is possible, that neurons might remain which had not been in any center of excitation so far.

Therefore they had been updated only by the neighborhood update which usually is not sufficient to place the units near the real surface. Having this in mind, Baader and Hirzinger have introduced a kind of reverse training. Unlike the normal training where for each input point a corresponding neural unit is determined and updated the procedure in the intermediate reverse training is reciprocal. For each unit u_j the part of the input data with the highest influence is determined and used for updating u_j , see figure 3.25.

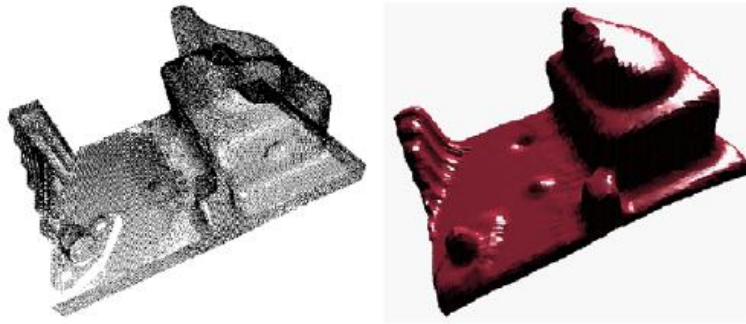


Figure 3.25: The combination of this normal and reverse training completes the algorithm of Baader and Hirzinger and has to be used in the training of the network.

3.3.4 Incremental surface-oriented construction

The idea of incremental surface-oriented construction is to build-up the interpolating or approximating surface directly on surface-oriented properties of the given data points. This can be done in quite different manner. For example, surface construction may start with an initial surface edge at some location of the given point set P , connecting two of its points which are expected neighboring on the surface. The edge is successively extended to a larger surface by iteratively attaching further triangles at boundary edges of the emerging surface. The surface-oriented algorithm of Boissonnat explained in the first subsection may be assigned to this category.

3.3.4.1 Boissonat's surface-oriented approach

Boissonat's surface oriented contouring algorithm [48] usually starts at the shortest connection between two points of the given point set P . In order to attach a new triangle at this edge, and later on to other edges on the boundary, a locally estimated tangent plane is computed based on the points in the neighborhood of the boundary edge. The points in the neighbourhood of the boundary edge are then projected onto the tangent plane. The new triangle is obtained by connecting one of these points to the boundary edge. That point is taken which maximizes the angle between at its edges in the new triangle, that is, the point sees edge boundary edge under the maximum angle, see figure 3.26 The algorithm terminates if

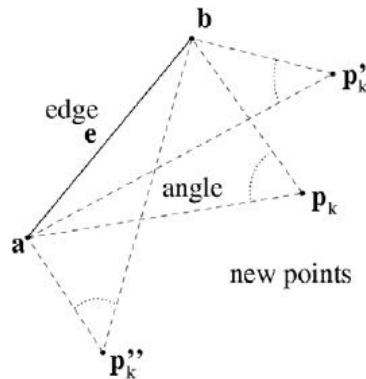


Figure 3.26: The point is taken which maximizes the angle between at its edges in the new triangle, that is, the point sees edge boundary edge under the maximum angle

there is no free edge available any more. The behavior of this algorithm can be seen in figure 3.27

3.3.4.2 Approach of Mencl and Muller

The solution of Mencl and Muller consists of seven main steps [19]

1. The computation of the EMST (Euclidean minimum spanning tree) of the point set.

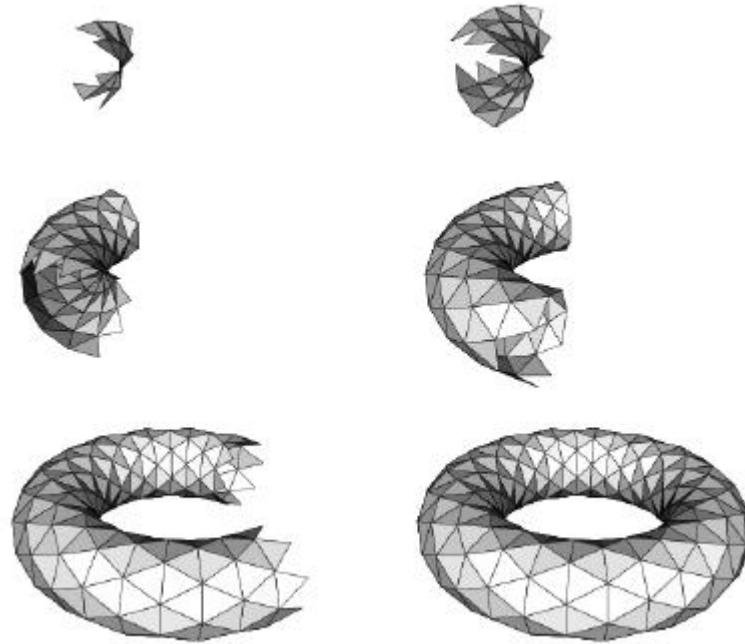


Figure 3.27: The algorithm terminates if there is no free edge available any more.

2. Extension of the graph at leaf points of the EMST.
3. Recognition of features.
4. Extraction of different objects out of the graph.
5. Connection of features of the same kind.
6. Connection of associated edges in the graph.
7. Filling the wire frame with triangles.

The first two steps are designed to build up an initial surface description graph (SDG). This is performed by computing the EMST (Euclidean minimum spanning tree) and an graph extension step afterwards, see figure 3.28. Next, a feature recognition is performed to gain necessary information considering the possible structure of the surface in the third step. As in object recognition of raster images Mencl and Muller consider features to be regions with special information about the objects structure

like paths, edges, point rings and so on. After that, these feature areas are disconnected and/or connected according to certain rules to have a proper description of the objects in the point set (step 4 and 5). In the last step before the triangle filling procedure, the so far computed graph is extended more by connecting associated edges in the graph under consideration of certain constraints. Finally, the triangles are filled into this surface description graph by using a rule system to assure a resulting surface with high accuracy.

As a main concept, Mencl and Muller introduce the concept of feature recognition and clustering to improve the accuracy of the surface description graph according to the assumed surface of the object. The idea is the possibility to integrate different kind of recognition algorithms in the main algorithm while maintaining the structural consistency of the SDG. In contrast to many other methods this approach returns a piecewise linear surface which interpolates exactly the input point set. The algorithm can handle point sets with high changes in point density. This makes it possible to describe objects with only the least necessary amount of points since it is not necessary to oversample areas with low local curvature. The reconstruction of sharp edges in artificial or synthetic objects can be done properly as well as the reconstruction of non-orientable surfaces like Mobius strips, for example.

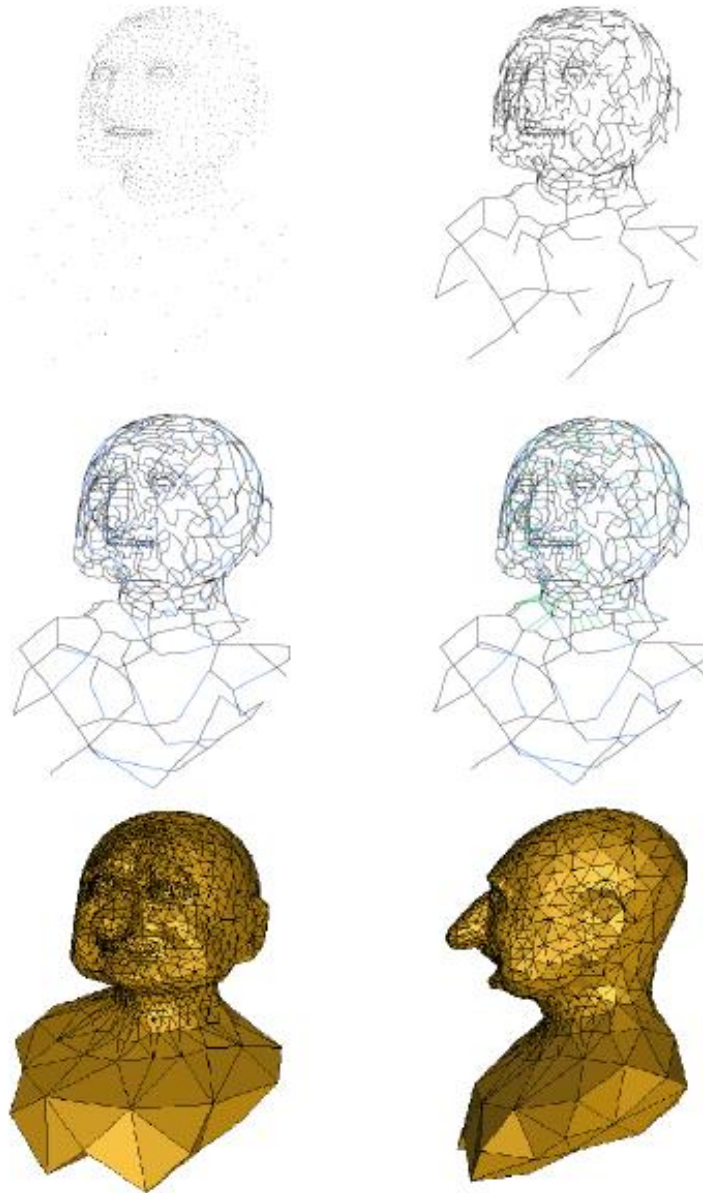


Figure 3.28: Approach of Mencl and Muller

Chapter 4

Filling hole in triangle mesh

4.1 Introduction

There has been a growing trend among shoe manufactures to introduce customized shoes to satisfy varying customer comfort needs. In the last few years with rapid development of 3D scanning that can easily and quickly acquire enormous number of surface points from a physical part, have now made automatic determination footwear feasible. Depending on the both of the complexity of the object and the adopted data acquisition technology some areas of the objects outer surface may never accessible. This induces some deficiencies in the point cloud and a set of holes in the triangle mesh. Moreover, data resulting from 3D scanning are given in an arbitrary position and orientation in 3D space. Thus , substantial post-processing is usually required before taking these models to footwear application. A general approach for filling hole in 3D model is described in this chapter.

4.2 Preliminaries

A triangular mesh is defined as a set of vertices and a set of oriented triangles that join these vertices. Two triangles are adjacent if they share

a common edge.

A boundary edge is an edge adjacent to exactly one triangle. A boundary vertex is a vertex that is adjacent to a boundary edge. A boundary triangle is a triangle that own one or two boundary vertices. A hole is a closed cycle of boundary edges. A given hole is assumed to have no islands.

1-ring triangles of vertex are all triangles that share one common vertex. 1-ring edges of vertex are all edges that share one common vertex and, all vertices on 1-ring edges of a vertex (except itself) are called 1-ring vertices of the vertex. A vertex based topological structure is used which records 1-rings vertices, 1-ring edges and 1-ring triangles of every vertex. Average normal of the 1-ring triangular of the vertex is defined vertex normal.

figure 4.1 illustrated the preliminaries.

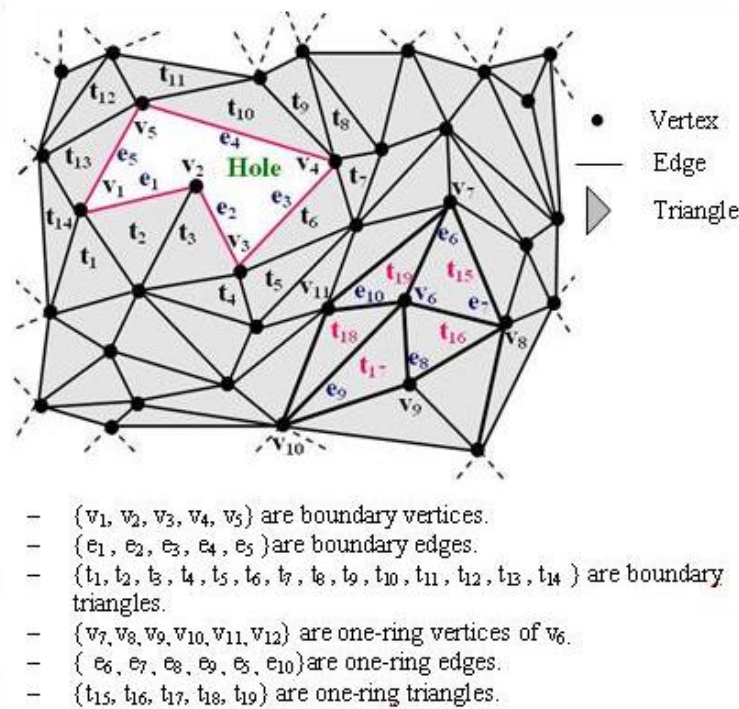


Figure 4.1: Preliminaries related to triangle mesh and hole.

4.3 Advance front mesh technique

The advancing front mesh generators is used for constructing mesh of the domain from its boundary [96, 60] The elements created are triangles (variations exist which enable to create quadrilaterals almost everywhere, depending on the number of sides forming the given boundary) and tetrahedral in three dimensions. The data required consists of the boundary, or more precisely, a polygonal discretization of it, input as a set of segments Additional items (points, edges or faces), which must be considered as prescribed item and thus which must be present in created triangulation, can be included in the data.

The process of any advancing-front method can be summarized as follows:

- Initialization of the front.
- Analysis of the front by determining the departure zone and analysis this region by:
 - (i) Creating internal points and internal elements.
 - (ii) Updating the front.
- As long as the front is not empty, go to analyse of the front

4.4 Differential geometry background

We take some basic theory of mappings from Kreyszig [67] suppose a surface $S \subseteq R^3$ has the parametric representation

$$x(u^1, u^2) = (x_1(u^1, u^2), x_2(u^1, u^2), x_3(u^1, u^2)) \quad (4.1)$$

for point (u^1, u^2) in some domain in R^2 . We call such a representation regular if (i) the functions x_1, x_2, x_3 are smooth, i.e., differentiable as many

times as we need for our discussion, and (ii) the vectors

$$x_1 = \frac{\partial X}{\partial u^1}, \quad x_2 = \frac{\partial X}{\partial u^2} \quad (4.2)$$

are linearly independent at every point (their cross product $x_1 \times x_2$ is nonzero).

Many properties of S are characterized by its first fundamental form, which is the square of the element of arc of a curve in S , the quadratic form

$$ds^2 = x_1 \cdot x_1 (du^1)^2 + 2x_1 \cdot x_2 du^1 du^2 + x_2 \cdot x_2 (du^2)^2 \quad (4.3)$$

Writing

$$g_{\alpha\beta} = x_\alpha \cdot x_\beta, \quad \alpha = 1, 2, \quad \beta = 1, 2, \quad (4.4)$$

and arranging the coefficients in a symmetric matrix

$$I = \begin{pmatrix} g_{11} & g_{12} \\ g_{12} & g_{22} \end{pmatrix} \quad (4.5)$$

we have

$$ds^2 = \begin{pmatrix} du^1 & du^2 \end{pmatrix} I \begin{pmatrix} du^1 \\ du^2 \end{pmatrix} \quad (4.6)$$

Often, the matrix I is itself referred to as the first fundamental form. Under the assumption of regularity, this matrix has a strictly positive determinant

$$g = \det I = g_{11}g_{22} - g_{12}^2 \quad (4.7)$$

the discriminant of the quadratic form. In this case, the form is positive definite. The coefficients $g_{\alpha\beta}$ are the components of a covariant tensor of second order, called the metric tensor, denoted simply by $g_{\alpha\beta}$.

Suppose now that S is a surface with coordinates (u^1, u^2) and that f is a mapping from S to a second surface S^* . Then we can define the parameterization $x^* = f \circ x$ of S^* , so that the coordinates of any image point $f(p) \in S^*$ are the same as those of the corresponding pre-image point $p \in S$, see figure

4.2. We say that the mapping f is allowable if the parameterization x^* is

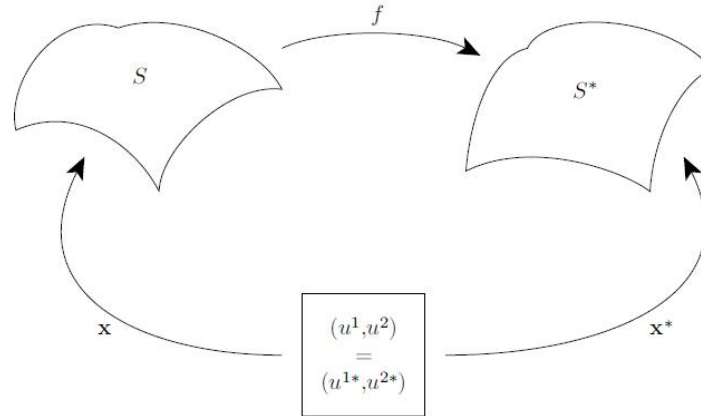


Figure 4.2: The mapping f from S to S^* and the parameterization x of S induce the parameterization $X^* = f \circ x$

regular. With this set up we will now consider various kinds of mappings.

4.4.1 Isometric mappings

An allowable mapping from S to S^* is isometric or length-preserving if the length of any arc on S^* is the same as that of its pre-image on S . Such a mapping is called an isometry.

For example, the mapping of a cylinder into the plane that transforms cylindrical coordinates into cartesian coordinates is isometric.

Theorem 1. An allowable mapping from S to S^* is isometric if and only if the coefficients of the first fundamental forms are the same, i.e.,

$$I = I^* \tag{4.8}$$

Two surfaces are said to be isometric if there exists an isometry between them. Isometric surfaces have the same Gaussian curvature at corresponding pairs of points (since Gaussian curvature depends only on the first fundamental form).

4.4.2 Conformal mappings

An allowable mapping from S to S^* is conformal or angle-preserving if the angle of intersection of every pair of intersecting arcs on S^* is the same as that of the corresponding pre-images on S at the corresponding point. For example, the stereographic and Mercator projections are conformal maps from the sphere to the plane, see figure 4.3

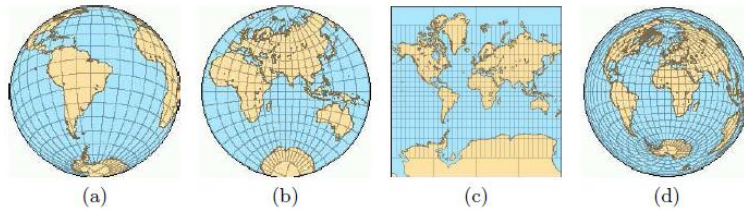


Figure 4.3: Orthographic (a), stereographic (b), Mercator (c), and Lambert (d) projection of the Earth.

Theorem 2. An allowable mapping from S to S^* is conformal or angle preserving if and only if the coefficients of the first fundamental forms are proportional, i.e.,

$$I = \eta(u^1, u^2)I^* \quad (4.9)$$

for some scalar function $\eta \neq 0$

4.4.3 Equiareal mappings

An allowable mapping from S to S^* is equiareal if every part of S is mapped onto a part of S^* with the same area. For example, the Lambert projection is an equiareal mapping from the sphere to the plane, see figure 4.3

Theorem 3. An allowable mapping from S to S^* is equiareal if and only

if the discriminants of the first fundamental forms are equal, i.e.,

$$g = g^* \quad (4.10)$$

The proofs of the above three results can be found in Kreyszig [67].

Theorem 4. Every isometric mapping is conformal and equiareal, and every conformal and equiareal mapping is isometric, i.e.,

$$\text{isometric} \iff \text{conformal} + \text{equiareal}.$$

We can thus view an isometric mapping as ideal, in the sense that it preserves just about everything we could ask for: angles, areas, and lengths. However, as is well known, isometric mappings only exist in very special cases. When mapping into the plane, the surface S would have to be developable, such as a cylinder. Many approaches to surface parameterization therefore attempt to find a mapping which either

- 1- is conformal, i.e., has no distortion in angles, or
- 2- is equiareal, i.e., has no distortion in areas, or
- 3- minimizes some combination of angle distortion and area distortion.

4.4.4 Planar mappings

A special type of mappings that we will consider now and then in the following are planar mappings $f : R^2 \rightarrow R^2, f(x, y) = (u(x, y), v(x, y))$. For these kind of mappings the first fundamental form can be written as

$$I = J^T J \quad (4.11)$$

where $J = \begin{pmatrix} u_x & u_y \\ v_x & v_y \end{pmatrix}$ is the Jacobian of f . It follows that the singular values σ_1 and σ_2 of J are just the square roots of the eigenvalues λ_1 and λ_2

of I and it is then easy to verify.

Proposition 1. For a planar mapping $f : R^2 \Rightarrow R^2$ the following equivalencies hold:

$$1- f \text{ is isometric} \iff I = \begin{pmatrix} 1 & 0 \\ 0 & 1 \end{pmatrix} \iff \lambda_1 = \lambda_2 = 1 \iff \sigma_1 = \sigma_2 = 1$$

$$2- f \text{ is conformal} \iff I = \begin{pmatrix} \eta & 0 \\ 0 & \eta \end{pmatrix} \iff \lambda_1/\lambda_2 = 1 \iff \sigma_1/\sigma_2 = 1$$

$$3- f \text{ is equiareal} \iff \det I = 1 \iff \lambda_1 \lambda_2 = 1 \iff \sigma_1 \sigma_2 = 1$$

4.4.5 Conformal and harmonic mappings

Conformal mappings have many nice properties, not least of which is their connection to complex function theory. Consider for the moment the case of mappings from a planar region S to the plane. Such a mapping can be viewed as a function of a complex variable, $w = f(z)$. Locally, a conformal map is simply any function f which is analytic in a neighbourhood of a point z and such that $f'(z) \neq 0$. A conformal mapping f thus satisfies the Cauchy- Riemann equations, which, with $z = x + iy$ and $w = u + iv$ are

$$\frac{\partial u}{\partial x} = \frac{\partial v}{\partial y}, \quad \frac{\partial u}{\partial y} = -\frac{\partial v}{\partial x} \quad (4.12)$$

Now notice that by differentiating one of these equations with respect to x and the other with respect to y , we obtain the two Laplace equations

$$\Delta u = 0, \quad \Delta v = 0 \quad (4.13)$$

where

$$\Delta = \frac{\partial^2}{\partial x^2} + \frac{\partial^2}{\partial y^2} \quad (4.14)$$

is the Laplace operator.

Any mapping $(u(x, y), v(x, y))$ which satisfies these two Laplace equations

is called a harmonic mapping. Thus a conformal mapping is also harmonic, and we have the implications

$$\text{isometric} \implies \text{conformal} \implies \text{harmonic}.$$

Why do we consider harmonic maps? Well, their big advantage over conformal maps is the ease with which they can be computed, at least approximately. After choosing a suitable boundary mapping (which is equivalent to using a Dirichlet boundary condition for both u and v), each of the functions u and v is the solution to a linear elliptic partial differential equation (PDE) which can be approximated by various methods, such as finite elements or finite differences, both of which lead to a linear system of equations. Harmonic maps are also guaranteed to be one-to-one for convex regions.

Theorem 5 (RKC). If $f : S \rightarrow R^2$ is harmonic and maps the boundary ∂S homeomorphically into the boundary ∂S^* of some convex region $S^* \subset R^2$ then f is one-to-one; see figure 4.4

On the downside, harmonic maps are not in general conformal and do not

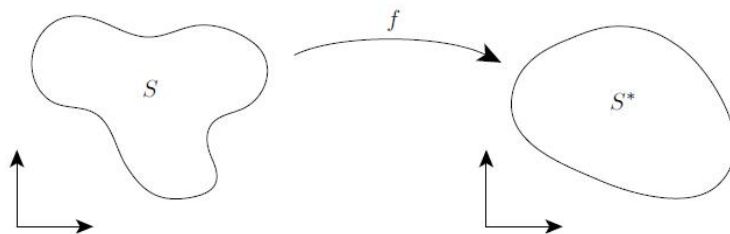


Figure 4.4: One-to-one harmonic mappings.

preserve angles. For example, it is easy to verify from the Cauchy-Riemann and Laplace equations that the bilinear mapping $f : [0, 1]^2 \rightarrow R^2$ defined by

$$u = x(1 + y), \quad v = y \tag{4.15}$$

is harmonic but not conformal. Indeed the figure 4.5 clearly shows that this harmonic map does not preserve angles. Another weakness of har-

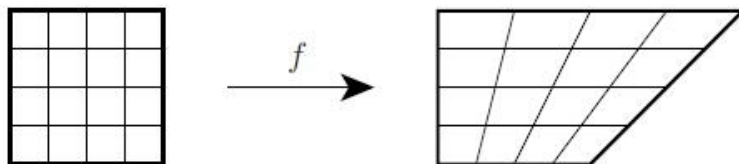


Figure 4.5: A harmonic mapping which is not conformal

monic mappings is their "one-sidedness". The inverse of a harmonic mapping is not necessarily harmonic. Again, the bilinear example above provides an example of this. It is easy to check that the inverse mapping $x = u/(1+v)$, $y = v$ is not harmonic as the function $x(u, v)$ does not satisfy the Laplace equation.

Despite these drawbacks, harmonic mappings do at least minimize deformation in the sense that they minimize the Dirichlet energy

$$E_D(f) = \frac{1}{2} \int_S \|\text{grad} f\|^2 = \frac{1}{2} \int_S (\|\nabla u\|^2 + \|\nabla v\|^2) \quad (4.16)$$

This property combined with their ease of computation explains their popularity.

When we consider mappings from a general surface $S \subset \mathbb{R}^3$ to the plane, we find that all the above properties of conformal and harmonic mappings are essentially the same. The equations just become more complicated. Any mapping f from a given surface S to the plane defines coordinates of S , say (u^1, u^2) . By theorem 2, If f is conformal then there is some scalar function $\eta \neq 0$ such that

$$ds^2 = \eta(u^1, u^2)((du^1)^2 + (du^2)^2) \quad (4.17)$$

Suppose that S has given coordinates $(\tilde{u}^1, \tilde{u}^2)$. After some analysis, one can show that the above equation implies the two equations

$$\begin{cases} \frac{\partial u^1}{\partial \tilde{u}^1} = \frac{\tilde{g}_{11}}{\sqrt{\tilde{g}}} \frac{\partial u^2}{\partial \tilde{u}^2} - \frac{\tilde{g}_{12}}{\sqrt{\tilde{g}}} \frac{\partial u^2}{\partial \tilde{u}^1} \\ \frac{\partial u^1}{\partial \tilde{u}^2} = \frac{-\tilde{g}_{22}}{\sqrt{\tilde{g}}} \frac{\partial u^2}{\partial \tilde{u}^1} + \frac{\tilde{g}_{12}}{\sqrt{\tilde{g}}} \frac{\partial u^2}{\partial \tilde{u}^2} \end{cases} \quad (4.18)$$

which are a generalization of the Cauchy-Riemann equations 4.12. Indeed, in the special case that S is planar, we can take

$$\tilde{g}_{11} = \tilde{g}_{22} = 1 \quad \tilde{g}_{12} = 0 \quad (4.19)$$

and we get simply

$$\frac{\partial u^1}{\partial \tilde{u}^1} = \frac{\partial u^2}{\partial \tilde{u}^2} \quad \frac{\partial u^1}{\partial \tilde{u}^2} = -\frac{\partial u^2}{\partial \tilde{u}^1} \quad (4.20)$$

Similar to the planar case, we can differentiate one equation in 4.18 with respect to \tilde{u}^1 and the other with respect to \tilde{u}^2 , and obtain the two generalizations of Laplace's equation,

$$\Delta_S u^1 = 0 \quad \Delta_S u^2 = 0 \quad (4.21)$$

where Δ_s is the Laplace-Beltrami operator

$$\Delta S = \frac{1}{\sqrt{\tilde{g}}} \left(\frac{\partial}{\partial \tilde{u}^1} \left(\frac{\tilde{g}_{22}}{\sqrt{\tilde{g}}} \frac{\partial}{\partial \tilde{u}^1} - \frac{\tilde{g}_{12}}{\sqrt{\tilde{g}}} \frac{\partial}{\partial \tilde{u}^2} \right) + \frac{\partial}{\partial \tilde{u}^2} \left(\frac{\tilde{g}_{11}}{\sqrt{\tilde{g}}} \frac{\partial}{\partial \tilde{u}^2} - \frac{\tilde{g}_{12}}{\sqrt{\tilde{g}}} \frac{\partial}{\partial \tilde{u}^1} \right) \right) \quad (4.22)$$

When this operator is differentiated out, one finds that it is a linear elliptic operator with respect to the coordinates $(\tilde{u}^1, \tilde{u}^2)$. The operator generalizes the Laplace operator (as can easily be checked by taking S to be planar with $\tilde{g}_{\alpha\beta}$ as in (4.19) and is independent of the particular coordinates (in this case $(\tilde{u}^1, \tilde{u}^2)$) used to define it. As explained by Klingenberg [64] it can also be written simply as

$$\Delta_s = \operatorname{div}_s \operatorname{grad}_s \quad (4.23)$$

Similar to the planar case, a harmonic map can either be viewed as the solution to equation (4.21), or as the minimizer of the Dirichlet energy

$$E_D f = \frac{1}{2} \int_S \| \text{grad}_s f \|^2 \quad (4.24)$$

4.4.6 Equiareal mappings

There are essentially only two quantities to consider minimizing in a mapping: angle distortion and area distortion. We know from the Riemann mapping theorem that (surjective) conformal mappings from a disk-like surface to a fixed planar simply-connected region not only exist but are also almost unique. For example, consider mapping the unit disk S into itself (treating S as a subset of the complex plane), and choose any point $z \in S$ and any angle $\theta, -\Pi < \theta < \Pi$. According to the theorem, there is precisely one conformal mapping $f : S \rightarrow S$ such that $f(z) = 0$ and $\arg f'(z) = \theta$. In this sense there are only the three degrees of freedom defined by the complex number z and the real angle θ in choosing the conformal map.

What we want to do now is to demonstrate that equiareal mappings are substantially different to conformal ones from the point of view of uniqueness as there are many more of them. The following example is to our knowledge novel and nicely illustrates the abundance of equiareal mappings. Consider again mappings $f : S \rightarrow S$ from the unit disk S into itself. Using the polar coordinates $x = r \cos \theta, y = r \sin \theta$ one easily finds that the determinant of the Jacobian of any mapping $f(x, y) = (u(x, y), v(x, y))$ can be expressed as

$$\det J(f) = u_x v_x - u_y v_x = \frac{1}{r} (u_r v_\theta - u_\theta v_r) \quad (4.25)$$

Consider then the mapping $f : S \rightarrow S$ defined by

$$r(\cos \theta, \sin \theta) \rightarrow r(\cos(\theta + \phi(r)), \sin(\theta + \phi(r))) \quad (4.26)$$

for $0 \leq r \leq 1$ and $-\Pi < \theta \leq \Pi$, where $\phi : [0, 1] \rightarrow R$ is an arbitrary function. This mapping maps each circle of radius r centred at the origin into itself, rotated by the angle $\phi(r)$ see figure 4.6 If ϕ is differentiable

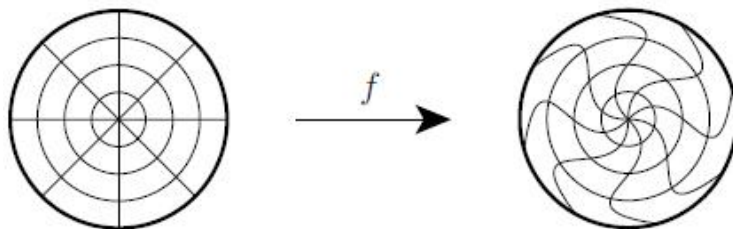


Figure 4.6: An equiareal mapping.

then so is f and differentiation shows that

$$u_r v_\theta - u_\theta v_r = r \quad (4.27)$$

independent of the function ϕ . We conclude that $\det J(f) = 1$ and therefore, according to Proposition 1, f is equiareal, irrespective of the chosen univariate function ϕ

It is not difficult to envisage other families of equiareal mappings constructed by rotating circles about other centres in S . These families could also be combined to make further equiareal mappings.

When we consider again the formulations of conformal and equiareal mappings in terms of the first fundamental form, the lack of uniqueness of equiareal mappings becomes less surprising. For, as we saw earlier, the property of conformality (1) essentially places two conditions on the three coefficients of the first fundamental form $g_{11}^*, g_{12}^*, g_{22}^*$ while the property of equiarealness (2) places only one condition on them (the three conditions together of course completely determine the three coefficients, giving an isometric mapping).

Considering not only the non-uniqueness, but also the rather strange rotational behaviour of the above mappings, we conclude that it is hardly

sensible to try to minimize area deformation alone. In order to find a well-behaved mapping we surely need to combine area-preservation with some minimization of angular distortion.

4.4.7 Discrete harmonic mappings

Common to almost all surface parameterization methods is to approximate the underlying smooth surface S by a piecewise linear surface S_T , in the form of a triangular mesh, i.e. the union of a set $T = \{T_1, \dots, T_n\}$ of triangles T_i such that the triangles intersect only at common vertices or edges. Nowadays in fact, surfaces are frequently simply represented as triangular meshes, and the smooth underlying surface is often not available. We will denote by V the set of vertices. If S_T has a boundary, then the boundary will be polygonal and we denote by V_B the set of vertices lying on the boundary and by V_I set of interior vertices.

The most important parameterization task is to map a given disk-like surface $S \subset R^3$ into the plane. Working with a triangular mesh S_T the goal is to find a suitable (polygonal) domain $S^* \subset R^2$ and a suitable piecewise linear mapping $f : S_T \rightarrow S^*$ that is linear on each triangle T_i in S_T and continuous; see Figure 4.7 Such a mapping is uniquely determined by the images $f(v) \in R^2$ of the vertices $v \in V$.

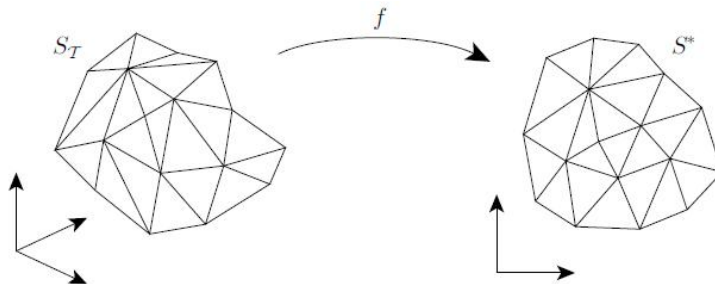


Figure 4.7: Piecewise linear mapping of a triangular mesh.

4.4.8 Finite element method

One of the earliest methods for mapping disk-like surfaces into the plane was to approximate a harmonic map using the finite element method based on linear elements. This method was introduced to the computer graphics community by Eck et al.[23] and called simply a discrete harmonic map, although a similar technique had earlier been used by Pinkall and Polthier for computing piecewise linear minimal surfaces [79]. The basic method has two steps.

- 1- First fix the boundary mapping, i.e. fix $f|_{\partial S_T} = f_0$ by mapping the polygonal boundary ∂S_T homeomorphically to some polygon in the plane. This is equivalent to choosing the planar image of each vertex in the mesh boundary ∂S_T and can be done in several ways [30, 47]
- 2- Find the piecewise linear mapping $f : S_T \rightarrow S^*$ which minimizes the Dirichlet energy

$$E_D = \frac{1}{2} \int_{S_T} \|\text{grad}_{S_T} f\|^2 \quad (4.28)$$

subject to the Dirichlet boundary condition $f|_{\partial S_T} = f_0$.

The main advantage of this method over earlier approaches is that this is a quadratic minimization problem and reduces to solving a linear system of equations. Consider one triangle $T = [v_1, v_2, v_3]$ in the surface S_T . Referring to figure 4.8 one can show that

$$2 \int_T \|\text{grad}_T f\|^2 = \cot \theta_3 \|f(v_1) - f(v_2)\|^2 + \cot \theta_2 \|f(v_1) - f(v_3)\|^2 + \cot \theta_1 \|f(v_2) - f(v_3)\|^2 \quad (4.29)$$

The normal equations for the minimization problem can therefore be expressed as the linear system of equations

$$\sum_{j \in N_i} w_{i,j} (f(v_j) - f(v_i)) = 0 \quad v_i \in V_I \quad (4.30)$$

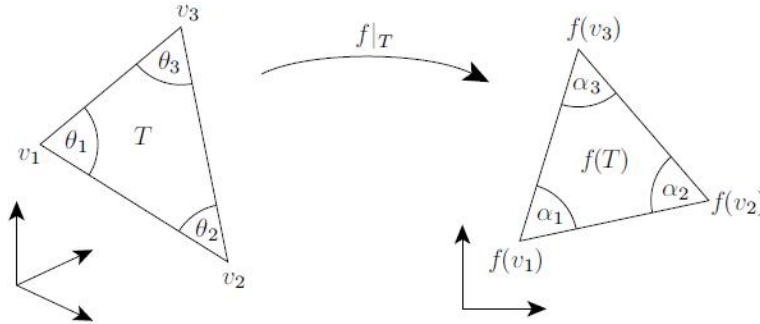


Figure 4.8: Atomic map between a mesh triangle and the corresponding parameter triangle.

where

$$w_{i,j} = \cot\alpha_{i,j} + \cot\beta_{i,j} \quad (4.31)$$

and the angles $\alpha_{i,j}, \beta_{i,j}$ are shown in the figure 4.9. Here we have assumed that the vertices in V are indexed (in any random order) and that N_i denotes the set of indexes of the neighbours of the vertex v_i (those vertices which share an edge with v_i).

The associated matrix is symmetric and positive definite, and so the

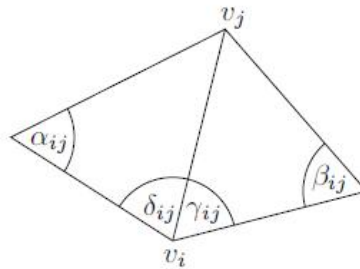


Figure 4.9: Angles for the discrete harmonic map and the mean value coordinates.

linear system is uniquely solvable. The matrix is also sparse and iterative methods are effective, e.g., conjugate gradients. Note that the system has to be solved twice, once for the x- and once for the y-coordinates of the parameter points $f(v_i), v \in V_I$. In practice the method often gives good

visual results.

4.5 Rotation about arbitrary axis in 3 dimensional

The problem of rotation about an arbitrary axis in three dimensions arises in many fields including computer graphics and molecular simulation. In this section we give an algorithm and matrices for calculating the motion. An algorithm is (see Figure 4.10):

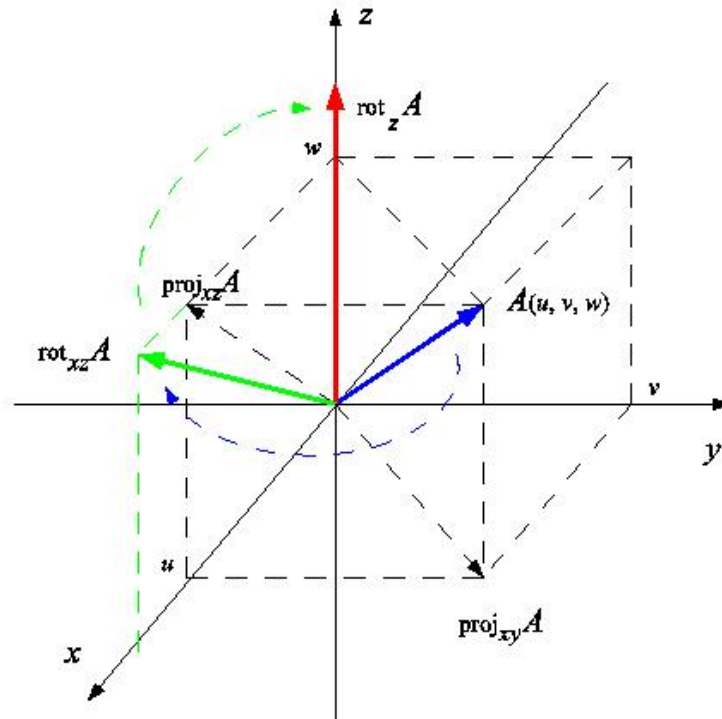


Figure 4.10: Moving the axis of rotation to the z axes

- 1- Translate space so that the rotation axis passes through the origin.
- 2- Rotate space about the z-axis so that the rotation axis lies in the xz plane.
- 3- Rotate space about the y-axis so that the rotation axis lies along z-axis.
- 4- Perform the desired rotation by θ about z-axis.

- 5- Apply the inverse of step (3).
- 6- Apply the inverse of step (2).
- 7- Apply the inverse of step (1).

This algorithm assumes that the axis of rotation is not parallel to the z axis. We will write our three-dimensional points in four homogeneous coordinates. i.e., (x,y,z) will be written as $(x,y,z,1)$. This enables us to do coordinate transformations using 4×4 matrices. Note that these 4×4 matrices are only necessary for translations, if we omitted translations from our movements we could do the motions with 3×3 rotation matrices obtained by deleting the last rows and last columns of the 4×4 matrices. In this thesis vectors are multiplied by matrices on the vector's left.

4.5.1 A translation matrix

The product $Tp.v$ is equivalent to the vector sum $\langle -a, -b, -c, 0 \rangle + v$, i.e, this transformation moves the point $P_1(a, b, c)$ to the origin

$$\begin{pmatrix} 1 & 0 & 0 & -a \\ 0 & 1 & 0 & -b \\ 0 & 0 & 1 & -c \\ 0 & 0 & 0 & 1 \end{pmatrix} \quad (4.32)$$

4.5.2 Rotation matrices

Here are the matrices for rotation by α around x - axis, β around y - axis and γ around the z - axis

$$R_x(\alpha) = \begin{pmatrix} 1 & 0 & 0 & 0 \\ 0 & \cos(\alpha) & -\sin(\alpha) & 0 \\ 0 & \sin(\alpha) & \cos(\alpha) & 0 \\ 0 & 0 & 0 & 1 \end{pmatrix} \quad (4.33)$$

$$R_y(\beta) = \begin{pmatrix} \cos(\beta) & 0 & \sin(\beta) & 0 \\ 0 & 1 & 0 & 0 \\ -\sin(\beta) & 0 & \cos(\beta) & 0 \\ 0 & 0 & 0 & 1 \end{pmatrix} \quad (4.34)$$

$$R_x(\gamma) = \begin{pmatrix} \cos(\gamma) & -\sin(\gamma) & 0 & 0 \\ \sin(\gamma) & \cos(\gamma) & 0 & 0 \\ 0 & 0 & 1 & 0 \\ 0 & 0 & 0 & 1 \end{pmatrix} \quad (4.35)$$

The general rotation matrix depends on the order of rotations. The first matrix rotates about x, then y, then z, the second rotations about z, then y, then x.

$$R_z R_y R_x = \begin{pmatrix} \cos\beta\cos\gamma & \cos\gamma\sin\alpha\sin\beta - \cos\alpha\sin\gamma & \cos\alpha\cos\gamma\sin\beta + \sin\alpha\sin\gamma & 0 \\ \cos\beta\sin\gamma & \cos\alpha\cos\gamma + \sin\alpha\sin\beta\sin\gamma & -\cos\gamma\sin\alpha + \cos\alpha\sin\beta\sin\gamma & 0 \\ -\sin\beta & \cos\beta\sin\alpha & \cos\alpha\cos\beta & 0 \\ 0 & 0 & 0 & 1 \end{pmatrix} \quad (4.36)$$

$$R_x R_y R_z = \begin{pmatrix} \cos\alpha\cos\beta & -\cos\gamma\sin\alpha + \cos\alpha\sin\beta\sin\gamma & \cos\alpha\cos\gamma\sin\beta + \sin\alpha\sin\gamma & 0 \\ \cos\beta\sin\alpha & \cos\alpha\cos\gamma + \sin\alpha\sin\beta\sin\gamma & \cos\gamma\sin\alpha\sin\beta - \cos\alpha\sin\gamma & 0 \\ -\sin\beta & \cos\beta\sin\gamma & \cos\beta\cos\gamma & 0 \\ 0 & 0 & 0 & 1 \end{pmatrix} \quad (4.37)$$

4.5.3 Transformations for moving a vector to the z-axis

In this section we introduce matrices to move a rotation vector $\langle u, v, w \rangle$ to the to the z - axis This is illustrated in figure 4.10. Note that we use the vector's components to form expressions for the cosines and sines. We require that the rotation vector not be parallel to the z - axis, else $u = v = 0$ and the denominators vanish.

The matrix to rotate a vector about the z - axis to the xz - plane is

$$R_{xz} = \begin{pmatrix} \frac{u}{\sqrt{u^2+v^2}} & \frac{v}{\sqrt{u^2+v^2}} & 0 & 0 \\ \frac{-v}{\sqrt{u^2+v^2}} & \frac{u}{\sqrt{u^2+v^2}} & 0 & 0 \\ 0 & 0 & 1 & 0 \\ 0 & 0 & 0 & 1 \end{pmatrix} \quad (4.38)$$

The matrix to rotate the vector in the xz – plane to the z – axis is

$$R_{xz2z} = \begin{pmatrix} \frac{w}{\sqrt{u^2+v^2+w^2}} & 0 & \frac{-\sqrt{u^2+v^2}}{\sqrt{u^2+v^2+w^2}} & 0 \\ 0 & 1 & 0 & 0 \\ \frac{\sqrt{u^2+v^2}}{\sqrt{u^2+v^2+w^2}} & 0 & \frac{w}{\sqrt{u^2+v^2+w^2}} & 0 \\ 0 & 0 & 0 & 1 \end{pmatrix} \quad (4.39)$$

4.5.4 Rotations about the origin

In this section we rotate the point (x, y, z) about the vector $\langle u, v, w \rangle$ by the angle θ . The matrix for rotations about the origin is the product

$$R_{xz}^{-1} R_{xz2z}^{-1} R_z(\theta) R_{xz2z} R_{xz} \begin{pmatrix} \frac{u^2+(v^2+w^2)\cos\theta}{u^2+v^2+w^2} & \frac{uv(1-\cos\theta)-w\sqrt{u^2+v^2+w^2}\sin\theta}{u^2+v^2+w^2} & \frac{uw(1-\cos\theta)+v\sqrt{u^2+v^2+w^2}\sin\theta}{u^2+v^2+w^2} & 0 \\ \frac{uv(1-\cos\theta)+w\sqrt{u^2+v^2+w^2}\sin\theta}{u^2+v^2+w^2} & \frac{v^2+(u^2+w^2)\cos(\theta)}{u^2+v^2+w^2} & \frac{uw(1-\cos\theta)-u\sqrt{u^2+v^2+w^2}\sin\theta}{u^2+v^2+w^2} & 0 \\ \frac{uw(1-\cos\theta)-v\sqrt{u^2+v^2+w^2}\sin\theta}{u^2+v^2+w^2} & \frac{vw(1-\cos\theta)+u\sqrt{u^2+v^2+w^2}\sin\theta}{u^2+v^2+w^2} & \frac{w^2+(u^2+v^2)\cos\theta}{u^2+v^2+w^2} & 0 \\ 0 & 0 & 0 & 1 \end{pmatrix} \quad (4.40)$$

If we multiply this times the point to be rotated, (x,y,z) , we get the rotated point

$$\begin{pmatrix} \frac{u(ux+vy+wz)+(x(v^2+w^2)-u(vy+wz))\cos\theta+\sqrt{u^2+v^2+w^2}(-wy+vz)\sin\theta}{u^2+v^2+w^2} \\ \frac{v(ux+vy+wz)+(y(v^2+w^2)-v(ux+wz))\cos\theta+\sqrt{u^2+v^2+w^2}(wx-uz)\sin\theta}{u^2+v^2+w^2} \\ \frac{w(ux+vy+wz)+(z(v^2+w^2)-w(vy+wz))\cos\theta+\sqrt{u^2+v^2+w^2}(-vx+uy)\sin\theta}{u^2+v^2+w^2} \\ 1 \end{pmatrix} \quad (4.41)$$

4.6 Rotation about an arbitrary line in 3 dimensional

We must give the axis an orientation so that positive and negative angles of rotation are defined. If the axis of rotation is given by two points $P_1 = (a, b, c)$ and $P_2 = (d, e, f)$, then the (oriented) vector of rotation can be given by $\langle u, v, w \rangle = \langle d - a, e - b, f - c \rangle$. The matrix for

rotation about an arbitrary line is given by the product:

$$T_{P_1}^{-1} R_{xz}^{-1} R_{xz}^{-1} R_z(\theta) R_{xz} R_{xz} T_{P_1}$$

This is the rotation operator for rotations about the line through $P_1(a, b, c)$ parallel to $\langle u, v, w \rangle$ by the angle θ . In hopes of fitting the matrix onto the page we make the substitution $L = \sqrt{u^2 + v^2 + w^2}$

$$\begin{pmatrix} \frac{a(v^2+w^2)+u(-bv-cw+ux+vy+wz)+(-a(v^2+w^2)+u(bv+cw-vy-wz)+(v^2+w^2)x)\cos\theta+\sqrt{u^2+v^2+w^2}(-cv+bw-wy+vz)\sin\theta}{u^2+v^2+w^2} \\ \frac{b(u^2+w^2)+v(-au-cw+ux+vy+wz)+(-b(u^2+w^2)+v(au+cw-ux-wz)+(u^2+w^2)y)\cos\theta+\sqrt{u^2+v^2+w^2}(cu-aw+wx-uz)\sin\theta}{u^2+v^2+w^2} \\ \frac{c(v^2+u^2)+w(-au-bv+ux+vy+wz)+(-c(v^2+u^2)+w(au+bv-ux-vy)+(u^2+v^2)z)\cos\theta+\sqrt{u^2+v^2+w^2}(-bu+av-vx+uy)\sin\theta}{u^2+v^2+w^2} \\ 1 \end{pmatrix} \quad (4.42)$$

4.7 Filling hole in triangle mesh

In the literature we have surveyed, existing approach to fill holes in meshes can be distinguished two main categories: the geometric and non-geometric approaches. Among the non-geometric approaches, authors in [4] detected the mesh areas that have to be filled with using volumetric representation. Davis et al [50] filled the gaps by applying volumetric process to extend a signed distance function through this volumetric representation until its zero set bridges whatever holes may be present. A similar approach has been developed by Authors in [32] for the simplification and the repairing of polygonal meshes. The advantage of this approach is working well for complex holes and drawback of current method include time-consuming and may generate incorrect topology in some case.

Considering the geometric approaches, the hole is filled in [80] with minimum area triangulation of its contour. Then the triangulation is refined so that the triangle density agrees with the density of the surrounding mesh triangles. Finally, the hole is smoothed with fairing technique based on

an umbrella operator [70]. A satisfactory hole filling method should: 1. run in reasonable time. 2. be able to patch an arbitrary holes for any model. 3. cover the missing geometry well. A hole filling process that is implemented here is summarized in following steps:

- Identify holes in triangle mesh. Holes can be identified automatically by looking close loop of boundary edges.
- Cover the holes with Advance Front Mesh technique.
- Modify the triangles in the initial patch mesh by estimating desirable normals instead relocating them directly.
- Rotate triangle by local rotation.
- Make algorithm more accurate by re-positioning these coordinate by solving the Poisson equation according to desirable normal and boundary vertices of the hole.
- Update the coordinate to make the smoothed patch mesh.

4.7.1 Hole patching

At first the hole is identified automatically by looking close loop of boundary edge. Then the Advance front mesh technique is applied over the hole to generate an initial patch mesh as follows:

Step 1: The angle α_i between two adjacent boundary edges at each vertex v_i on the front is calculated.

Step 2: When the angle α is less than or equal to 75° , we simply connect the neighboring vertices of V_1 , namely V_0 and V_2 , to form a new triangle. When the angle is larger than 75° , but less than or equal to 135° .

As figure 4.11.(b) depicts, a new vertex V_3 is inserted along the bisection line of vectors $V_0 V_1$ and $V_1 V_2$ to determine the new vertex. When the angle is larger than 135° , as figure 4.11.(c), two new vertices, V_3 and V_4 are inserted, equally distributed on two triple-section lines of vectors $V_0 V_1$ and $V_1 V_2$.

Step 3: The distance between the new vertex and related boundary vertexes is calculated when the distance is less than given threshold, they should merge.

Step 4: Update the front and repeat the algorithm until the hole is patched with new triangles.

4.7.2 Harmonic-based desirable normal computing

The earliest purpose of discrete harmonic functions is to map a disk-like surface ST onto a plane S^* . The basic idea is to find a piecewise linear mapping $f : S_T \rightarrow S^*$ to minimize the Dirichlet energy

$$E_D = \frac{1}{2} \int_{S_T} \|\text{grad}_{S_T} f\|^2 \quad (4.43)$$

subject to the Dirichlet boundary condition $f|_{\partial S_T} = f_0$. As for triangle $T = \{v_1, v_2, v_3\}$ the Dirichlet energy can be expressed as:

$$2 \int_T \|\text{grad}_T f\|^2 = \cot \theta_3 \|f(v_1) - f(v_2)\|^2 + \cot \theta_2 \|f(v_1) - f(v_3)\|^2 + \cot \theta_1 \|f(v_2) - f(v_3)\|^2 \quad (4.44)$$

The equation for the minimization problem can therefore be re-expressed as the following linear system

$$\sum_{v_j \in N_i} w_{i,j} (f(v_j) - f(v_i)) = 0 \quad v_i \in V_I \quad (4.45)$$

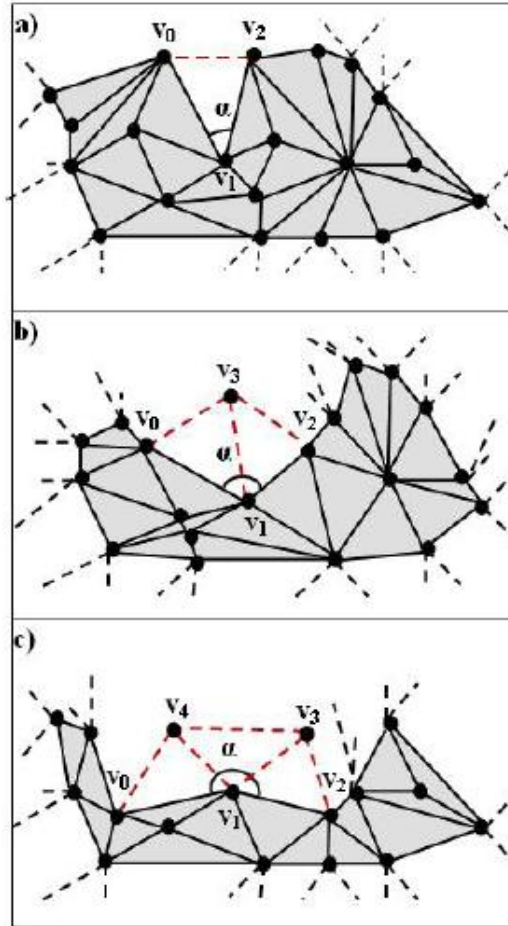


Figure 4.11: Rules for generating initial patch over the hole.

where $w_{i,j} = \cot\alpha_{i,j} + \cot\beta_{i,j}$ the angles $\alpha_{i,j}$ and $\beta_{i,j}$ are shown in figure Fig 4.12 and N_i refers to the 1-ring vertices of vertex v_i . The associated matrix is symmetric and positive and sparse, and so the linear system is uniquely solvable. The system can be solved efficiently with iterative methods such as conjugate gradient method. Note that system has to be solved three times. Once for x-, once for y- and once for z-coordinate. Now the desirable normal of all vertices in initial patch mesh is obtained. However, Poisson equation requires a discrete guidance field, i.e., w , defined on the triangles of the patch mesh. The guidance vector field is constructed

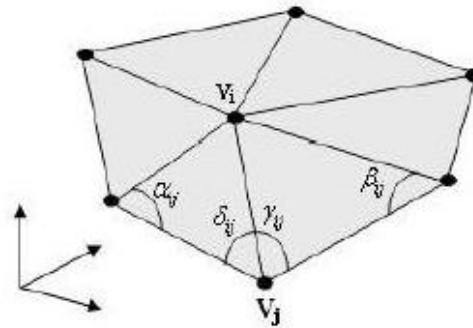


Figure 4.12: 1-ring vertex of v_i and angles opposite to edge $v_i v_j$.

by triangle rotation. Local rotation is applied to each triangle of initial patch mesh. Let n be the original normal of triangle and n' be the new normal of triangle that is calculated with desirable normal of vertices of triangle and c be the center of triangle. The rotation can be obtained by rotating n to n' around c . See 4.13. After rotation, the original patch mesh is torn a part and triangles are not connected any more and this torn triangles are used to construct a guidance vector field for Poisson equation. Finally, the disconnected triangles are stitched by solving Poisson equation.

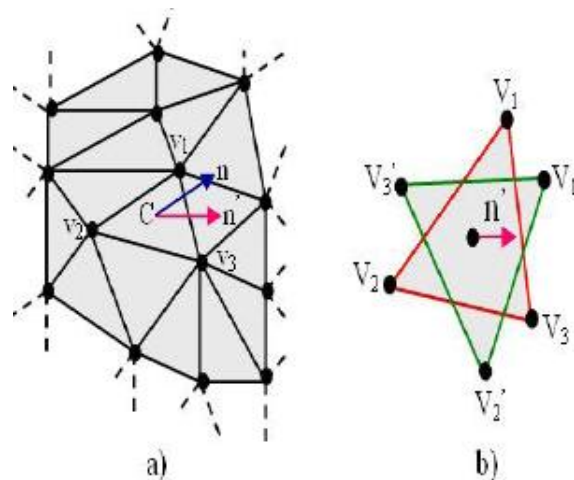


Figure 4.13: a) Initial patch mesh in triangle mesh, (b) A triangle red is initial patch mesh and its locally rotated version is green.

4.7.3 Poisson equation

In this section, we introduced the details of Poisson equation for reconstruction smooth and accurate patch mesh. We regard the mesh geometry (coordinates) as scalar function. The Poisson equation is originally appeared from [58]. The aim of this method is solving an unknown target mesh with known topology but unknown geometry (vertex coordinate). Poisson equation like Harmonic equation has to solved three time.

The Poisson equation with Dirichlet boundary condition [81], [111] is formulated as

$$\nabla^2 f = \nabla \cdot w \quad \text{over } \Omega, \quad \text{with } f|_{\partial\Omega} = f^*|_{\partial\Omega} \quad (4.46)$$

where

- f is an unknown scalar function defined over interior of Ω .
- f^* is a known scalar function that provides the desirable values on the boundary $\partial\Omega$.
- $\nabla^2 = (\frac{\partial^2}{\partial x^2}, \frac{\partial^2}{\partial y^2}, \frac{\partial^2}{\partial z^2})$ is Laplacian operator.
- w is a Guidance Vector Filed and $\nabla \cdot w = \frac{\partial w_x}{\partial x} + \frac{\partial w_y}{\partial y} + \frac{\partial w_z}{\partial z}$ is the divergence of $w = (w_x, w_y, w_z)$.

Thus it can be defined as least-squares minimization problem:

$$\min_f \int \int_{\Omega} |\nabla f - w|^2 \quad \text{with } f|_{\partial\Omega} = f^*|_{\partial\Omega} \quad (4.47)$$

A discrete vector field on a triangle mesh is defined to be a piecewise constant vector function whose domain is the set of point on the mesh surface. A constant vector is defined for each triangle, and this vector is coplanar with the triangle. For discrete vector field w on a mesh, its divergence at vertex v_i can be defined to be

$$(\text{div } w)(v_i) = \sum_{T_k \in N(v_i)} \nabla B_{ik} \cdot w|_{T_k} \quad (4.48)$$

where N_i is the 1-ring vertices of v_i , $|T_k|$ is the area of triangle T_k , and ∇B_{ik} is the gradient vector of B_i within T_K .

The discrete gradient of the scalar function f on a discrete mesh is expressed as

$$\nabla f(v) = \sum_i f_i \nabla \phi_i(v) \quad (4.49)$$

with $\phi_i(\cdot)$ being the piecewise linear basis function valued 1 at vertex v_i and 0 at all other vertices and f_i being the value of f at v_i and it is one of the coordinates of v_i . The discrete Laplacian operator can be determined as follows

$$\Delta f(v_i) = \frac{1}{2} \sum_{v_j \in N_i} (\cot \alpha_{i,j} + \cot \beta_{i,j})(f_i - f_j) \quad (4.50)$$

where $\alpha_{i,j}$ and $\beta_{i,j}$ are the two angles opposite to edge in the two triangles sharing edge $(v_i$ and $v_j)$ and N_i is the set of the 1-ring vertices of vertex v_i , see Figure 4.12. Finally the discrete Poisson equation is expressed as follows: $\nabla^2 f \equiv \text{div}(\nabla f) = \nabla w$

Discrete Poisson equation with Dirichlet boundary condition can be defined by the sparse linear system. It can be represented as the following form:

$$Ax = b \quad (4.51)$$

where the coefficient matrix A is determined by Eq.4.50 and the vector b is determined by Eq.4.48 and unknown vector x is the coordinate of all vertices on the patch mesh.

The smooth and accurate patch mesh is constructed as follows: *First*, Compute the gradient of each new vertex on the adjacent triangle by using Eq.4.49. *Next*, calculate the divergence of every boundary vertex by using Eq.4.48 *then*, determine the coefficient matrix A by Eq.4.50. Vector b in this equation is determined by using the divergence of all boundary vertices.

Finally, solve the Poisson equation and obtain the new coordinate of all vertices of the patch mesh.

Chapter 5

Alignment of the scanned foot with shoe last data base

5.1 Introduction

With recent improvement of in the methods for the acquisitions and rendering of 3D models, the method for retrieval of models from large repositories of 3D shapes has gained prominence in the graphic and vision communities. A variety of methods have been proposed that enable the efficient querying of model repositories for a desired 3D shape. Many of these methods use a 3D models as query and attempt to receive models from the data base that have a similar shape.

One of the specific challenges in matching 3D shapes arise from the fact that in many application, models should be considered to be same if they differ by a similarity transformation. Thus in order to match two models, a measure of similarity needs to be computed at the optimal transformation, scale and rotation. A general approaches for alignment of 3D client foot scan with shoe last data base is described in this chapter.

5.2 Problem Description

Triangle mesh models are used for representation of objects can be generated using a variety of techniques which is described in chapter 3. 3D-model are given in arbitrary orientation, scales and positions in 3D-space R^3 . 3D model alignment can be defined in such a way that invariance with respect to translation, rotation, scaling and reflection (flipping) of mesh.

An example of pose estimation (normalization) is depicted in figure 5.1. Three 3D-models of shoe last are shown in the original position, orientation, and scale(a, b, c), while the canonical frame are displaced in the second row(d, e, f). The models are aligned parallel with x-y space.

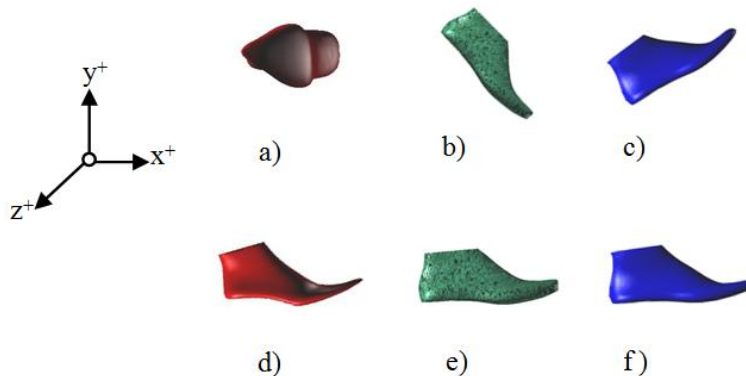


Figure 5.1: Models of shoe last are initially given in arbitrary units, position, and orientation (a, b, and c). The out come of the pose estimation procedure is the canonical positioning of each model (d, e, and f) which is parallel with x-y space.

There have been several approaches for estimating the pose of a 3D model The most prominent tool for solving the problem is the Principal Component Analysis (PCA)[62], also known as the discrete Karhunen-Loeve transform, or the Hotelling transform, which is described in details in section 5.3. Since applying the PCA to the set of vertices of a mesh model can produce undesired normalization results, the modification of the PCA are given in this chapter. We will present "weighted" principal component analysis (WPCA) for alignment of 3D foot scan of client with

shoe last data base.

Pose estimation of a 3D-mesh model based on the Extended Gaussian Images (EGIs) is one of the first approaches reported in the literature. An EGI defines a function on a unit sphere, by using normal vectors of faces of the mesh. The method is sensitive to polygon tessellations of a 3D-shape, noise, and face orientation. More details about the technique can be found in [62].

In [75], the pose estimation is also based on the PCA wherein the underlying 3D-model is supposed to be a solid. However, 3D-models are not guaranteed to consist of closed surfaces bounding one or more solids, and it would be a difficult and questionable undertaking to enforce objects to be solids by stitching up surfaces with boundaries. Therefore, the approach is suitable only for a small class of 3D models. The other significant drawback lies in the fact that the procedure is timeconsuming.

We consider that the pose normalization should be both efficient and effective. Also, meshes in different levels-of-detail representing the same real-world object, should be reasonably aligned in the canonical frame.

5.3 Pricipal Componentet Analysis

The principal component analysis(PCA)[102, 36, 76], is widely used in signal processing, statistics(data analysis), compression, and neural computing. In some applications areas, the PCA also called the(discrete) Karhunen-loeve transform, or Hotelling transform. The following presentation of the original PCA analysis is adapted from [36]. The PCA is based on the statistical representation of random variable. Suppose we have finite set of data vectors V , where

$$V = \left\{ v \mid v = (v_1, v_2, \dots, v_n) = [v_1, v_2, \dots, v_n]^T \in R^n, n \in N \right\} \quad (5.1)$$

Let m_v be mean of the set V

$$m_v = E \{V\} = \frac{1}{|V|} \sum_{v \in V} v \quad (5.2)$$

Where $|V|$ denotes the number of elements of set V (i.e, the cardinal number). The associated covariance matrix of the same data set is given by

$$C_v = [c_{ij}]_{n \times n} = E \{(v - m_v)(v - m_v)^T\} = \frac{1}{|V|} \sum_{v \in V} (v - m_v)(v - m_v)^T \quad (5.3)$$

matrix C_v is, by definition, symmetric real matrix with non-negative elements. Elements $c_{ij}(i \neq j)$ represent the covariance between the components v_i and v_j (5.1). If two components v_i and v_j of the data are uncorrelated, then their covariance is zero ($c_{ij} = c_{ji} = 0$). The element c_{ij} represents the variance of the component v_i , which indicates the spread of the component value around its means value. Eigenvalues and eigenvectors of the covariance matrix are used to form an orthogonal basis of the space R^n . We recall that the eigenvectors $e_i(\|e_i\| = 1)$ and the corresponding eigenvalues λ_i are the solutions of equations

$$C_V e_i = \lambda_i e_i \quad (i = 1, \dots, n) \quad (5.4)$$

We stress that in the case of a symmetric non-negative matrix all eigenvalues are non-negative real numbers. By ordering the eigenvectors according to the order of descending eigenvalues, we obtain an orthonormal basis with the first eigenvector coinciding with the direction of largest variance of the set V . Directions of largest variance are usually regarded as directions in which the original data set possesses the most significant amounts of energy.

Let A be a matrix consisting of ordered eigenvectors of the covariance matrix as the row vectors. The ordered eigenvectors can be seen as basis of a new coordinate frame with the origin placed at the point m_v . We regard the new coordinate system as the PCA coordinate system (frame). A data

vector $v \in V$ from the original system is transformed into the vector p in the PCA frame

$$p = A(v - m_V) \quad (5.5)$$

In the PCA frame data are uncorrelated, i.e., the non-diagonal elements of the covariance matrix are equal to zero. Before explaining how we engage the PCA for 3D-model alignment purposes, we present application of the PCA in data compression and image processing.

Data can be compressed using the PCA in the following manner. The original vector v , which is projected on the coordinate axes of the PCA frame (5.6), can be reconstructed by applying an affine map to the projection p given by,

$$v = A^T p + m_V \quad (5.6)$$

where we used the property of an orthogonal matrix $A^{-1} = A^T$ (A^T denotes the transpose of matrix A). If we do not use all the eigenvectors of the covariance matrix, the data can be represented in a lower dimensional space, whose dimension is determined by the number of used eigenvectors, i.e., basis vectors of the orthonormal basis.

Let A_k be the matrix consisting of the first k (ordered) eigenvectors as the row vectors. By substituting A with A_k in equation(5.5), we obtain

$$p = A_k(v - m_V) \quad \text{and} \quad \hat{v} = A_k^T P + m_V \quad (5.7)$$

Hence, we project the original data vector from an n -dimensional linear metric space R^n on a new k -dimensional vector space R^K , whose orthonormal basis consists of the first k eigenvectors of the covariance matrix. Then, we perform a kind of reverse transform. However, we cannot reconstruct the original data vector, i.e., $\hat{v} \neq v$ because the matrix A_k of the matrix $k \times n$ possesses the following properties:

$A.A^T = I_k$, but $A^T.A \neq I_n$, where I_n denotes the identity matrix of type $n \times n$. We regard \hat{v} as approximation of v , which is represented in a lower

dimensional space. If we choose $K \ll n$ then the original data is compressed by the factor of k/n . It can be proven [102] that described linear dimension reduction technique is optimal in mean square scene. In other words, the mean-square error between the original data v and the reconstructed data \hat{v} obtained by using a given number of eigenvectors is minimized.

Data compression using the PCA possesses the following useful properties:

- The computational costs of the subsequent processing steps are reduced.
- The presence of noise in original data will be reduced, because the directions of largest spreads (the first components) are more robust to noise than directions of lowest variance
- By setting $k = 3$ (or $k = 2$), a high-dimensional space is projected so that data can be visualized.

The value of sorted eigenvalues $\lambda_1 \geq \lambda_2 \geq \dots \geq \lambda_n$ carry a useful information. Namely, the value of λ_i is proportional to the variance (energy) along the direction determined by the eigenvector e_i . For applications in which a varying amount of energy of the original data should be preserved, we simply fix the number of used eigenvectors. Alternatively, the total amount of energy carried by the first k eigenvectors can be used to determine the dimensionality. For instance,

$$k = \max \left\{ j \mid \sum_{i=1}^j \lambda_i \leq t \sum_{i=1}^n \lambda_i \right\} \quad (5.8)$$

where $t \in [0, 1]$ is a threshold. In this case, the total amount of energy (information) is approximately consistent with a varying dimensionality k .

Thus, dealing with a lossy compression gained by the PCA introduces a trade-off between the reduction of vector dimension (we want to simplify

the representation as much as possible) and the loss of information (we want to preserve as much as possible of the original information content). The PCA offers convenient mechanisms (fixed k vs. fixed t) to control this trade-off.

Properties of the PCA can be depicted using an application in image processing. Suppose that we have a color image of dimensions $M \times N$. Each pixel is represented by a triplet of red, green, blue(RGB) component values. We consider that each image consists of three band, i.e., three gray scale images each of which is represents pixel values of the corresponding color. If we want to generate a single grayscale image so that the most details are shown, then we apply the PCA to the set of 3D points, which are obtained by treating color triplets of pixels as points in R^3 .

An example of RGB image and the outcome of PCA are shown in figure 5.2. Pixels of the given image are represented as points in a 3D space, where x , y , and z represent values of red, green and blue componenets, respectively. The first eigenvalue (P_1) having the largest eigenvalue points to the direction of largest variance(spread) whereas the second (P_2) and the third (P_3) eigenvectors are orthogonal to the first one.

In this example the first eigenvalue corresponding to the first eigenvector

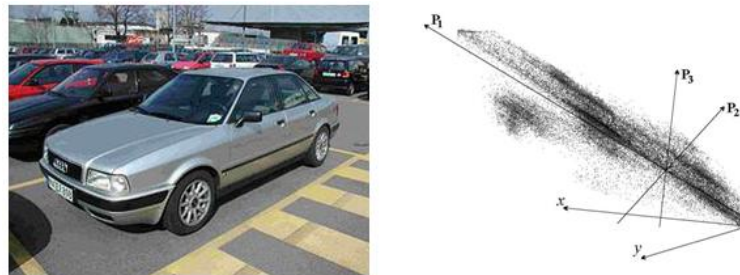


Figure 5.2: The analyzed image (left) and the pixels of the image in the color space (right). Axes x , y , and z represent values of red, green, and blue components, respectively. The PCA coordinate axes are denoted by P_1, P_2 and P_3

is $\lambda_1 = 9211.79$ while other eigenvectors are $\lambda_2 = 437.38$ and $\lambda_3 = 74.29$. Hence, the first eigenvector contains almost all energy. This means that

the data could be well approximated with one-dimensional representation. The result is depicted in figure 5.3. In the first row, red, green, and blue bands of the original image (figure 5.3) are represented by grayscale images. The first image in the second row (P_1) is created by normalizing the first coordinate of each point in the PCA frame.

In this example, we deal with 8-bit gray scale and the pixel values are normalized so that the lowest value of the first PCA coordinate is mapped to 0, the highest to 255, while the values in between are proportionally set. The last two images in figure 5.3 are obtained analogously.

The example of finding largest spreads of a point set (right-hand side in figure 5.2) suggests an analogous application to the point set I of a mesh model.

5.4 Modifications of the PCA

We may apply PCA to sets of 3D point-clouds, but different sizes of triangle meshes cannot be considered. In order to account for different sizes of triangle Paquet et al. [77] established weights associated to center of gravity of triangles and Vranic et al. [106] used weighting factors associated to vertices. These two methods showed improvements if compared to the classical PCA. The "weighted" PCA analyses were designed to approximate the PCA of the whole point set of the model. All the models should be aligned at equal position, in order to have equivalent cross sections from center of mass of each model towards the heel and toe. To achieve the alignment we described the main steps and details of "weighted" PCA in the next section. First, we applied Step 1 through Step 3 for the first model in shoe last data base (See Figure 5.3). Then, for alignment of another models with the first model we applied Steps 1, 2, 4, 5. See Figure 5.4.

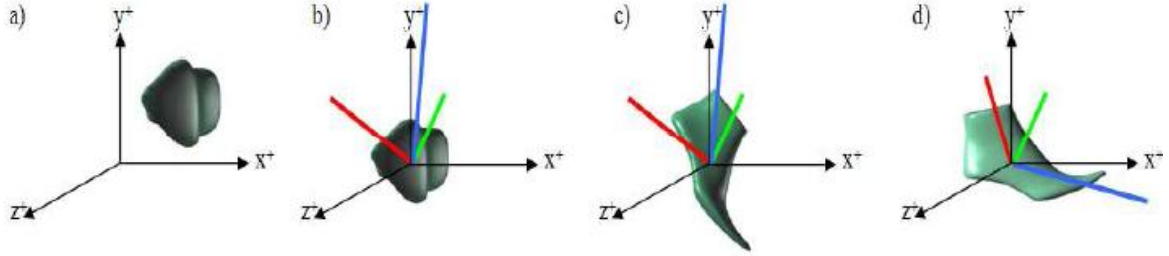


Figure 5.3: *a)* Input 3D smooth triangle. *b)* Translated center of gravity to the origin. The red, green and blue lines are eigenvectors. *c)* Rotated 3D model with its eigenvectors. *d)* Target model.

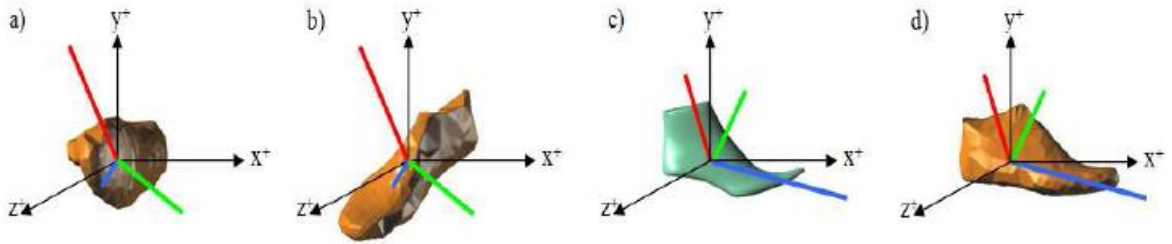


Figure 5.4: *a)* Translated center of gravity to the origin. *b)* Rotated 3D foot model. *d)* The alignment of 3D foot in b with shoe last in c.

Let $T = \{t_1, \dots, t_n\}$ ($t_i \subset \mathbb{R}^3$) be a set "triangle mesh" $V = \{v_1, \dots, v_n\}$ ($v_i = (x_i, y_i, z_i) \in \mathbb{R}^3$) be a set of "vertices" associated to triangle mesh and c be the "center of gravity" of the model.

Step1. Translate center of gravity to the origin and create a new list of vertices, I , such that:

$$c = \sum_{i=0}^n \frac{v_i}{n} \quad (5.9)$$

$$I = \{V_1 - c, \dots, V_n - c\} \quad (5.10)$$

Step 2. Let A be the total sum of the areas of all triangles in the mesh, let A_k be the area of triangle k within the mesh, let ct_i "center of gravity of each triangle" and ct the total sum of "center of gravity" of all of triangles

in mesh. The covariance matrix $3 * 3$ is determined by:

$$ct = \frac{\sum_{i=0}^n ct_i}{n} (ct = (x_i, y_i, z_i \in R^3)) \quad (5.11)$$

$$CM = \begin{pmatrix} Cov_{xx} & Cov_{xy} & Cov_{xz} \\ Cov_{yx} & Cov_{yy} & Cov_{yz} \\ Cov_{zx} & Cov_{zy} & Cov_{zz} \end{pmatrix} \quad (5.12)$$

$$Cov_{xx} = \frac{\sum_{i=0}^n A_i (ct_i - ctx)(ct_ix - ctx)}{A} \quad (5.13)$$

Covariance matrix CM is a symmetrical real matrix, therefore its eigenvectors are positive real numbers and orthogonal. We sort eigenvalues in decreasing order to find the corresponding eigenvectors and to scale them in Euclidean unit lengths. The rotational matrix R is constructed with eigenvectors in rows. We apply this matrix to all of the vertices of a triangle and we form a new vertex sets called:

$$I' = \{R \times I_1, \dots, R \times I_n\} \quad (5.14)$$

Step3. Rotate first shoe last with its eigenvectors in figure 5.3.c up to a position where the foot shape becomes parallel with $x - y$ space, see figure 5.3.d. Record the new position of these 3 eigenvectors in the file as the origin matrix, O_{em}

$$CM = \begin{pmatrix} OrgionEig_1x & OrgionEig_2x & OrgionEig_3x \\ OrgionEig_1y & OrgionEig_2y & OrgionEig_3y \\ OrgionEig_1z & OrgionEig_2z & OrgionEig_3z \end{pmatrix} \quad (5.15)$$

step 4. Let matrix N_{em} be transpose of a matrix R and O_{em} be the origin matrix that is recorded in step 3. The alignment is accomplished by constructing a rotation matrix R' through the following formula:

$$R' = O_{em} \times N_{em} \quad (5.16)$$

step 5. Get the matrix R' in Step 4 and apply it to all I' . New point sets I'' are calculated, See figure 5.4.

$$I'' = \{R'_1 \times I'_1, \dots, R'_n \times I'_n\} \quad (5.17)$$

5.5 Search for similarity estimation

The similarity search algorithm is based on the cutting foot triangle mesh into several sections towards the heel and the toe. Then the area of each section (available contour) is calculated and compared with the area of equal sections in shoe last data base. Let M be the mesh structure of the model. A triangular mesh is defined as a set of vertices and a set of edges and triangles that join these vertices. The two triangles which share a common edge are called adjacent triangles. The model consists of three list V, E, T as follows: Triangle list consists of 3 edges, edges list consists of 2 vertices and adjacent triangles and Vertex list consists of coordinates in 3D $v_i = (x_i, y_i, z_i) \in R^3$ is illustrated these basic concepts see figure 5.6.

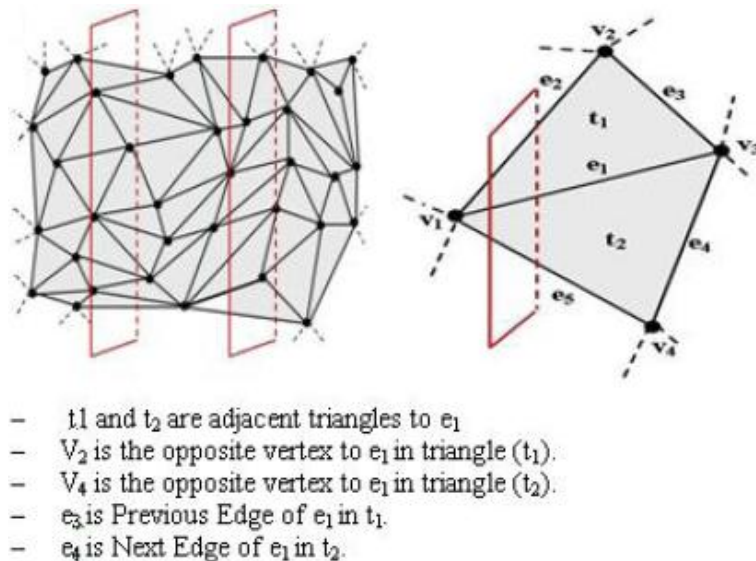


Figure 5.5: Preliminaries related to triangle mesh with intersection planes for cutting shape to several sections.

The algorithm has the following steps summarized in Figure 5.7.

Step 1: Find the intersection of the cutting plane with the edge of a triangle and create new vertex.

Step 2: Choose the edge with the endpoints on the opposite sides of the intersection points.

Step 3: Find the next edge and the previous edge of the current edge.

Step 4: Build a new edge between the intersection point and the opposite vertices of the current edges triangles.

Step 5: Build a new triangle between the new edges.

Step 6: Update the triangles and vertices of the current edge.

Step 7: Add the new triangle and the edge to the list.

The output of our algorithm is set of vertices and edges related to each contour as illustrated in Figure 5.7.

Let $V_c = v_1; \dots; v_n (v_i = (x_i; y_i; z_i) \in R^3)$ be a set of "vertices" and $E_c = \{e_1; \dots; e_n\}$ the set of "edges" associated to the contours.

Step 1: Let c_c be center of gravity of contour determined as follow:

$$c_c = \frac{\sum_{i=0}^N V c_i}{N} \quad (c_c = x_i, y_i, z_i \in R^3) \quad (5.18)$$

Step 2: For calculating the area of each contour. We divide the vertices of contours edge and center of gravity of contour in triangles. Let A_i be the area of each associated triangle in the contour and N be the number of triangles that associated with edges and center of gravity of contour. The area of each contour can be calculated as follow:

$$A = \sum_{i=0}^N A_i \quad (5.19)$$

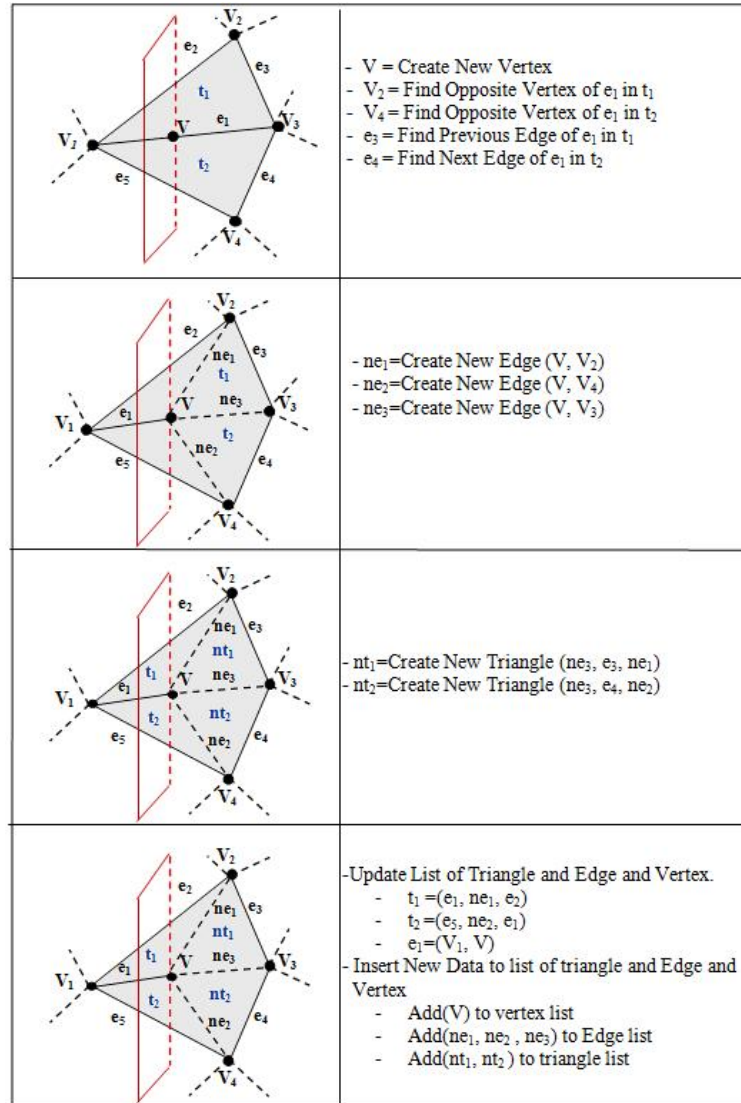


Figure 5.6: Steps for cutting shape to several sections.

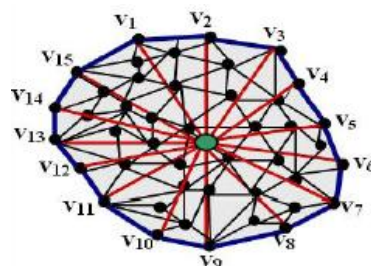


Figure 5.7: The illustrated contour after cutting mesh.

Chapter 6

Conclusion

As consumers are becoming increasingly selective of what they wear on their feet, footwear manufacturing industry encountered the problem of developing footwear which is fulfils consumers requirement better than its computerise. Thus production of custom tailored product is widely required in manufacturing industry nowadays and the business paradigm is moving from producer- centered productivity to consumer-centered customization.

Very few standards exist for finding products to people. Footwear fit is a noteworthy example for consumer consideration when purchasing shoes. Thus mass customization starts with understanding individual customers requirements and it finishes with fulfilment process of satisfying the target customer with near mass production efficiency.

Loose shoes (even thought function may be impaired) are not as uncomfortable as when the shoes are tight. Unlike any other consumer product, personalized footwear or the matching of footwear to feet is not easy if delivery of discomfort is predominantly by a shoe that has designed unsuitable for the particular shape of foot. Properly constructed footwear contribute to fit and comfort . The design of new shoes starts with the design of the new shoe last.

Traditionally, foot dimensions are measured using some devices such as the Ritz Stick device, the Brannock device, the Scholl device; callipers and tapes are also used for measurement of foot dimensions. Foot measuring always takes a lot of time and shoe making industry in order to make an accurate custom shoe last, must manually measure the specific consumers foot, and sometimes, more than thirty measurement are required. The last is also manually manufactured by experienced last maker. Thus the process of foot measuring and last manufacturing process and custom footwear is expensive to produce and time-consuming because of the complexity constraints imposed by footwear manufacturing process. Nowadays, the combination of 3D scanning system with mathematical technique makes it possible, automating the process of producing custom tailored footwear based on consumers foot shape.

We presented an approaches for addressing the computerize footwear fit customization in industry problem. The basic idea of solution is to compare the lasts which were used to manufacture the shoes and the scanned feet of the clients.

During the surface reconstruction process, a mesh is calculated from cloud points. Depending on both the complexity of the object to be reverse engineered and the adopted data acquisition system technology (e.g. coordinate measuring machines or laser scanning), some areas of the object outer surface may never be accessible. This induces some deficiencies in the point cloud and a set of holes in the triangle mesh. This defficiency is not acceptable when the 3D model is taking into actual application. Thus certain repair must be done before taking these models into actual application.

We presented robust algorithm for filling hole in triangle mesh .Our algorithm is based on the advancing front mesh technique to cover the hole, modifying the triangles in the initial patch mesh by estimating Harmonic

normals instead of relocating them directly and the Poisson equation according to desirable normal and boundary vertices of the hole to optimize the missing geometry more accurately. After obtaining complete 3D model, the result data must be generated and aligned.

One of the specific challenges faced in the area of shape matching is that a shape and its image under a similarity transformation are considered to be the same.

The most prominent tool for solving the problem is the Principal Component Analysis (PCA). PCA also is known as the discrete Karhunen-Loeve transform, or the Hotelling transform aligns a model by considering its centre of mass as the coordinate system origin, and its principle axes as the coordinate axes. The purpose of the PCA applied to a 3D model is to make the resulting shape feature vector independent to translation and rotation as much as possible. By applying the PCA to a set of vertices of a 3D-mesh, different sizes of triangles are not taken into account. Thereby we presented Weight Principal Components Analysis (WPCA) for alignment of 3D-mesh model. After these substantial post processing methods, the 3D foot model is ready for sophisticated modelling operations. Our new approach will be based on the efficient algorithm for cutting 3D triangle mesh to several sections toward heel and toe. Then the area of each contour is calculated and compared with area of equal section in shoe last data base for finding footwear fit .

Bibliography

- [1] A.Baader and G.Hirzinger. "*Three-dimensional surface reconstruction based on a self-organizing feature map*". pp. 273-278. In Proc. 6th Int. Conf. Advan. Robotics, Tokyo, 1993.
- [2] A.Baader and G.Hirzinger. "*A self-organizing algorithm for multi-sensory surface reconstruction*". In International Conf. on Robotics and Intelligent Systems IROS'94, Munich,. Computer Graphics forum, 1994.
- [3] A.Ullrich, N.Studincka, J.Riegl, and S.Orlandini. "*Longrange High performance time-of-flight-based 3d imaging sensors*". pp.852-855. in: 3D Data Processing Visualization and Transmission, Padova, Italy,, 2002.
- [4] B.Curless and M.levoy. "*A volumetric method for building complex models from range images*". pp. 30312,. In: Processing of siggraph,, 1996.
- [5] B.Guo, J.Menon, and B.Willette. "*Surface reconstruction using alpha-shapes.*". 16(4), pp. 177-190. Computer Graphics forum, 1997.
- [6] F. Blais. "*Review of 20 years of range sensor development*". Journal of Electronic Imaging, 13(1):231240, January 2004.

- [7] B.M.Nigg, G.Frei, B.Segesser, and B.Weber. "*Bewegungsanalyse fr Schuhkorrekturen (Movement analysis for shoe corrections)*". Medita 9a:160-163, 1977.
- [8] Brannock. <http://www.brannock.com/>, 2006.
- [9] C.Bajaj and D.Schikore. "*Error-bounded reduction of triangle meshes with multivariate data.*". pp. 34-45. In Proceedings of SPIE Symposium on Visual Data Exploration and Analysis III, 1996.
- [10] C.Bajaj, F.Bernardini, and G.Xu. "*Automatic reconstruction of surfaces and scalar fields from 3d scans*". pp. 109-118. Computer Graphics Proceedings, SIGGRAPH'95, Annual Conference Series, 1995.
- [11] C.Bajaj, F.Bernardini, and G.Xu. "*Reconstructing surfaces and functions on surfaces from unorganized 3d data*". Algorithmica, 19, pp. 243-261. 1997.
- [12] C.COLLAZZO. "*A 1986 1987 study of consumer problems in shopping for foot wear , with emphasis on size and fit*". 16(4), 421 424. Journal of Testing and Evaluation, 1988.
- [13] C.matabosch, J.Salvi, and J.Forest. "*Stereo rig geometry determination by fundamental matrix decomposition*". pp.405-412. in workshop on European Scientific and industrial collaboration, 2003.
- [14] M. W. Cox and R. Alm. "*The right stuff; America's move to mass customization*". 3-26. Annual Report, 1998.
- [15] B. Curless. "*From range scans to 3D models*". 33(4). Computer Graphics,, 1999.
- [16] D.Attali. "*r-regular shape reconstruction from unorganized points*". pp. 248-253. In ACM Symposium on Computational Geometry, Nice, France, 1997.

-
- [17] S. Davis. *"From future perfect: Mass customizing"*. 17 (2), 16-21. Planning Review, 1989.
- [18] T. K. Dey and J.Giesen. *"Detecting undersampling in surface reconstruction"*. pp.257-263. Proc. of 17th ACM Sympos. Comput. Geometry, 2001.
- [19] D.Ruprecht and H.Muller. *"Spatial free form deformation with scattered data interpolation methods"*. 19, pp. 63-71. Computers and Graphics, 1995.
- [20] D.Terzopoulos, A.Witkin, and M.Kass. *"Constraints on deformable models: Recovering 3d shape and nonrigid motion"*. 36, pp. 91-123. Artificial Intelligence,, 1988.
- [21] D.Terzopoulos and D.Metaxas. *"Dynamic 3d models with local and global deformations: Deformable superquadrics"*. 13(7), pp. 703-714. IEEE Transactions on Pattern Analysis and Machine Intelligence, 1991.
- [22] E.Bittar, N.Tsingos, and M-P.Gascuel. *"Automatic reconstruction of unstructured data: Combining a medial axis and implicit surfaces"*. 14(3), pp. 457-468. Computer Graphics forum,, 1995.
- [23] M. Eck, T. D. DeRose, T. Duchamp, H. Hoppe, M. Lounsbery, and W. Stuetzle. *"Multiresolution analysis of arbitrary meshes"*. pages 173-182. In Proceedings of SIGGRAPH, 1995.
- [24] Weller F. *"Stability of voronoi neighborhood under perturbations of the sites"*. In Proceedings 9th Canadian Conference on Computational Geometry, 1997.

- [25] F. Bernardini and C. Bajaj. "*Sampling and reconstructing manifolds using alpha-shapes.*". In Proc. of the Ninth Canadian Conference on Computational Geometry, 1997.
- [26] F. Bernardini, C. Bajaj, J. Chen, and D. Schikore. "*Automatic reconstruction of 3d cad models from digital scans*". Technical Report CSD-97-012, Department of Computer Sciences, Purdue University, 1997.
- [27] E. Feitzinger and H. Lee. "*Mass customization at Hewlett-Packard: The power of postponement*". 75 (1), 116-121. Harvard Business Review, 1997.
- [28] E. Feitzinger and H. Lee. "*Mass customization at Hewlett-Packard: The power of postponement*". 75 (1), 116-121. Harvard Business Review, 1997.
- [29] F. Isselhard, G. Brunnett, and T. Schreiber. "*Polyhedral reconstruction of 3d objects by tetrahedra removal*". 288-97. Technical report, Fachbereich Informatik, University of Kaiserslautern, Germany, 1997.
- [30] M. S. Floater. "*Parameterization and smooth approximation of surface triangulations.*". 14(3):231-250. Computer Aided Geometric Design, 1997.
- [31] F. Preparata and M. Shamos. "*Computational Geometry: An Introduction*". Springer Verlag, 1985.
- [32] F. S. Nooruddin and G. Turk. "*Simplification and repair of polygonal models using volumetric techniques,*". vol. 9(2), pp. 191-205. IEEE Transactions on Visualization and Computer Graphics, 2003.

- [33] G.Herman and H.Liu. "*Three-dimensional displays of human organs from computed tomograms*". 9, pp. 1-21. Computer Graphics and Image Processing, 1979.
- [34] J. Gilmore and J. Pine. "*The four faces of mass customization*". 75 (1),91-101. Harvard Business Review, 1997.
- [35] G.Li and A.Jneja. "*A morphing-based surface blending operator for footwear cad*". Proceeding of International Mechanical Engineering Congress and Exposition, 2004.
- [36] R. C. Gonzalez and R. E. Woods. "*Digital image processing*". Addison Wesley. 2001.
- [37] R. S. Goonetilleke and A.Luximon. "*Designing for Comfort: A Footwear Application*". Proceedings of the Computer-Aided Ergonomics and Safety Conference '01, Maui, Hawaii. Plenary session paper, 2001.
- [38] G.Roth and E.Wibowoo. "*An efficient volumetric method for building closed triangular meshes from 3d image and point data*". pp. 173-180. In Graphics Interface'97,, 1997.
- [39] M. Haglind and J. Helander. "*Development of value networks- an empirical study of networking in Swedish manufacturing industries*". pp. 350-358. Proceedings of the International Conference on Engineering and Technology Management, 1999.
- [40] M.R Hawes and D. Sovak. "*Quantitative morphology of the human foot in a north American population*". 37, 12131226. Ergonomics, 1994.

- [41] H.Edelsbrunner. "*Weighted alpha shapes*". Technical Report UIUCDCS-R-92-1760, Department of Computer Science, University of Illinois at Urbana-Champaign, Urbana, Illinois,, 1992.
- [42] H.Edelsbrunner and E.Mucke. "*Three-dimensional alpha shapes*". 13(1), pp. 43-72. ACM Transactions on Graphics, 1994.
- [43] H.Hoppe, T.DeRose, T.Duchamp, J.McDonald, and W.Stuetzle. "*Surface reconstruction from unorganized points*". Computer Graphics, 26(2), pp. 71-78. Proceedings of Siggraph'92, 1992.
- [44] H.Hoppe, T.DeRose, T.Duchamp, J.McDonald, and W.Stuetzle. "*Mesh optimization*". In Computer Graphics Proceedings, Annual Conference Series, pp. 21-26,. Proceedings of Siggraph'93, 1993.
- [45] Univ. of Washington H.Hoppe. "*Surface Reconstruction from Unorganized Points*". PhD thesis, 1994.
- [46] H.Hu, Z.Li, J.Yan, X.wang, H.Xiao, J.Duan, and L.Zheng. "*Anthropometric measurement of the Chinese elderly living in the Beijing area*". 37: 303-311. International Journal of Industrial Ergonomics, 2007.
- [47] K. Hormann. "*Theory and Applications of Parameterizing Triangulations*". PhD thesis, Department of Computer Science, University of Erlangen, 2001.
- [48] J-D.Boissonnat. "*Geometric structures for three-dimensional shape representation*". 3(4), pp. 266-286. ACM Transactions on Graphics,, 1984.
- [49] D.J. Janisse. "*The art and science of fitting shoes*". 13(5): 257-62. Foot Ankle, 1992.

- [50] J.Davis, SR.Marschner, M.Garr, and M. Levoy. "*Filling holes in complex surfaces using volumetric diffusion*". In: Processing of the first international symposium on 3D data, visualization and transmission, 2002.
- [51] J.Forest and J.Salvi. "*An overview of laser slit 3d digitizers*". pp.73-78. in: International Conference on Robots and Systems,Lausanne,, 2002.
- [52] J.Hoschek and D.Lasser. "*Fundamentals of Computer Aided Geometric Design*". A.K. Peters, 1993.
- [53] J. Jiao, M. Tseng, V. Duffy, and F. Lin. "*Product family modeling for mass customization*". 35(3-4). Computers and Industrial Engineering, 1998.
- [54] J.J.Gibson. "*The perception of the visua world*". Hoghton Mifflin, boston, 1950.
- [55] J.Miller, D.Breen, W.Lorensen, R.O'Bara, and M.Wozny. "*Geometrical deformed models: a method for extrcting closed geometric models from volum data*". pages 217-226. Proceeding of SIGGRAPH. Computer Graphics, 1991.
- [56] J.Miller, D.Breen, W.Lorensen, R.O'Bara, and M.Wozny. "*Geometrically deformed models: A method for extracting closed geometric models from volume data*". pp. 217-226. Proceedings of SIGGRAPH'91, 1991.
- [57] P. Johansson and J. Olhager. "*Linking productprocess matrices for manufacturing and industrial service operations*". 104, 615-624. International journal of production economics, 2006.

- [58] J.Tohline. "Origin of the poisson equation,".
<http://www.phys.lsu.edu/astro/HBook:current=Context=PGE=poisson.origin.text.pdf>.
- [59] J.Y.Wang. "Imaging laser radar - an overview. , 1986.". In Proceedings of the 9th International Conference on laser, pages 19-29, 1986.
- [60] J.Z.Zhu, O.C.Zienkiewicz, H.HInton, and J.Wu. "A new approach to development of automatic quadrilateral mesh generation". Int.j.nummer,method. Int.j.nummer,method, 1991.
- [61] P. Kanchanasevee, G. Biswas, K. Kawamura, and S. Tamura. "Contract-net based scheduling for holonic manufacturing systems". 3203, 108-115. Proceedings of the SPIE - The International Society for Optical Engineering, 1999.
- [62] S. B. Kang and K. Ikeuchi. "-D Object Pose Determination Using Complex EGI,". Tech. Rep. CMU-RI-TR-90-18, The Robotics Institute, Carnegie Mellon University, Pittsburgh, Pennsylvania,. 1990.
- [63] K.Kimk, K.lee, and T.Hwang. "A grouping algorithm for custom-tailored products". pp. 618625. Journal of Materials Processing Technology, 2002.
- [64] W. Klingenberg. "A Course in Differential Geometry". Springer, Berlin, Heidelberg,, 1978.
- [65] S. Kotha. "Mass Customization: Implementing the Emerging Paradigm for Competitive Advantage". vol. 16 (special issue), pp. 2142. Strategic Management Journal, 1995.

- [66] S. kotha. "*Mass-customization: a strategy for knowledge certain and organizational learning*". 11 (7/8), 846-858. International Journal of Technology Management, 1996.
- [67] E. Kreyszig. "*Differential Geometry*". Dover, New York,, 1991.
- [68] J. Lampel and H. Mintzberg. "*Customizing customization*". 38,21-30. Sloan Management Review, 1996.
- [69] R. Lau. "*Mass customization: The next industrial revolution*". 37 (5), 18-19. Industrial Management, 1995.
- [70] L.Kobbelt, S.Campagna, J.Vorsatz, and H-P.Seidel. "*Interactive multiresolution modeling on arbitrary meshes*". pp. 10514,. In: Proceedings of SIGGRAPH, 1998.
- [71] M-E.Algorri and F.Schmitt. "*Surface reconstruction from unstructured 3d data*". Computer Graphics forum, 15(1), pp. 47-60,, 1996.
- [72] M.Levoy, J.Ginsberg, J.Shade, D.Fulk, K.Pulli, B.Curless, S.Rusinkiewicz, D.Koller, L.Pereira, M.Ginzton, S.Anderson, and J.Davis. "*The digital Michelangelo project: 3D scanning of large statues*". 131144. Conference on Comp. Graphics and Inter. Techniques, 2000.
- [73] M.Mochimaru, M.Kouchi, and M.Dohi. "*Analysis of 3d human foot forms using the free form deformation method and its application in grading shoe lasts*". vol. 43, no. 9, pp. 13011313. Ergonomics, 2000.
- [74] F. T. Cheng nad D. B.Perng. "*A Systematic Approach for Developing a Foot Size Information System for Shoe Last Design*". vol. 25, pp. 171-183. International Journal of Industrial Ergonomics, 1999.
- [75] M. Novotni and R. Klein. "*A Geometric Approach to 3D Object Comparison,*". pp. 167-175. in Proc. SMI 2001, Genova, Italy, 2001.

- [76] E. Paquet and M. Rioux. "*nefertiti: a query by content system for threedimensional model and image databases management*". 17:157. Image and Vision Computing,, 1999.
- [77] E. Paquet, M. Rioux, A. Murching, T. Naveen, and A. Tabatabai. "*Description of Shape Information for 2-D and 3-D Objects*". 16(1-2):103-122. Signal Processing: Image Communication, 2000.
- [78] J. Pine. "*Mass customizing products and services*". 21 (4),6-13. Planning Review, 1993.
- [79] U. Pinkall and K. Polthier. "*Computing discrete minimal surfaces and their conjugates.*". 2(1):15-36. Experimental Mathematics, 1993.
- [80] P.Liepa. "*Filling holes in meshes,*". vol. 23, pp. 2005. In: Proceedings of the eurographics/ACM SIGGRAPH symposium on geometry processing, 2003.
- [81] P.Perez, P.Gangnet, and A.Blake. "*Poisson image editing*". pp. 313318,. In: Processing of SIGGRAPH, San Diego, California, USA,, 2003.
- [82] Laetitia Radder and Lynette Louw. "*Mass customization and mass production*". 11:35-40. MCB UP Ltd, 1999.
- [83] P. R.Cavanagh. "*The Running Shoe Book*". Mountain View, CA: Anderson World, 1980.
- [84] R.Duda and P.Hart. "*Pattern Classification and Scene Analysis.*". Wiley and Sons, 1973.
- [85] Ritz. <http://www.ritzstick.com/>.
- [86] R.Mencl and H.Mller. "*Graph based surface reconstruction using structures in scattered point sets*". pp.298-312. Proc. CGI, 1998.

- [87] R.S.Goonetilleke, A.Luximon, and K.L.Tsui. "*A fit metric for footwear customization*". Proceeding of the World Congress on Mass Customization and Personalization, 2001.
- [88] R.Szeliski and D.Tonnesen. "*Surface modeling with oriented particle systems*". pp. 185-194. Computer Graphics, Proceedings of Siggraph'92, 1992.
- [89] R.Veltkamp. "*Closed object boundaries from scattered points*". In Lecture Notes in Computer Science 885. Springer Verlag, 1994.
- [90] R.Veltkamp. "*Boundaries through scattered points of unknown density*". 57(6), pp. 441-452,. Graphics Models and Image Processing, 1995.
- [91] J. Salvi, J. Page's, and J. Batlle. "*Pattern codification strategies in structured light systems*". 37(4), 827-849. Pattern Recogn, 2004.
- [92] B. Ture savadkkoohi, R. De Amicis, and G.Conti. "*An overview of technology for 3D acquisition and registration*". 104-109. World-Com'09, International conference on computer graphic and virtual reality, Las Vegas, Nevada, USA, 2009.
- [93] B.Ture savadkkoohi and R.De Amicis. "*A CAD system for evaluating footwear fit*". First international conference on computer graphic, multimedia, biraod casting, korea, Springer-Verlag, 2009.
- [94] B.Ture savadkkoohi and R.De Amicis. "*Similarity Estimation for computerize footwear fit*". In 19th International Conference on Computer Graphic and Vision, Moscow, Russia, 2009.
- [95] B.Ture savadkkoohi and R.De Amicis. "*Post-processing of 3D scanning data for custom footwear manufacture*". WSCG'2010, In 18th

International Conference on Computer Graphics, Visualization and Computer Vision, Plizen, Czech Republic, 2010.

- [96] S.H.LO. "Automatic mesh generation and adaption by using contours". 31,689-707. Int.j.nummer,method, 1991.
- [97] G. Da Silveria, D.Borenstein, and F.Fogliatto. "Mass customization: literature review and research directions". 72, 1-13. International journal of production economics, 2001.
- [98] S.Muraki. "Volumetric shape description of range data using "blobby model". pp. 217-226. Computer Graphics,, 1991.
- [99] J. E. Spencer. "Robotics Technology and Advent of Agile Manufacturing Systems in the Footwear Industry". 16/3:10-15. Assembly Automation, 1996.
- [100] J. Spira. "Mass customization through training at Lutron Electronics". 30 (3),171-174. Computers in Industry, 1996.
- [101] TightCocone. <http://www.cse.ohio-state.edu/tamaldey/cocone.html>.
- [102] I. T.Jolliffe. "Principal component analysis". Springer-Verlag, 1986.
- [103] F. T.Piller and C.Schaller. "Individualization Based Collaborative Customer Relationship Management: Motives, Structures, and Modes of Collaboration for Mass Customization and CRM". ISSN 0942-5098. Technische Universitt Mnchen, May 2002.
- [104] T.Schreiber. "Approximation of 3d objects". In Proceedings of the 3rd Conference on Geometric Modeling, Dagstuhl, Germany,, 1997.
- [105] T.Schreiber and G.Brunnett. "Approximating 3d objects from measured points". In Proceedings of 30th ISATA, Florence, Italy, 1997.

- [106] D. V. Vranic and D. Saupe. "*3D Model Retrieval*". 89-93. in Proc. Spring Conference on Computer Graphics and its Applications (SCCG2000), B. Falcidieno, Ed., Budmerice Manor, Slovakia, May 2000.
- [107] W.Friedman. "*Nike Picks up the Pace in Race to Harness Web*". 71/10:S4. Advertising Age, 2000.
- [108] B.De Wita, D.De Clercq, and P.Aertsb. "*Biomechanical analysis of the stance phase during barefoot and shod running*". Pages 269-278. Journal of Biomechanics, 2000.
- [109] W.Lorensen and H.Cline. "*Marching cubes: A high resolution 3d surface construction algorithm.*". Computer Graphics, 21(4), pp. 163-169,, 1987.
- [110] R. B. Woodruff. "*Customer Value: The Next Source for Competitive Edge*". vol. 25, no. 2, pp. 139-153. Journal of the Academy of Marketing Science, 1997.
- [111] X.Shi, H.Guo, B.Shum, Y.Yu, and K.Zhou. "*Mesh editing with poisson-based gradient field manipulation*". pp. 644-651, ACM Press. In PROCEEDINGS of Siggraph, Los Angeles, California, USA, vol., 2004.

